

# **High barrier waterborne polymer-clay nanocomposites**

Dissertation

zur Erlangung des akademischen Grades eines

Doktors der Naturwissenschaften (Dr. rer. nat)

im Fach Chemie

an der Fakultät für Biologie, Chemie und Geowissenschaften

der Universität Bayreuth

vorgelegt von

Evgeny S. Tsurko

aus Moskau (Russland)

Bayreuth

2017

Die vorliegende Arbeit wurde in der Zeit von März 2012 bis März 2017 in Bayreuth am Lehrstuhl Anorganische Chemie I unter Betreuung von Herrn Professor Dr. Josef Breu angefertigt.

Vollständiger Abdruck der von der Fakultät für Biologie, Chemie und Geowissenschaften der Universität Bayreuth genehmigten Dissertation zur Erlangung des akademischen Grades eines Doktors der Naturwissenschaften (Dr. rer. nat.).

Dissertation eingereicht am: 07.08.2017

Zulassung durch die Promotionskommission: 10.08.2017

Wissenschaftliches Kolloquium: 07.12.2017

Amtierender Dekan: Prof. Dr. Stefan Peiffer

Prüfungsausschuss:

Prof. Dr. Josef Breu (Erstgutachter)

Prof. Dr. Jürgen Senker (Zweitgutachter)

Prof. Dr. Peter Strohriegl (Vorsitz)

Prof. Dr. Georg Papastavrou

*This thesis is dedicated to my parents  
for their love and endless support*

My most sincere acknowledgement of my supervisor

**Professor Dr. Josef Breu**

for his guidance, encouragement and enthusiastic support throughout the course of this research program.

## **Acknowledgement**

This thesis is a culmination of 5 years of research since I first joined Professor Breu's group in 2012. In the meantime, I have worked with a large number of people who have contributed to my research in different ways. I would like to express my appreciation to all of them in this acknowledgment.

First of all, I would like to thank my supervisor, Professor Dr. Josef Breu, for his trust, as well as for the great opportunities he has provided me since I first joined his research group. He has always been a great source of motivation and guidance throughout my research.

During my academic study period I was lucky enough to meet many people who proved to be of great help to me, in particular Dr. Matthias Stöter and Dr. Sabine Rosenfeldt. I would like to thank my colleagues in the laboratory and the entire ACI group. Additionally, I would like to thank Patrick Feicht and Christoph Habel for their contributions to the manuscripts and scientific discussions.

The technical staff, in particular Lena Geiling, conducted so many of the measurements included in this thesis, so I would like to thank all of them. I also extend my gratitude to the secretaries of the ACI department, Petra Seidler and Iris Raithel.

Many thanks go to both the electronic and mechanical workshops of Bayreuth University for building the automatic spray coating system.

I would also like to express my thanks to my professors back home at Moscow State University, Natalya E. Sorokina and Olga N. Shornikova.

Finally, I would like to thank my family for their support and encouragement. I am grateful for the endless love and support I receive from my parents, my sister and my girlfriend.

## Content

---

1. Summary – Zusammenfassung .....	1
2. Introduction.....	5
2.1. Polymer nanocomposites .....	5
2.2. Theory of gas permeability .....	6
2.3. Tortuous pathway models .....	7
2.4. Factors contributing to barrier performance .....	10
2.4.1. Crystallinity of the polymer matrix.....	10
2.4.2. Interactions between the filler and the modifier .....	10
2.4.3. Filler texturing .....	11
2.5. Polymer-filler-modifier system.....	11
2.5.1. Waterborne polymer matrix .....	11
2.5.2. Synthetic Na-fluorohectorite as a superior filler.....	12
2.5.3. Modifier .....	13
2.5.4. Nanocomposites preparation techniques.....	14
3. Synopsis .....	15
3.1. Motivation.....	15
3.2. Oxygen and water vapor barrier of PVA-clay nanocomposites .....	16
3.3. Oxygen and water vapor barrier of PEIE-PAA-clay nanocomposites.....	20
3.4. Helium barrier of PVA-clay nanocomposites .....	24
4. Bibliography .....	27
5. Individual contribution to joint publications.....	33
6. Results.....	35
6.1. Appendix 1.....	35
6.2. Appendix 2.....	47
6.3. Appendix 3.....	60
7. Declaration – Erklärung.....	71

**Abbreviations**

$\alpha$	filler aspect ratio
$\beta$	least-square parameter from Gusev-Lusti equation equal to 0.71
$\kappa$	geometric factor in Fredrickson-Bicerano model equal to $\pi/\ln \alpha$
$\mu$	geometric factor
$\sigma$	the standard deviation in the flake size
$\phi$	filler volume fraction
$a_1$	coefficient in Fredrickson-Bicerano model equal to $(2 - \sqrt{2})/4$
$a_2$	coefficient in Fredrickson-Bicerano model equal to $(2 + \sqrt{2})/4$
AFM	atomic-force microscopy
$C$	concentration
cv	coefficient of variation
$D$	diffusion coefficient
$D_0$	diffusion coefficient of unfilled film
$\bar{D}$	mean value of platelet length
$f$	tortuosity factor
HA	6-aminocaprohydroxamic acid hydrochloride
HAHec	6-aminocaprohydroxamic acid hydrochloride modified NaHec
HeTR	helium transmission rate
$J_x$	penetrant flux along the $x$ axis
$l$	thickness of the barrier film
NaHec	sodium fluorohectorite
OLED	organic light-emitting diode
OP	oxygen permeability
OPV	organic photovoltaics
OTR	oxygen transmission rate
$p$	pressure
$P$	permeability of filled nanocomposite
$P_0$	permeability of unfilled nanocomposite
PAA	polyacrylic acid
PEI	polyethyleneimine

## Abbreviations

---

PEIE	ethohylated polyethyleneimine
PET	polyethylene terephthalate substrate film
PVA	polyvinyl alcohol
PXRD	powder X-ray diffraction
RH	relative humidity
$S$	solubility coefficient
$S_0$	solubility coefficient of unfilled film
SAXS	small-angle X-ray scattering
TEM	transmission electron microscopy
$p_u$	upstream pressure
$p_d$	downstream pressure
WVP	water vapor permeability
WVTR	water vapor transmission rate
$x_0$	least-square parameter from Gusev-Lusti equation equal to 3.47
XRD	X-ray diffraction

## 1. Summary – Zusammenfassung

### Summary

This dissertation focuses on the creation of waterborne polymer-clay nanocomposites with superb barrier properties ( $O_2$ ,  $H_2O$ , He), even at elevated relative humidity (RH). The high sensitivity of waterborne polymer nanocomposites to water vapor was mitigated by improving the donor-acceptor interactions between the polymer matrix and filler, increasing the polymer matrix crystallinity and by the self-assembly of the polymer-filler domains in the smectic phase. Furthermore, a special approach was used in spray coating to contribute to a perfect parallel alignment of the filler nanoplatelets.

The permeability ( $P$ ) of barrier nanocomposites is the product of the diffusivity ( $D$ ) and solubility ( $S$ ) of the penetrant.  $D$  is influenced by the incorporation of the impermeable platelets, thus increasing the diffusion path (tortuous pathway). According to the tortuous pathway models [1,2],  $D$  mainly depends on the filler aspect ratio ( $\alpha$ ) and volume fraction ( $\phi$ ). Utilization of a large aspect ratio ( $\alpha \approx 20000$ ) synthetic sodium fluorohectorite (NaHec) as nanofiller together with a high loading (10-35 vol%) significantly decreases the diffusivity.  $S$  mainly depends on the affinity between the penetrant and the barrier, wherein polar molecules are basically more soluble in polar than in nonpolar matrices and vice versa. Accordingly, waterborne nanocomposites are typically poor barriers for polar water molecules. The remarkable oxygen barrier properties of such nanocomposites at a very low RH inevitably degrade at more elevated RH levels ( $> 35\%$ ). Increased amounts of water molecules sorbed on polar functional groups interrupt the polymer chain interactions and cause plastification and swelling of the polymer matrix. Modification of the filler with a hydrogen bond-capable modifier—for example, 6-aminocaprohydroxamic acid hydrochloride (HA)—reduces the hydrophilicity of the filler to some extent and incites donor-acceptor interactions between the modifier and polymer matrix, thus decreasing the free volume and limiting swelling of the polymer matrix.

Modification of the NaHec with HA (HAHec) reduces swelling of the filler in polyvinyl alcohol (PVA)—clay nanocomposites. Furthermore, the crystalline domains of the PVA polymer matrix show reduced water vapor sensitivity as well. Spray coating yields a perfectly textured film. A combination of the above-mentioned effects shifts the onset of significant swelling in the PVA nanocomposites to high RH regions. As a result, even at 23 °C and 90% RH, surprisingly low

oxygen (OTR) and water vapor (WVTR) transmission rates ( $0.11 \text{ cm}^3 \text{ m}^{-2} \text{ day}^{-1} \text{ bar}^{-1}$  and  $0.18 \text{ g m}^{-2} \text{ day}^{-1}$  respectively, for a coating of  $0.42 \text{ }\mu\text{m}$ ) are observed.

Polyacrylic acid (PAA), ethoxylated polyethyleneimine (PEIE) and HAHeC form a perfectly homogeneous suspension in water. Doctor blading and spray coating produce highly textured nanocomposites containing polymer-clay domains in the smectic phase. Nevertheless, spray coating is superior to doctor blading because it yields significantly better ordered structures. The improved regularity enhances the electrostatic interaction between filler and matrix via the Madelung constant, which eventually reduces the transmission rates. As a result, the OTR and WVTR of the spray-coated waterborne nanocomposite coating with a thickness  $21.4 \text{ }\mu\text{m}$  at  $38 \text{ }^\circ\text{C}$  and  $90\% \text{ RH}$  are equal to  $0.24 \text{ cm}^3 \text{ m}^{-2} \text{ day}^{-1} \text{ bar}^{-1}$  and  $0.003 \text{ g m}^{-2} \text{ day}^{-1}$  respectively.

PVA nanocomposites were tested on the much more sophisticated gas, helium, as well. NaHeC increases the barrier properties of the PVA polymer matrix against helium by a factor of about 1000. It was also shown that decreasing the PVA molar mass leads to improvement of the helium barrier.

Thus, high-barrier waterborne polymer-clay nanocomposites were obtained. Nanocomposites possess excellent barrier properties not only for nonpolar  $\text{O}_2$  and He, but also for polar water vapor. A combination of various effects shifts the swelling of waterborne nanocomposites to the high RH region, whereby superb barrier performance persists even at elevated RH. The achieved barrier properties of these waterborne polymer nanocomposites are not only applicable as a possible low-tech food packaging solution, but can also be put to use in high-tech display encapsulation or lighter-than-air applications.

## Zusammenfassung

Die vorliegende Dissertation befasst sich mit der Herstellung wasserlöslicher Polymer-Schichtsilikate-Nanokomposite mit ausgezeichneten Barriereigenschaften ( $O_2$ ,  $H_2O$ , He), selbst bei erhöhter relativer Feuchtigkeit (RH). Mit dem Ziel die hohe Wasserdampfempfindlichkeit von wasserbasierten Polymer-Nanokompositen zu verringern, wurden die Donor-Akzeptor-Wechselwirkungen zwischen den Polymermatrizen und dem Füllstoff erhöht. Dadurch wurde die Kristallinität der Polymermatrix und die Selbstassemblierung der Polymer-Füllstoffdomänen in der smektischen Phase erhöht. Darüber hinaus trägt die Methode der Sprühbeschichtung zu einer perfekten, parallelen Ausrichtung der Füllstoff-Nanoplättchen zusätzlich bei.

Die Permeabilität ( $P$ ) des Barriere-Nanokomposits ist das Produkt aus der Diffusivität ( $D$ ) und der Löslichkeit ( $S$ ) des Penetrationsmittels.  $D$  wird durch den Einbau impermeabler Plättchen beeinflusst. Auf diese Weise wird der Diffusionsweg (engl. Tortuous pathway) erhöht. Dem Tortuous Pathway-Modellen nach [1,2] hängt  $D$  hauptsächlich vom Höhe-Durchmesser-Verhältnis ( $\alpha$ ) und dem Volumenanteil ( $\phi$ ) ab. Das Verwenden eines synthetischen Na-Hectorit (NaHec) mit großen  $\alpha$  ( $\alpha \approx 20000$ ) als Nanofüllstoff vermindert bei gleichzeitig hohem Füllstoffanteil (10-35 vol%)  $D$  signifikant.  $S$  hängt hauptsächlich von der Affinität des Penetrationsmittels zur Barrierschicht ab. Typischerweise sind daher wasserlösliche Nanokomposite schlechte Barriermaterialien für polare Wassermoleküle. Die bemerkenswerten Sauerstoff-Barriere-Eigenschaften derartiger Nanokomposite nehmen mit steigender RH ( $> 35\%$ ) ab. Eine erhöhte Menge an Wassermolekülen, die an den polaren funktionellen Gruppen sorbiert sind, unterbricht die Polymerketten-Wechselwirkungen und verursacht Plastifizierung und Quellen der Polymermatrix. Die Modifizierung des Füllstoffs mit einem Modifikator, welcher Wasserstoffbrückenbindungen ausbilden kann, beispielsweise 6-Aminocaprohydroxamsäure-Hydrochlorid (HA), reduziert die Hydrophilie des Füllstoffs bis zu einem gewissen Grad und regt Donor-Akzeptor-Wechselwirkungen zwischen Modifikator und Polymermatrix an, wodurch das freie Volumen verringert und die Quellung der Polymermatrix begrenzt.

Die Modifizierung des NaHec mit HA (HAHec) reduziert die Quellung des Füllstoffs in Polyvinylalkohol (PVA)-Schichtsilikate-Nanokompositen. Weiterhin weisen die kristallinen Domänen der PVA-Polymermatrix auch eine verminderte Wasserdampfempfindlichkeit auf. Die Sprühbeschichtung ergibt eine perfekt strukturierte Folie. Die Kombination der Effekte

verschiebt den kritischen Wert, ab dem eine bedeutende Quellung der PVA-Nanokompositen einsetzt, in hohe RH Regionen. Infolgedessen werden selbst bei 23 °C und 90% RH überraschend niedrige Sauerstoff- (OTR) und Wasserdampftransmissionsraten (WVTR) beobachtet ( $0.11 \text{ cm}^3 \text{ m}^{-2} \text{ Tag}^{-1} \text{ bar}^{-1}$  und  $0.18 \text{ g m}^{-2} \text{ Tag}^{-1}$  für eine Beschichtung von  $0.42 \text{ }\mu\text{m}$ ).

Polyacrylsäure (PAA), ethoxyliertes Polyethylenimin (PEIE) und HAHeC bilden eine perfekt homogene Suspension in Wasser. Rakeln und Sprühbeschichtung als Beschichtungsmethoden erzeugen hochstrukturierte Nanokomposite mit Polymer-Schichtsilikate-Domänen in der smektischen Phase. Trotzdem ist die Sprühbeschichtung der Rakel insofern überlegen, dass deutlich geordnetere Strukturen erzeugt werden. Die verbesserte Regularität erhöht die elektrostatische Wechselwirkung zwischen Füllstoff und Matrix über die Madelung-Konstante, die die Transmissionsraten schließlich reduziert. Im Ergebnis sind die OTR und WVTR von einer sprühbeschichteten wasserlöslichen Nanokompositbeschichtung mit einer Dicke von  $21.4 \text{ }\mu\text{m}$  bei 38 °C and 90% RH gleich  $0.24 \text{ cm}^3 \text{ m}^{-2} \text{ Tag}^{-1} \text{ bar}^{-1}$  und  $0.003 \text{ g m}^{-2} \text{ Tag}^{-1}$ .

PVA-Nanokomposite wurden auch auf/an einem anspruchsvollen Gas, nämlich Helium, getestet. NaHeC erhöht die Barriereigenschaften der PVA-Polymermatrix gegen Helium um einen Faktor von etwa 1000. Es wurde auch gezeigt, dass eine Verringerung der PVA-Molmasse zur Verbesserung der Barriereigenschaften gegenüber Helium führt.

In der Folge wurden wasserlösliche Polymer-Schichtsilikate-Nanokomposite gewonnen. Diese Nanokomposite besitzen ausgezeichnete Barriereigenschaften nicht nur gegenüber unpolaren Gasen wie Sauerstoff und Helium, sondern auch gegenüber polaren Permeaten, wie Wasserdampf. Die Kombination verschiedener Effekte verlagert das Quellen von wasserlöslichen Nanokompositen in die Hoch-RH-Region, wodurch die ausgezeichneten Barriereigenschaften auch bei erhöhter RH bestehen bleiben. Die erzeugten Barriereigenschaften machen wasserlösliche Polymer-Nanokomposite nicht nur für Low-Tech-Verpackungen nutzbar, sondern auch für Hightech-Display-Verkapselung oder Anwendungen in der Luftfahrt.

## 2. Introduction

### 2.1. Polymer nanocomposites

Polymer nanocomposites represent a multiphase system where the nanofiller phase is dispersed in the polymer matrix [3]. In general, nanofillers can be classified by their shape: 0-dimensional (nanoparticles); 1-dimensional (fibers, carbon nanotubes); 2-dimensional (clays, graphene, and graphene oxide). By definition, at least one dimension of the filler is smaller than 100 nm in a nanocomposite. As this dissertation focuses on incorporation of 2-dimensional clay (NaHec) into a polymer matrix, nanocomposites with 2-dimensional fillers will be described in detail.

Nanofiller incorporation predominantly improves the following characteristics of the neat polymer matrix: mechanical properties [4,5], fire retardancy [6,7] and barrier performance [8,9]. Stiff filler platelets redispersed in a polymer matrix effectively dissipate applied loads, thereby improving the mechanical properties, e.g. stiffness and toughness [10]. Incorporation of nanoplatelets also improves fire retardancy, as the filler effectively prevents spreading of the fire. Therefore, polymer nanocomposites possess higher ignition time and lower heat release rate.

Gas barrier is among the most common polymer nanocomposite application. Barriers are required in many fields, from low-tech food packaging to high-tech display encapsulation. The primary factor determining the expiration date of food is permeability of the packaging. Most, if not all, packaged food requires restricted permeability for both hydrophobic ( $O_2$ ,  $N_2$ ) and hydrophilic (water vapor,  $CO_2$ ) penetrants. Developing technically benign, water-based, chlorine- and metal-free polymer nanocomposites with improved flex-crack resistance and barrier properties for both hydrophobic and hydrophilic penetrants will reduce food wastage that is currently prevalent.

Ultra-high barrier materials are required for encapsulations of flexible organic photovoltaics (OPV) solar cells and organic light-emitting diode (OLED) displays. Both OLED and OPV are sensitive to oxidation by atmospheric water vapor and oxygen. The protective glass cover that is used currently is an excellent barrier for both oxygen and water vapor, but it is brittle and not flexible. Barrier polymer nanocomposites can replace glass as protective coatings, thereby providing new classes of flexible electronic devices. For sufficient lifetime of the OLED displays, OTR and WVTR have to be lower than  $10^{-5} \text{ cm}^3 \text{ m}^{-2} \text{ day}^{-1} \text{ bar}^{-1}$  and  $10^{-6} \text{ g m}^{-2} \text{ day}^{-1}$ ,

respectively [11]. Apart from OPV and OLED encapsulation, ultra-high barrier materials are required for effective storage of hydrogen and helium [12] and lighter-than-air applications [13].

## 2.2. Theory of gas permeability

Transfer of a penetrant through the homogeneous nonporous barrier film can be divided into three stages [14]:

- absorption of the gas at one side of the barrier film;
- diffusion of the liquid penetrant through the barrier film due to a concentration gradient;
- evaporation of the penetrant from other side of the barrier film in the gaseous state.

Diffusion is a kinetic process of penetrant transfer from a region of high concentration to a region of low concentration. Fick's first law [15] relates the flux of penetrant diffusing through the barrier film ( $J_x$ ) with the concentration ( $C$ ) gradient from both sides of the film. When the penetrant mainly transfers in one direction (thin barrier film) for simplification, the Fick's first law can be expressed using the following equation:

$$J_x = -D \frac{\partial C}{\partial x} \quad (1)$$

According to Henry's law of solubility [16], concentration of the dissolved gas in the barrier film is proportional to the applied gas pressure ( $p$ ):

$$C = S(C, p)p \quad (2)$$

If Henry's law is satisfied, it is possible to estimate the penetrant flux through the barrier film. For the film with a thickness  $l$  and pressures on both sides of the film,  $p_u$  (upstream) and  $p_d$  (downstream), the penetrant flux can be expressed by combining equations 1 and 2 [17]:

$$J = DS \left( \frac{p_u - p_d}{l} \right) \quad (3)$$

The product of diffusivity and solubility coefficients is the permeability coefficient ( $P$ ):

$$P = DS \quad (4)$$

The expression  $(p_u - p_d)/l$  is the applied pressure gradient across the film with the thickness  $l$ . Therefore, the penetrant flux is the product of the permeability coefficient and pressure gradient across the barrier film:

$$J = P \frac{\Delta p}{l} \quad (5)$$

### 2.3. Tortuous pathway models

According to equation 4, the permeability coefficient of the neat unfilled polymer film is a product of the diffusivity and the solubility. In the simplest models, the filler has no effect on the polymer matrix and no specific interactions with the penetrant. This assumption implies that the solubility decreases proportionally to the filler volume fraction, since filler platelets are supposed to be impermeable to the penetrant, and decrease the volume available for penetrant dissolution [3,18]:

$$S = S_0(1 - \phi) \quad (6)$$

Where  $S$  and  $S_0$  are the solubility coefficients of filled and unfilled film, respectively.

The filler incorporation effect on the diffusion coefficient is more complicated. Impermeable fillers significantly increase the path taken for penetrant to diffuse from one side to the other side of the barrier film, commonly known as tortuous pathway (Figure 1). Most tortuous pathway models associate the decrease in the neat polymer permeability with the volume fraction of the incorporated filler, together with its aspect ratio and shape. Alignment of the filler platelets perpendicular to the penetrant flux is equally important, since this disposition maximizes the tortuous pathway. In general, the change in the diffusion coefficient after filler incorporation can be expressed using the following equation:

$$D = D_0 f \quad (7)$$

Where  $D$  and  $D_0$  are the diffusion coefficients of filled and unfilled film, respectively;  $f$  is the tortuosity factor.

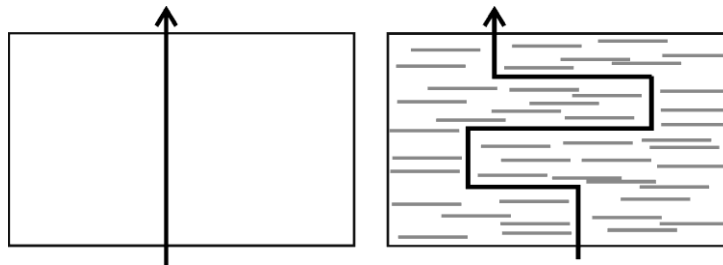


**Figure 1.** Illustration of the tortuous pathway. Polymer matrix without filler (left) and polymer matrix with random array of monodisperse nanoplatelets (right).

By combining the equations 4, 6 and 7, one can determine the total effect of filler incorporation on the permeability coefficient:

$$P = DS = D_0 f S_0 (1 - \phi) = P_0 f (1 - \phi) \quad (8)$$

Where  $P$  and  $P_0$  are the permeability coefficients of filled and unfilled film, respectively.

From the equation 8, the tortuosity factor  $f$  can be expressed as:

$$f = \frac{P}{P_0 (1 - \phi)} \quad (9)$$

Tortuous pathway models consider the influence of filler incorporation on the tortuosity factor or on the decrease in the permeability coefficient  $P/P_0$ . The Nielsen model considers ribbon-shaped filler platelets that are uniformly and completely dispersed in a polymer matrix aligned parallel to the surface [19]. These platelets have defined width and thickness with an infinite length. The 2-dimensional Nielsen model establishes decrease in permeability with the filler volume fraction and aspect ratio via simple geometric calculations. The Nielsen model is suitable for 'the dilute regime', where there is no overlap between the filler platelets, suitable for the situation where  $\alpha\phi \ll 1$ . According to the equation 10 (Table 1), increase in the filler aspect ratio and the volume fraction improves the barrier performance.

Cussler and coworker's models further develop Nielsen's theory, using similar but more complicated geometric considerations. The Cussler model sequentially moves from the ideal system of monodisperse and regular filler alignment [1] to a more realistic monodisperse and random alignment [20], and finally to a polydisperse and random alignment of the filler [20] (equations 11-13). The last assumption is the closest to real systems, since majority of the nanocomposites contain polydisperse and randomly aligned fillers. In contrast to the Nielsen model, the Cussler-Aris model considers 'semi-dilute regime' with a high level of filler overlap, which is satisfied when  $\alpha\phi \gg 1$ . The geometric factor ( $\mu$ ) of the filler introduced into the equations is not completely clear. For the periodic and ribbon-like platelets with significantly larger lengths, as compared to the width,  $\mu$  can be taken as 1 [21]. For the periodic hexagons platelets, for example NaHec, the geometric factor is equal to 4/9 [22]. For the random platelets,  $\mu$  can vary from 2/27 to  $\pi^2 / 16 \ln^2 \alpha$  [2,22].

**Table 1.** Tortuous pathway models.

Model	Filler geometry	Model dimension	Platelets/ Array	Equation	№
Nielsen	Ribbon	2D	Monodisperse, Regular	$\frac{P}{P_0} = \frac{1-\phi}{1+\frac{\alpha\phi}{2}}$	10
Cussler-Aris	Ribbon	2D	Monodisperse, Regular	$\frac{P}{P_0} = \left(1 + \mu \frac{\alpha^2 \phi^2}{1-\phi}\right)^{-1}$	11
Cussler-Lape	Ribbon	2D	Monodisperse, Random	$\frac{P}{P_0} = \frac{1-\phi}{\left(1 + \frac{2}{3}\alpha\phi\right)^2}$	12
Cussler-Lape	Ribbon	2D	Polydisperse, Random	$\frac{P}{P_0} = \frac{1-\phi}{\left(1 + \left(\frac{\sigma}{D}\right)^2\right)^2 \left(1 + \frac{\alpha}{3}\phi\right)^2}$	13
Fredrickson-Bicerano	Disc	3D	Monodisperse, Random	$\frac{P}{P_0} = \frac{1}{4} \left( \frac{1}{1+a_1\kappa\alpha\phi} + \frac{1}{1+a_2\kappa\alpha\phi} \right)^2$	14
Gusev-Lusti	Disc	3D	Polydisperse, Random	$\frac{P}{P_0} = \exp\left(-\frac{\alpha\phi}{x_0}\right)^\beta$	15

Dependence of the relative permeability (equation 11) on  $\alpha$  and  $\phi$  of the filler is graphically presented in Figure 2. The horizontal line marks  $\alpha$  of the applied synthetic NaHec ( $\alpha \approx 20000$ ) and predicts theoretical improvement of barrier performance over a wide range of  $\phi$ .

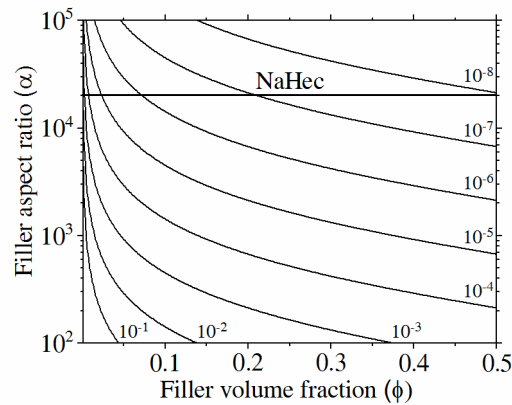


**Figure 2.** Schematic representation of the effect of filler incorporation on relative permeability, according to the Cussler-Aris model.

The Fredrickson-Bicerano model can be regarded as a complex continuation of the Nielsen model and the Cussler model [2]. They consider a 3-dimensional model with disc-shaped, randomly aligned filler platelets. Fredrickson and Bicerano offer solutions for both dilute and semi-dilute composite regimes (equation 14).

The Gusev-Lusti model proposes computer calculations for investigation of the filler incorporation effect [23]. The model focuses on the geometric factor and changes in the permeability due to molecular-level transformations in the polymer matrix. The Gusev-Lusti model analyzes 3-dimensional systems with randomly aligned disc shaped fillers. An exponential equation (equation 15) is obtained on varying the volume fraction and aspect ratio of the filler.

## **2.4. Factors contributing to barrier performance**

### **2.4.1. Crystallinity of the polymer matrix**

Polymer matrix in the nanocomposite represents an amorphous phase or a mixture of amorphous and crystalline phases, a semi-crystalline phase. The ability to crystallize mainly depends on the polymer structure: straight chains with regularly-spaced small side groups tend to crystallize. Nevertheless, the degree of crystallinity in the semi-crystalline polymers is typically between 10 and 80% [24].

The polymer crystalline regions, in contrast to the amorphous regions, are impermeable to the penetrant [25–27]. Thus, increased crystallinity of the polymer matrix [28–31] improves barrier performance of the barrier nanocomposites. A filler simply acts as a nucleating agent, thereby improving the crystallinity of the polymer matrix [32]. Preparation technique or/and annealing of nanocomposites higher than the polymer glass transition temperature further the crystallinity [33].

### **2.4.2. Interactions between the filler and the modifier**

Incorporation of the filler into the neat polymer matrix leads to an increase in the free volume due to disruption of the polymer structure by highly anisotropic platelets. Additional free volume in the nanocomposite films increases both diffusivity and solubility, thereby it increases the barrier permeability. Donor-acceptor interactions between the polymer matrix and the filler reduce the free volume on incorporation of the filler [9]. However, strong interactions between the polymer matrix and the filler possibly hinder the swelling of the polymer, which is important for creating high water barrier nanocomposites at elevated RH. Cross-linking agents, for example

glutaraldehyde [34,35] or multivalent ions like  $\text{Ca}^{2+}$ ,  $\text{Mg}^{2+}$ ,  $\text{Cu}^{2+}$ ,  $\text{Al}^{3+}$ ,  $\text{Fe}^{3+}$  [36,37], improve interactions between the polymer and the filler. Nevertheless, the possible aggregation caused by the cross-linking agents limits their application and impedes the utilization of one-component systems.

Filler modification is another method of improving interactions. Interlayer charge of the clay allows modification, thereby changing the initial properties of the clay. For example, NaHec modification with trimethyl aminoethyl methacrylate makes hydrophilic clay hydrophobic and increases its solubility in organic solvents [8]. Modification of NaHec with hydroxamic or amino acids that form hydrogen bonds improve interactions of the filler with waterborne polymers like PVA, PEI, and PAA.

### **2.4.3. Filler texturing**

Tortuous pathway models basically assume an ideal parallel-to-substrate alignment of the filler platelets that minimizes diffusion. However, due to anisotropic nature of the filler, in real systems, although nanoplatelets occupy predominantly parallel alignment, it is far from ideal ordering. Nanocomposite preparation techniques greatly influence the filler texture, which differs from one method to another. It was shown that for HAHec – PEIE – PAA system, spray coating produces more textured nanocomposites, as compare to doctor blading system [38].

Apart from parallel texturing, self-assembly of the nanocomposites in smectic phase [39] also improves the barrier properties. Uniform alignment of the filler with equivalent distances between the platelets reduces the free volume. Due to ideal crystallinity of such nanocomposites, the tortuosity increases significantly and improves the barrier performance. Smectic phase self-assembly mostly depends on the interactions between the filler and the polymer matrix. However, quality of crystallinity also depends on the preparation technique.

## **2.5. Polymer-filler-modifier system**

### **2.5.1. Waterborne polymer matrix**

Environmental pollution is an urgent problem of the 21<sup>th</sup> century. Environmentally friendly, waterborne polymer-clay nanocomposites would be preferred barrier materials, but they fail to meet particular standards of for high water vapor barriers. Various synthetic waterborne polymers are used for the creation of barrier nanocomposites: PVA, PEI, PAA, polyvinylpyrrolidone, polyethylene oxide, polyacrylamide, and carboxymethylcellulose sodium

salt. Waterborne PVA and PEI-PAA nanocomposites are excellent barrier materials for nonpolar gases, such as oxygen, especially at very low RH. Sensitivity of waterborne nanocomposites to water vapor significantly limits the area of their application. Improving the water vapor barrier and limiting the swelling of polymer matrix at high RH can make waterborne barrier formulations applicable for food packaging.

PVA is thermoplastic semi-crystalline polymer that is widely used for preparation of films. Due to the hydroxyl groups, PVA is able to form polymer-polymer and polymer-filler hydrogen bonds. Hydrogen bonds and polarity of hydroxyl groups presumably determine excellent oxygen barrier properties of nanocomposites at very low RH. Increase in the moisture content disrupts the polymer-polymer interactions because of sorbed water on polar hydroxyl groups [40]. Subsequent swelling of the polymer matrix deteriorates the oxygen barrier, whereas the water vapor barrier of PVA nanocomposites is initially poor. Increase in the filler loading shifts swelling of PVA nanocomposites to higher RH region [41]. Increase in the PVA polymer matrix crystallinity contributes to improvement of the barrier performance, since crystalline regions are impermeable [28–31]. PVA crystallinity improvement is mostly achieved by temperature treatment of the nanocomposites during or after nanocomposite preparation [33].

PAA [42] and linear PEI are crystalline, while branched PEI [43] is an amorphous polymer matrix. PEI-PAA barrier nanocomposites are usually produced using the layer-by-layer technique, consistently separating positively charged PEI and negatively charged PAA during deposition. Similar to PVA, the barrier performance of hydrophilic PEI-PAA nanocomposites is very sensitive to RH. Utilization of cross-linking agents like glutaraldehyde [34] and pH variation [9] for improving donor-acceptor interactions are the main ways for barrier enhancement.

### **2.5.2. Synthetic Na-fluorohectorite as a superior filler**

Layered silicates are most commonly used as nanofillers. Fluorohectorite, for example, belongs to the 2:1 smectite family, and shows a sandwich-like structure comprising of two tetrahedral and one octahedral layers. Its composition, similar to the synthetic fluorohectorite used in this work, is as follows:  $[\text{Na}_{0.5}]^{\text{inter}}[\text{Mg}_{2.5}\text{Li}_{0.5}]^{\text{oct}}[\text{Si}_4]^{\text{tet}}\text{O}_{10}\text{F}_2$  [44].

The tetrahedral sheets of fluorohectorite are composed of  $\text{SiO}_4^{4-}$ , which are linked together by sharing three corners of the basal oxygen atoms, the fourth being the apical oxygen atom. Each

of the basal  $O^{2-}$  connects to a  $Si^{4+}$ - $Si^{4+}$  cation pair. The octahedral sheet of fluorohectorite contains cations –  $Li^+$  and  $Mg^{2+}$ , coordinated by four shared oxygen atoms and two additional fluoride groups. The isomorphous substitution of cations in the octahedral layer introduces negative charges, which are counterbalanced by the interlayer cation –  $Na^+$  [45].

Melt-synthesized NaHec nanosheets, moreover, are available in large sizes ( $>20 \mu m$ ), making synthetic fluorohectorite a superb filler for barrier nanocomposites [46,47]. Additionally, this synthetic clay can be delaminated into single layers, each with thickness of 0.96 nm, simply by osmotic swelling. Interlayer spacing can be easily modified through ion exchange using cationic modifiers, such as quaternary ammonium salts or polyelectrolytes. High cation exchange capacity allows significant changes in the properties of the NaHec, providing better dispersibility of clay in the polymer matrix.

### **2.5.3. Modifier**

PVA and PEI-PAA polymer matrices can form donor-acceptor hydrogen bonds via functional groups. Donor-acceptor interactions reduce the free volume and limit the swelling of polymer matrix, thereby improving barrier properties. Modification of NaHec with hydrogen bonds inducing modifier can implement donor-acceptor interactions between the polymer matrix and the filler. Two classes of organic compounds currently appear to be the most effective for this purpose: hydroxamic acids and amino acids.

Hydroxamic acids contain an  $R-C(O)-N(H)-OH$  functional group. Due to the presence of carbonyl, amino and hydroxyl groups hydroxamic acids form several strong hydrogen bonds per one molecule [48]. Thereby hydroxamic acids are well known chelating agents [49]. So far, the most proven modifier is 6-aminocaprohydroxamic acid hydrochloride (HA). Modification of NaHec with HA creates a highly stable suspension, which remains delaminated, even in a mixture with PVA or PEI-PAA polymer matrices. Simplicity and low cost of production via one step reaction of caprolactam and hydroxylamine sulfate are equally important criteria [50].

Amino acids are another class of modifiers that are also highly effective. Combination of amino and carboxyl groups promotes hydrogen bond interactions between modifier and polymer matrix. The terminal amino groups that contain arginine, histidine, glutamine and lysine can be easily protonated and ion-exchanged with the clay interlayer cation.

#### **2.5.4. Nanocomposites preparation techniques**

The nanocomposite preparation method depends on the required characteristics of nanocomposite and initial parameters of the polymer-filler system. Simple suspension casting [4], spin coating [51], doctor blading [8], layer-by-layer [52], spray coating [39] techniques are among the most popular laboratory methods. This dissertation focuses on doctor blading and spray coating techniques.

##### **Doctor blading**

Doctor blading is a fast and large scalable process that consists of two steps: deposition of one-component polymer-filler suspension and subsequent suspension drying. During deposition, raker removes excess of the suspension from the substrate surface. Height of the raker, moving speed, and substrate temperature are main parameters of the deposition step. Spreading the suspension above the substrate is a crucial condition for the preparation of homogeneous films.

The following film drying procedure is equally important, although it restricts the nanocomposite thickness. Effective solvent evaporation from inner regions of the applied liquid layer could be hampered because of high thickness or barrier of the coating, forming blisters and bubbles on the surface. Thus, doctor blading is limited in the preparation of ultra-high barrier nanocomposites.

##### **Spray coating**

The method involves spraying the suspension on the substrate. During the spraying process, the suspension passes through the airbrush nozzle under high pressure, atomizes to small droplets, and crashes against the substrate at a huge speed. Different variations of the spray coating technique exist, including spraying of one- or multi-component suspensions or using fixed or movable airbrush/substrates. Similar to doctor blading, spray coating also consists of two steps: spraying and drying. Therefore, the main parameters to be considered are as follows:

- Spraying rate of the suspension;
- Speed of the conveyor belt and/or the substrate;
- Atomization pressure;
- Distance between the airbrush and the substrate;
- Drying time;
- Temperature of the substrate surface.

### **3. Synopsis**

#### **3.1. Motivation**

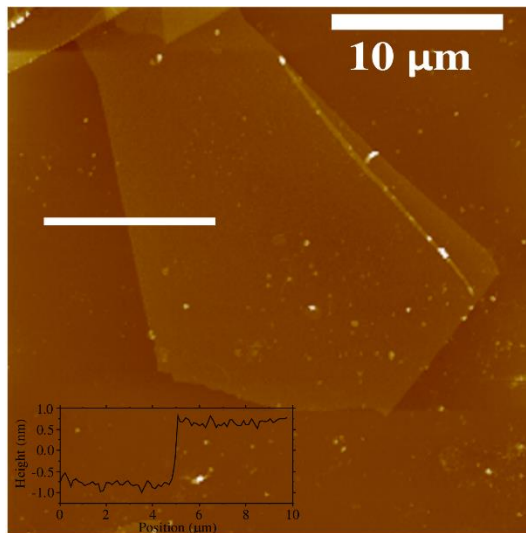
Flexible transparent barrier coatings are required for applications in food packaging and display encapsulation. Most barriers require restricted permeability for both hydrophobic (O<sub>2</sub>, N<sub>2</sub>, H<sub>2</sub>, and He) and hydrophilic (water vapor, CO<sub>2</sub>) permeates. Such multi-permeate barriers can only be realized by using less favorable laminated structures of polar and nonpolar polymers or by reducing diffusion rates in a nonselective manner. Environmentally friendly and waterborne polymer-clay nanocomposites would be preferred, but they fail to meet the particular standards for ultra-high water vapor barriers.

PVA and PEI-PAA system are well-known waterborne polymer matrices having a great oxygen barrier at very low RH. Such nanocomposites, however, show high solubility, hygroscopicity and swelling in water, and consequently high water vapor permeability (WVP). Moreover, water uptake by swelling at an elevated RH leads to a drastic increase in the permeability of not only of water vapor, but also of oxygen. Reducing the significant swelling at higher RH regions can not only improve the oxygen barrier performance of waterborne nanocomposites, but can also achieve the ultra-high water vapor barrier properties. Superior oxygen and water vapor barrier properties at elevated RH may render waterborne polymer nanocomposites useful for low-tech food packaging application, high-tech display encapsulation, and lighter than air applications.

### 3.2. Oxygen and water vapor barrier of PVA-clay nanocomposites

Water uptake of PVA nanocomposites by swelling at an elevated RH ( $> 35\%$ ) leads to a drastic increase in the oxygen permeability. Grunlan *et al.* [41] has shown that the critical RH, where swelling followed by a significant loss in the oxygen barrier sets in, can be shifted to a higher RH by incorporating Na-montmorillonite as a platy impermeable filler.

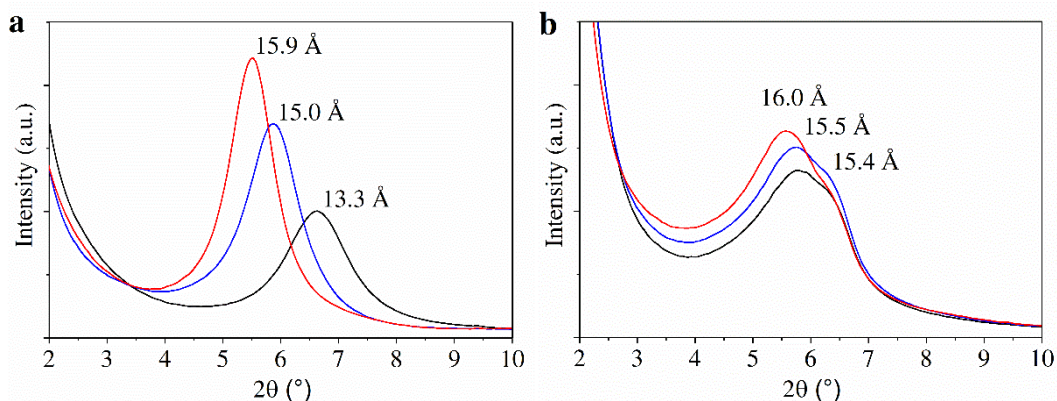
Melt-synthesized NaHec (Figure 3), used in this work, possesses unique combination of large aspect ratio ( $> 20000$ ) and charge homogeneity, thus making it a superior filler for polymer nanocomposites. High filler loading (50 wt%) drastically decreased the diffusion coefficient and decreased the swelling. Modification of NaHec with HA reduced hydrophilicity of the filler to some extent. However, the modifier is known to form very strong hydrogen bonds via the hydroxamic acid functional group. Ion exchange did not trigger any restacking, evidenced by the absence of reflection at the basal spacing of HAHec stacks in the small-angle X-ray scattering (SAXS) curves of aqueous suspensions. The stability of both NaHec and HAHec suspensions was not affected by mixing with PVA solutions, indicated by the absence of reflections at the basal spacing of NaHec or HAHec stacks in the SAXS patterns.



**Figure 3.** Typical AFM image of delaminated NaHec.

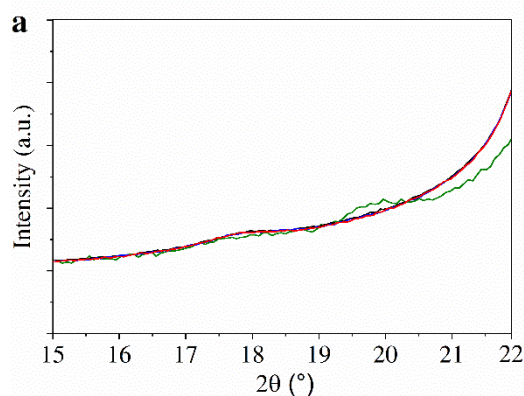
These highly stable delaminated suspensions of dissolved PVA and NaHec or HAHec were spray coated on PET substrates, whereupon thin, flexible, and transparent barrier films were obtained. As expected, modification with HA, capable of forming hydrogen bonds, limited the

swelling of the modified clay in PVA-HAhec, as compared to that in PVA-NaHec nanocomposite films (Figure 4).



**Figure 4.** The powder X-ray diffraction (PXRD) curves of PVA-NaHec (a) and PVA-HAhec (b) at 50% (black), 75% (blue), and 90% (red) RH.

PVA crystalline domains showed reflections at  $2\theta \approx 18^\circ$  and  $\approx 20^\circ$ . Peak at  $\approx 20^\circ$ , corresponding to non-swollen PVA domains, appeared at 0% RH. Increasing the RH ( $> 50\%$ ) shifted this reflection to  $\approx 18^\circ$ , corresponding to swollen PVA domains (Figure 5a). Surprisingly, the crystalline domains of the PVA matrix in nanocomposite films showed reduced water vapor sensitivity. The reflection, associated with crystalline domains in PVA-NaHec, remained at  $20^\circ$  at 50% RH, but shifted to  $18^\circ$  at 75% and 90% RH values (Figure 5b). On the contrary, swelling of the crystalline PVA domains for PVA-HAhec nanocomposite film was hampered even at 90% RH (Figure 5c). The significantly reduced swelling sensitivity of both HAhec and crystalline PVA domains will contribute to the greatly reduced water sensitivity of the PVA-HAhec coatings. This might be due to potential hydrogen bonding between modifier and crystalline PVA domains attached to the filler surface.



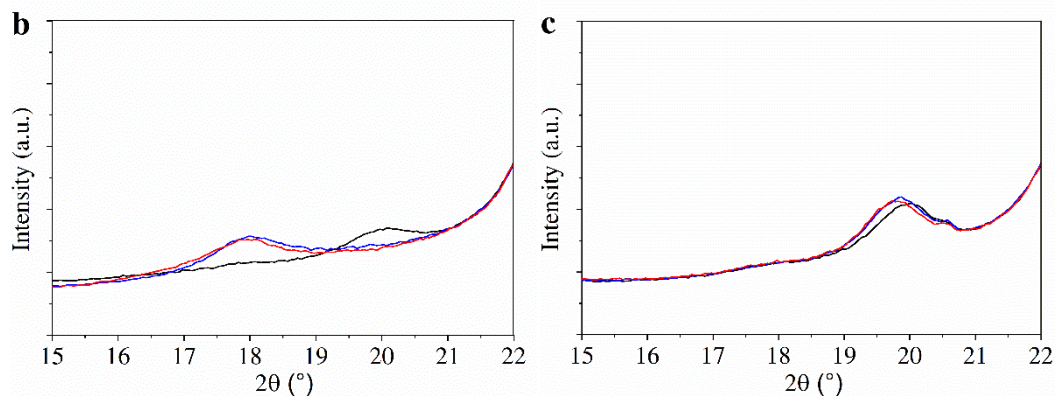


**Figure 5.** Diffractograms of PVA (a) PVA-NaHec (b) and PVA-HAhec (c) films at 0% (green), 50% (black), 75% (blue), and 90% (red) RH.

Spray coating produced perfectly textured nanocomposite films. The mean derivation angle of the orientation distribution of the stacks was  $1.45^\circ$ , according to the SAXS measurements (Figure 6a). The perfect parallel orientation of the large aspect ratio nanoplatelets of PVA-HAhec was confirmed from a transmission electron microscopy (TEM) cross-sectional image (Figure 6b). This high quality of parallel orientation of clay platelets is the key for an appreciable tortuous pathway, and will, therefore, contribute significantly to the superior barrier properties.

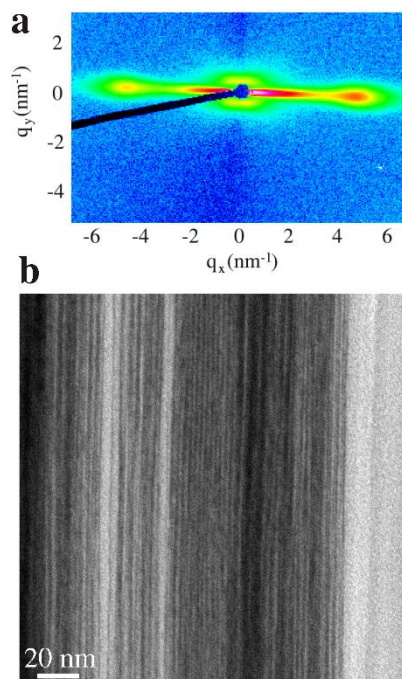


**Figure 6.** SAXS (a) and TEM (b) images of PVA-HAhec nanocomposite film.

Thus, waterborne polymer nanocomposites possess superior oxygen and water vapor barrier properties at high RH. Moreover, due to potential hydrogen bonds between modifier and filler and shifting of the polymer matrix swelling to a higher RH region, performance of PVA-HAhec nanocomposite film is surprisingly good. Even at 23 °C and 90% RH, unexpectedly low OTR and WVTR ( $0.11 \text{ cm}^3 \text{ m}^{-2} \text{ day}^{-1} \text{ bar}^{-1}$  and  $0.18 \text{ g m}^{-2} \text{ day}^{-1}$ , respectively, for a coating of  $0.42 \text{ }\mu\text{m}$ ) values were observed.

### **Details and further discussion**

Appendix 1: Can high oxygen and water vapor barrier nanocomposite coatings be obtained with a waterborne formulation?

### 3.3. Oxygen and water vapor barrier of PEIE-PAA-clay nanocomposites

PEI-PAA nanocomposites are usually produced using a layer-by-layer technique, which separates oppositely charged polyelectrolytes during deposition. Recently, Grunlan *et al.* presented a stable coacervate one-component PEI-PAA suspension, obtained by increasing the ionic strength [53]. In our work, stable PEIE-PAA suspension was obtained by pre-neutralization of PAA with ammonia solution and subsequent addition of PEIE.

Mixing of the PEIE-PAA system with HAHeC led to perfectly homogeneous suspension, as confirmed from SAXS measurements (Figure 7). Singular silicate layers were separated by a uniform distance of 27.5 nm, as indicated by a 001 series visible up to the tenth order.

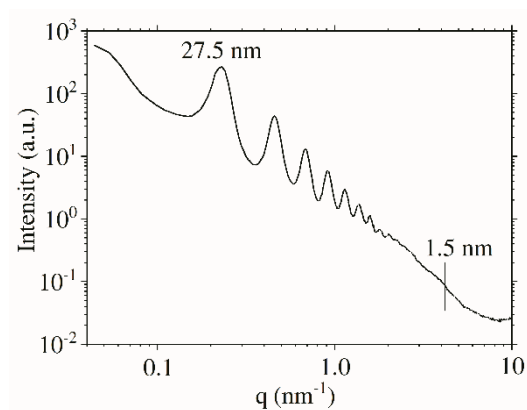


**Figure 7.** SAXS pattern of PEIE-PAA-HAHeC gel.

Therefore, highly homogeneous one-component polymer-filler suspension can be applied via doctor blading or spray coating. Novel approach in spray coating was implemented using a specially created automatic spray coating system, equipped with a SATA 4000 LAB HVLP 1.0 mm spray gun (Figure 8).

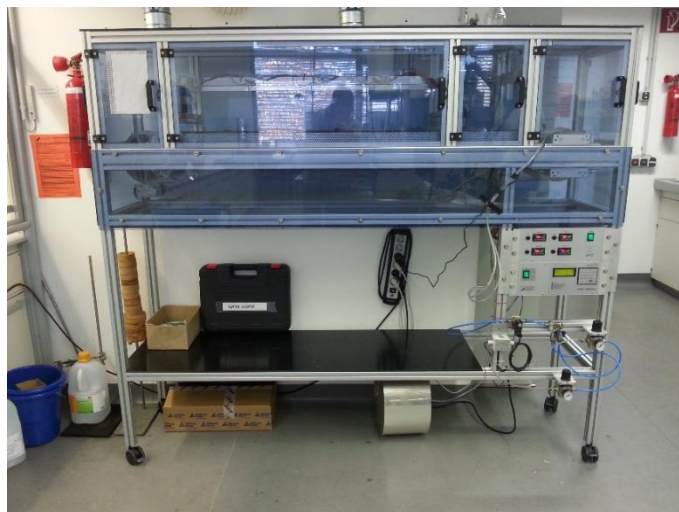


**Figure 8.** Automatic spray coating system.

A fixed airbrush sprayed the suspension ( $4 \text{ bar}$ ,  $1 \text{ mL s}^{-1}$ ) on the PET substrate attached to the conveyor belt, moving at a certain speed (Figure 9a). The speed of the conveyor belt/substrate was set to  $1 \text{ m s}^{-1}$ , and the distance between the airbrush and the substrate was fixed at  $24 \text{ cm}$ . The thickness of the suspension layer applied in one spraying step was  $\approx 2 \text{ }\mu\text{m}$ , corresponding to  $\approx 20 \text{ nm}$  of dry film thickness. For drying the suspension layer, the sample was stopped under infrared lamps until the solvent evaporated completely (Figure 9b). The drying time was  $180 \text{ s}$ , and the power of the lamps was adjusted to obtain a substrate surface temperature of  $50 \text{ }^\circ\text{C}$ . Films were prepared by repeating 1000 spraying/drying cycles.

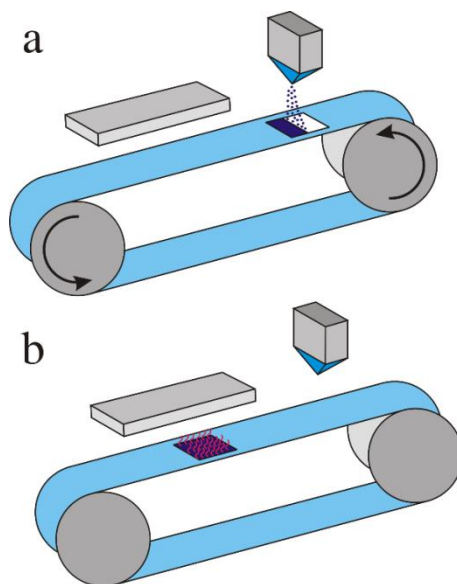


**Figure 9.** Schematic representation of the spray coating process: (a) spraying and (b) drying.

The obtained nanocomposite films possessed 1D crystalline nature, as confirmed from PXRD measurements (Figure 10). The quality of the 1D crystalline order is indicated by the coefficient of variation (cv) and the intensity and maximum visible order of the 00l series. Doctor-bladed films showed a significantly higher cv, and the intensities of the 00l reflections decreased much faster with an increasing scattering angle. Thereby, spray coating yielded a better 1D crystallinity, as compared to doctor blading.

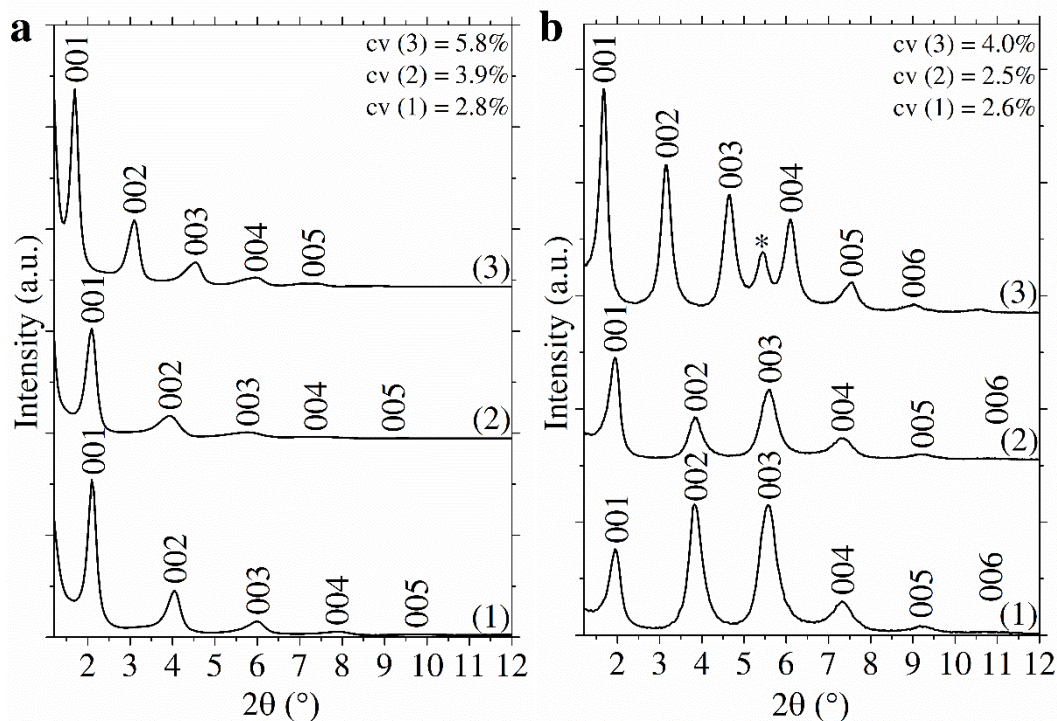


**Figure 10.** PXRD patterns of nanocomposite films equilibrated at different temperature/RH conditions. (a) Doctor-bladed nanocomposite film. (b) Spray-coated nanocomposite film recorded at 23 °C/0% RH (1), 23 °C/50% RH (2), and 38 °C/90% RH (3), respectively.

No significant swelling with water vapor was observed upon increasing the RH from 0% to 50%, as indicated by no significant changes in interlayer distances. This finding is quite surprisingly for a waterborne nanocomposite. Significant swelling, however, set in at 38 °C/90% RH, where the interlayer distance increased by about 15%, corresponding to a significant volume of water being dissolved in the nanocomposite films.

For a homogeneous, single phase 1D crystalline (smectic) nanocomposite film with utterly delaminated equidistantly distributed HAhec in the polymer, an interlayer distance of 10 nm (1

nm platelet thickness + 9 nm organic volume) was expected. Both doctor-bladed and spray-coated nanocomposite films showed significantly lower interlayer distances (4.21 and 4.55 nm, respectively). A thermodynamically favored partial phase separation occurs upon drying the nanocomposite films that is visible in the TEM images (Figure 11).

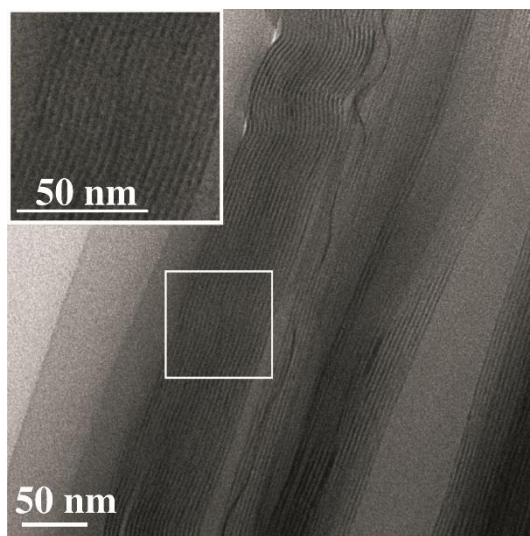


**Figure 11.** TEM image of free-standing spray-coated nanocomposite film.

Spray-coated nanocomposite films have better oxygen and water vapor barrier properties, as compared to doctor-bladed nanocomposite films at both measured conditions. Most remarkably, OTR and WVTR at 23 °C and 50% RH of spray-coated nanocomposite films are  $<0.0005 \text{ cm}^3 \text{ m}^{-2} \text{ day}^{-1} \text{ bar}^{-1}$  and  $0.0007 \text{ g m}^{-2} \text{ day}^{-1}$  respectively, satisfying the tough requirements for encapsulation of organic photovoltaics. The WVP of the spray coated film did not increase at 38 °C and 90% RH, despite significant swelling of the smectic polymer-clay domains observed from PXRD. As the processing technique has a significant impact on the quality of the 1D crystallinity of the smectic polymer-clay domains, the order in the nanocomposite film might be a so-far overlooked key factor for improving the barrier performance of spray-coated film, as compared to that of doctor-bladed nanocomposite film.

### **Details and further discussion**

Appendix 2: Large scale self-assembly of smectic nanocomposite films by doctor blading versus spray coating: impact of crystal quality on barrier properties.

### 3.4. Helium barrier of PVA-clay nanocomposites

New wind energy concepts, wherein helium acts as a lifting agent, requires new materials with excellent multi-permeate barriers against helium, oxygen, and water vapor. The effects of PVA molar mass and NaHec loading on helium barrier properties were investigated. Triple phase system (PVA, water, and NaHec) was homogeneously dispersed, according to the SAXS measurements (Figure 12).

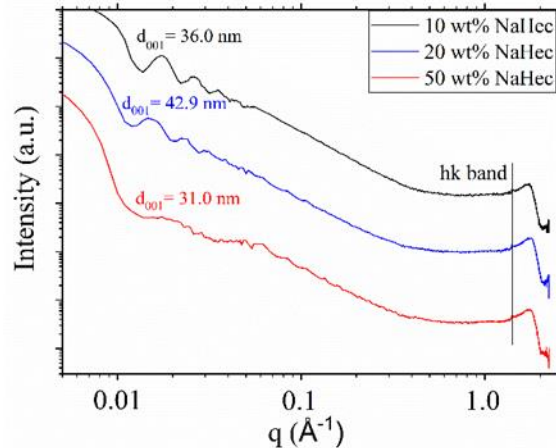


**Figure 12.** SAXS measurements of PVA-NaHec gels at different filler loadings.

These highly delaminated suspensions were doctor-bladed onto the PET substrate. According to the PXRD measurements (Figure 13), polymer nanocomposite films showed reflections at  $12.4$   $\text{\AA}$ , corresponding to NaHec aggregates that appear during drying of films. A characteristic broad peak at about  $20^\circ$  corresponds to PVA crystalline domains that are regarded as impermeable, contributing to better barrier performance.

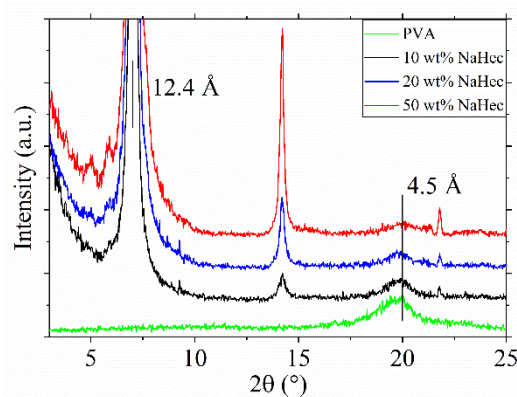


**Figure 13.** PXRD measurements of the PVA-NaHec nanocomposites with different filler loadings.

Helium permeability of nanocomposites emphasized the impact of PVA molar mass on barrier properties (Table 2). Increasing molar mass resulted in increased permeability of the composite, a consequence of increasing number of entanglements. Therefore, the free volume increased and the barrier properties deteriorated. Incorporation of 50 wt% filler, the permeability of PVA-NaHec nanocomposite decreased by a factor of about 1000, as compared to that of unfilled PVA coating.

**Table 2.** Helium permeability values of the PVA-NaHec nanocomposite films at 2-10% RH.

Sample	NaHec (wt%)	Coating thickness ( $\mu\text{m}$ )	Permeability $\text{cm}^3 \mu\text{m m}^{-2} \text{day}^{-1} \text{atm}^{-1}$
PET	0	0.0	62640
PVA 20-98	0	1.4	19860
PVA 20-98	50	1.0	44
PVA 18-88	50	1.0	37
PVA 10-98	50	1.0	18.5

One of the disadvantages of using PVA as a matrix is the plasticization effect at a relative humidity over 35%. We have already shown [54] that a decreasing plasticization effect for oxygen and water vapor, and therefore, we also expect it with helium as a test gas (Table 3).

**Table 3.** Helium transmission rates of the nanocomposite systems at 0% and 75% RH.

Sample	HeTR	Permeability
	$\text{cm}^3 \text{m}^{-2} \text{day}^{-1} \text{atm}^{-1}$ <i>0% RH / 75% RH</i>	$\text{cm}^3 \mu\text{m m}^{-2} \text{day}^{-1} \text{atm}^{-1}$ <i>0% RH / 75% RH</i>
PET + PVA + 10 wt%	<i>0.8</i>	<i>31.3</i>
NaHec	<i>7.1</i>	<i>266.3</i>
PET + PVA + 50 wt%	<i>0.8</i>	<i>30.3</i>
NaHec	<i>1.7</i>	<i>63.3</i>

The helium transmission rates (HeTR) at a relative humidity of about 75% increased because of the polymer matrix swelling, as expected. Nevertheless, this plasticization effect is much lower

than that observed in the neat polymer matrix, because in that case, the permeability at about 75% RH would have been in the region of a neat PET substrate with a value of about  $60000 \text{ cm}^3 \mu\text{m m}^{-2} \text{ day}^{-1} \text{ atm}^{-1}$ . Moreover, the increase in the transmission rate of the sample with 50 wt% filler content was lesser than the increase in the sample with 10 wt%.

### **Details and further discussion**

Appendix 3: An excellent helium barrier for lighter than air applications.

---

## 4. Bibliography

- [1] E.L. Cussler, S.E. Hughes, W.J. Ward, R. Aris, Barrier membranes, *J. Membr. Sci.* 38 (1988) 161–174.
- [2] G.H. Fredrickson, J. Bicerano, Barrier properties of oriented disk composites, *J. Chem. Phys.* 110 (1999) 2181-2188.
- [3] T. Sabu, J. Kuruvilla, S.K. Malhotra, G. Koichi, M.S. Sreekala, Polymer Composites, Volume 2, Nanocomposites, Wiley-VCH, 2013.
- [4] Y.Q. Li, T. Yu, T.Y. Yang, L.X. Zheng, K. Liao, Bio-Inspired nacre-like composite films based on graphene with superior mechanical, electrical, and biocompatible properties, *Adv. Mater.* 24 (2012) 3426–3431.
- [5] P. Podsiadlo, M. Michel, J. Lee, E. Verploegen, N. Wong, S. Kam, V. Ball, J. Lee, Y. Qi, A.J. Hart, P.T. Hammond, N.A. Kotov, Exponential Growth of LBL Films with Incorporated Inorganic Sheets, *Nano Lett.* 8 (2008) 1762-1770.
- [6] J. Zhu, A.B. Morgan, F.J. Lamelas, C.A. Wilkie, Fire Properties of Polystyrene - Clay Nanocomposites, *Chem. Mater.* 13 (2001) 3774–3780.
- [7] A. Edenharter, P. Feicht, B. Diar-Bakerly, G. Beyer, J. Breu, Superior flame retardant by combining high aspect ratio layered double hydroxide and graphene oxide, *Polymer.* 91 (2016) 41–49.
- [8] D.A. Kunz, J. Schmid, P. Feicht, J. Erath, A. Fery, J. Breu, Clay-based nanocomposite coating for flexible optoelectronics applying commercial polymers, *ACS Nano.* 7 (2013) 4275–4280.
- [9] Y.-H. Yang, M. Haile, Y.T. Park, F.A. Malek, J.C. Grunlan, Super Gas Barrier of All-Polymer Multilayer Thin Films, *Macromolecules.* 44 (2011) 1450–1459.
- [10] B.L. Smith, T.E. Schäffer, M. Viani, J.B. Thompson, N.A. Frederick, J. Kindt, A. Belcher, G.D. Stucky, D.E. Morse and P.K. Hansma, Molecular mechanistic origin of the toughness of natural adhesives, fibres and composites, *Nature.* 399 (1999) 761–763.

- 
- [11] M.T. Scherner, C. Konrad, A. Bizzarri, M. Suppan, M. Cajlakovic, V. Ribitsch, F. Stelzer, Opto-chemical method for ultra-low oxygen transmission rate measurement, *Proc. IEEE Sensors*. (2009) 1660–1665.
- [12] L.J. van Rooyen, J. Karger-Kocsis, O.C. Vorster, L.D. Kock, Helium gas permeability reduction of epoxy composite coatings by incorporation of glass flakes, *J. Membr. Sci.* 430 (2013) 203–210.
- [13] R.J.M. Penedo, T.C.D. Pardal, P.M.M.S. Silva, N.M. Fernandes, T.R.C. Fernandes, High Altitude Wind Energy from a Hybrid Lighter-than-Air Platform Using the Magnus Effect, Airborne Wind Energy. Chapter 29 (2013) 491–500.
- [14] T.V. Naylor, Chapter 20 – Permeation Properties. Comprehensive Polymer Science and Supplements, Volume 2 (1989) 643-648, Pergamon Press.
- [15] A. Fick, Über Diffusion, *Annalen der Physik*. 170 (1855) 59-86.
- [16] W. Henry, Experiments on the Quantity of Gases Absorbed by Water, at Different Temperatures, and under Different Pressures, *Philosophical Transactions of the Royal Society of London*. 93 (1803) 29-42+274-276.
- [17] M.H. Klopffer, B. Flaconnèche, Transport Properties of Gases in Polymers: Bibliographic Review, *Oil gas sci. technol.* 56 (2001) 223–244.
- [18] S. Takahashi, H.A. Goldberg, C.A. Feeney, D.P. Karim, M. Farrell, K. O’Leary, D.R. Paul, Gas barrier properties of butyl rubber/vermiculite nanocomposite coatings, *Polymer*. 47 (2006) 3083–3093.
- [19] L.E. Nielsen, Models for the Permeability of Filled Polymer Systems, *J. Macromol. Sci. A*. 1 (1967) 929-942.
- [20] N.K. Lape, E.E. Nuxoll, E.L. Cussler, Polydisperse flakes in barrier films, *J. Membr. Sci.* 236 (2004) 29–37.
- [21] J.P. DeRocher, B.T. Gettelfinger, J. Wang, E.E. Nuxoll, E.L. Cussler, Barrier membranes with different sizes of aligned flakes, *J. Membr. Sci.* 254 (2005) 21–30.
- [22] G.D. Moggridge, N.K. Lape, C. Yang, E.L. Cussler, Barrier films using flakes and reactive additives, *Progr. Org. Coat.* 46 (2003) 231–240.

- 
- [23] A.A. Gusev, H.R. Lusti, Rational Design of Nanocomposites for Barrier Applications, *Adv. Mater.* 13 (2001) 1641–1643.
- [24] G. W. Ehrenstein, Polymeric materials structure, properties, applications. Carl Hanser Verlag GmbH & Co. KG, 2001.
- [25] M. Drieskens, R. Peeters, J. Mullens, D. Franco, P.J. Lemstra, D.G. Hristova-Bogaerds, Structure versus properties relationship of poly(lactic acid). I. Effect of crystallinity on barrier properties, *J. Polym. Sci. Part B Polym. Phys.* 47 (2009) 2247–2258.
- [26] Y.S. Hu, R.Y.F. Liu, M. Rogunova, D. Schiraldi, S. Nazarenko, A. Hiltner, E. Baer, Oxygen-barrier properties of cold-crystallized and melt-crystallized poly(ethylene terephthalate-co-4,4'-biphenylene), *J. Polym. Sci. Part B: Polym. Phys.* 40 (2002) 2489–2503.
- [27] J. Lin, S. Shenogin, S. Nazarenko, Oxygen solubility and specific volume of rigid amorphous fraction in semicrystalline poly(ethylene terephthalate), *Polymer.* 43 (2002) 4733–4743.
- [28] H.M. Kim, J.K. Lee, H.S. Lee, Transparent and high gas barrier films based on poly(vinyl alcohol)/graphene oxide composites, *Thin Solid Films.* 519 (2011) 7766–7771.
- [29] J. Ma, Y. Li, X. Yin, Y. Xu, J. Yue, J. Bao, T. Zhou, Poly(vinyl alcohol)/graphene oxide nanocomposites prepared by in situ polymerization with enhanced mechanical properties and water vapor barrier properties, *RSC Adv.* 6 (2016) 49448–49458.
- [30] H.D. Huang, P.G. Ren, J. Chen, W.Q. Zhang, X. Ji, Z.M. Li, High barrier graphene oxide nanosheet/poly(vinyl alcohol) nanocomposite films, *J. Membr. Sci.* 409–410 (2012) 156–163.
- [31] J.-T. Chen, Y.-J. Fu, Q.-F. An, S.-C. Lo, Y.-Z. Zhong, C.-C. Hu, K.-R. Lee, J.-Y. Lai, Enhancing polymer/graphene oxide gas barrier film properties by introducing new crystals, *Carbon.* 75 (2014) 443–451.
- [32] E. Doblhofer, J. Schmid, M. Rieß, M. Daab, M. Suntinger, C. Habel, H. Bargel, C. Hugenschmidt, S. Rosenfeldt, J. Breu, T. Scheibel, Structural Insights into Water-Based Spider Silk Protein – Nanoclay Composites with Excellent Gas and Water Vapor Barrier Properties, *Appl. Mater. Interfaces.* 8 (2016) 25535–25543.

- 
- [33] H.E. Assender, A.H. Windle, Crystallinity in poly(vinyl alcohol). 1. An X-ray diffraction study of atactic PVOH, *Polymer*. 39 (1998) 4295–4302.
- [34] Y.-H. Yang, L. Bolling, M. Haile, J.C. Grunlan, Improving oxygen barrier and reducing moisture sensitivity of weak polyelectrolyte multilayer thin films with crosslinking, *RSC Adv.* 2 (2012) 12355–12363.
- [35] A. Walther, I. Bjurhager, J.M. Malho, J. Pere, J. Ruokolainen, L.A. Berglund, O. Ikkala, Large-Area, Lightweight and Thick Biomimetic Composites with Superior Material Properties via Fast, Economic, and Green Pathways, *Nano Lett.* 10 (2010) 2742–2748.
- [36] S. Park, K.-S. Lee, G. Bozoklu, W. Cai, S.T. Nguyen, R.S. Ruoff, Graphene Oxide Papers Modified by Divalent Ions—Enhancing Mechanical Properties via Chemical Cross-Linking, *ACS Nano*. 2 (2008) 572-578.
- [37] P. Podsiadlo, A.K. Kaushik, B.S. Shim, A. Agarwal, Z. Tang, A.M. Waas, E.M. Arruda, N.A. Kotov, Can Nature’s Design be Improved Upon? High Strength, Transparent Nacre-Like Nanocomposites with Double Network of Sacrificial Cross Links, *J. Phys. Chem. B*. 112 (2008) 14359–14363.
- [38] E.S. Tsurko, P. Feicht, F. Nehm, K. Ament, S. Rosenfeldt, I. Pietsch, K. Roschmann, H. Kalo, J. Breu, Large Scale Self-Assembly of Smectic Nanocomposite Films by Doctor Blading versus Spray Coating: Impact of Crystal Quality on Barrier Properties, *Macromolecules*. 50 (2017) 4344-4350.
- [39] M. Wong, R. Ishige, K.L. White, P. Li, D. Kim, R. Krishnamoorti, R. Gunther, T. Higuchi, H. Jinnai, A. Takahara, R. Nishimura, H.-J. Sue, Large-scale self-assembled zirconium phosphate smectic layers via a simple spray-coating process, *Nat. Commun.* 5 (2014) 1–12.
- [40] H.B. Hopfenberg, A. Apicella, D.E. Saleeby, Factors affecting water sorption in and solute release from glassy ethylene—vinyl alcohol copolymers, *J. Membr. Sci.* 8 (1981) 273–282.
- [41] J.C. Grunlan, A. Grigorian, C.B. Hamilton, A.R. Mehrabi, Effect of clay concentration on the oxygen permeability and optical properties of a modified poly(vinyl alcohol), *J. Appl. Polym. Sci.* 93 (2004) 1102–1109.

- 
- [42] C.Y. Pan, Q.Q. Liu, X.H. Xu, Z.H. Chen, Measurements of surface crystallinity of PAA and PAANa coatings and its effect on hydrophilicity of coatings, *Trans. Nonferrous Met. Soc. China*. 13 (2003) 988–993.
- [43] R. Bahulekar, N.R. Ayyangar, S. Ponrathnam, Polyethyleneimine in immobilization of biocatalysts, *Enzyme Microb. Technol.* 13 (1991) 858–868.
- [44] B.K.G. Theng, Formation and Properties of Clay-polymer Complexes 4 Elsevier Science, LandcareResearch, Palmerston North, New Zealand, 2012.
- [45] M.F. Brigatti, E. Galan, B.K.G. Theng, Chapter 2, Structures and Mineralogy of Clay Minerals, in Developments in Clay Science Handbook of Clay Science, Volume 1 ed.; Faiza Bergaya, B. K. G., editor; Elsevier: Amsterdam, 2006; pp. 19-86.
- [46] M. Stöter, D.A. Kunz, M. Schmidt, D. Hirsemann, H. Kalo, B. Putz, J. Senker, J. Breu, Nanoplatelets of Sodium Hectorite Showing Aspect Ratios of  $\approx 20\,000$  and Superior Purity, *Langmuir*. 29 (2013) 1280–1285.
- [47] M. Stöter, S. Rosenfeldt, J. Breu, Tunable Exfoliation of Synthetic Clays, *Annu. Rev. Mater. Res.* 45 (2015) 129-151.
- [48] R. Kohli, Hydrogen Bonding Abilities of Hydroxamic Acid and Its Isosteres, Anchor Academic Publishing, Hamburg, 2016.
- [49] N. Türkel, Stability of Metal Chelates of Some Hydroxamic Acid Ligands, *J. Chem. Eng. Data*. 56 (2011) 2337–2342.
- [50] E.N. Zilberman, O.D. Strizhakov, S.V. Svetozarskiy, Synthesis of  $\epsilon$ -aminocaprohydroxamic acid, *J. Gen. Chem. USSR* (Engl. Transl.). 35 (1965) 857–860.
- [51] C. Lü, Z. Cui, Y. Wang, Z. Li, C. Guan, B. Yang, J. Shen, Preparation and characterization of ZnS–polymer nanocomposite films with high refractive index, *J. Mater. Chem.* 13 (2003) 2189–2195.
- [52] P. Tzeng, C.R. Maupin, J.C. Grunlan, Influence of polymer interdiffusion and clay concentration on gas barrier of polyelectrolyte/clay nanobrick wall quadlayer assemblies, *J. Membr. Sci.* 452 (2014) 46–53.

- [53] M. Haile, O. Sarwar, R. Henderson, R. Smith, J.C. Grunlan, Polyelectrolyte Coacervates Deposited as High Gas Barrier Thin Films, *Macromol. Rapid Commun.* 38 (2016) 1600594.
- [54] E.S. Tsurko, P. Feicht, C. Habel, T. Schilling, M. Daab, S. Rosenfeldt, J. Breu, Can high oxygen and water vapor barrier nanocomposite coatings be obtained with a waterborne formulation?, *J. Membr. Sci.* 540 (2017) 212–218.

## 5. Individual contribution to joint publications

The publications/manuscripts, which are presented in the appendix, were obtained in cooperation with other co-workers at different departments. My contribution to each publication are specified below and asterisk denotes the corresponding author.

### 5.1. Appendix 1

This work is published in Journal of Membrane Science under the title «**Can high oxygen and water vapor barrier nanocomposite coatings be obtained with a waterborne formulation?**». By Evgeny S. Tsurko, Patrick Feicht, Christoph Habel, Theresa Schilling, Matthias Daab, Sabine Rosenfeldt, Josef Breu\*.

- I created the automatic spray coating system; performed synthesis of modifier, modification of NaHec, creation of barrier nanocomposites and their characterization in addition to writing the manuscript.
- Patrick Feicht and Christoph Habel helped with WVTR measurements and also contributed to the scientific discussion.
- Matthias Daab helped with XRD measurements in temperature-humidity chamber.
- Dr. Sabine Rosenfeldt performed the SAXS measurements.
- Prof. Josef Breu contributed to proofreading the manuscript and the scientific discussion.

My contribution to this work was ca. 80%.

### 5.2. Appendix 2

This work is published in Macromolecules under the title «**Large Scale Self-Assembly of Smectic Nanocomposite Films by Doctor Blading versus Spray Coating: Impact of Crystal Quality on Barrier Properties**». By Evgeny S. Tsurko, Patrick Feicht, Frederik Nehm, Kevin Ament, Sabine Rosenfeldt, Ines Pietsch, Konrad Roschmann Hussein Kalo, and Josef Breu\*.

- I created the automatic spray coating system; performed synthesis of modifier, modification of NaHec, creation of barrier nanocomposites and their characterization in addition to writing the manuscript.
- Patrick Feicht contributed to the scientific discussion and writing manuscript.
- Frederik Nehm performed WVTR measurements of spray-coated nanocomposites.
- Kevin Ament performed the TEM measurements.
- Dr. Sabine Rosenfeldt performed the SAXS measurements.

- Dr. Ines Pietsch, Dr. Konrad Roschmann and Dr. Hussein Kalo contributed to creation of one-component PEIE-PAA suspension.
- Prof. Josef Breu contributed to proofreading the manuscript and the scientific discussion.

My contribution to this work was ca. 70%.

### 5.3. Appendix 3

This work will be submitted in Journal of Membrane Science under the title «**An excellent helium barrier for lighter than air applications**». By Christoph Habel, Evgeny S. Tsurko, Patrick Feicht, Matthias Daab, Sabine Rosenfeldt, Josef Breu\*.

- I performed SAXS and PXRD analysis of the nanocomposite films in addition to writing the manuscript.
- Christoph Habel created nanocomposite films, measured helium barriers in addition to writing the manuscript.
- Patrick Feicht contributed to the scientific discussion.
- Matthias Daab and Sabine Rosenfeldt helped with SAXS measurements.
- Prof. Josef Breu contributed to proofreading the manuscript and the scientific discussion.

My contribution to this work was ca. 50%.

## 6. Results

### 6.1. Appendix 1

#### **Can high oxygen and water vapor barrier nanocomposite coatings be obtained with a waterborne formulation?**

Evgeny S. Tsurko<sup>a,b</sup>, Patrick Feicht<sup>a,b</sup>, Christoph Habel<sup>a,b</sup>, Theresa Schilling<sup>a,b</sup>, Matthias Daab<sup>a,b</sup>,  
Sabine Rosenfeldt<sup>a,c</sup>, Josef Breu<sup>a,b,\*</sup>

<sup>a</sup> Bavarian Polymer Institute, Universitätsstraße 30, Bayreuth 95447, Germany

<sup>b</sup> Department of Inorganic Chemistry I, University of Bayreuth, Universitätsstraße 30, Bayreuth 95447, Germany

<sup>c</sup> Department of Physical Chemistry I, University of Bayreuth, Universitätsstraße 30, Bayreuth 95447, Germany

\* Corresponding author:

Prof. Dr. Josef Breu

Universitätsstr. 30

95440 Bayreuth

Germany

\* E-mail address: [Josef.Breu@uni-bayreuth.de](mailto:Josef.Breu@uni-bayreuth.de)

Journal of Membrane Science, DOI: [10.1016/j.memsci.2017.06.051](https://doi.org/10.1016/j.memsci.2017.06.051).



Contents lists available at ScienceDirect

Journal of Membrane Science

journal homepage: [www.elsevier.com/locate/memsci](http://www.elsevier.com/locate/memsci)

## Can high oxygen and water vapor barrier nanocomposite coatings be obtained with a waterborne formulation?



Evgeny S. Tsurko<sup>a,b</sup>, Patrick Feicht<sup>a,b</sup>, Christoph Habel<sup>a,b</sup>, Theresa Schilling<sup>a,b</sup>, Matthias Daab<sup>a,b</sup>, Sabine Rosenfeldt<sup>a,c</sup>, Josef Breu<sup>a,b,\*</sup>

<sup>a</sup> Bavarian Polymer Institute, Universitätsstraße 30, Bayreuth 95447, Germany

<sup>b</sup> Department of Inorganic Chemistry I, University of Bayreuth, Universitätsstraße 30, Bayreuth 95447, Germany

<sup>c</sup> Department of Physical Chemistry I, University of Bayreuth, Universitätsstraße 30, Bayreuth 95447, Germany

### ARTICLE INFO

#### Keywords:

Layered silicates  
Polymer nanocomposites  
Hydrogen bonds  
Gas barrier  
Spray coating

### ABSTRACT

Modification of synthetic, high aspect ratio clay with 6-aminocaprohydroxamic acid hydrochloride pushes the interaction between the polyvinyl alcohol (PVA) matrix and the filler to the level where the waterborne nanocomposite becomes rather insensitive to swelling, even at an elevated relative humidity (RH). The modifier can form strong hydrogen bonds with the hydroxyl groups of PVA via the hydroxamic acid functional group. This prevents the swelling of crystalline PVA domains. Perfectly textured nanocomposite films are obtained by spraying polymer-filler suspensions. The combination of the various effects shifts the onset of significant swelling of the nanocomposites to high RH regions. Even at 90% RH, surprisingly low oxygen and water vapor transmission rates ( $0.11 \text{ cm}^3 \text{ m}^{-2} \text{ day}^{-1} \text{ bar}^{-1}$  and  $0.18 \text{ g m}^{-2} \text{ day}^{-1}$ , respectively, for a coating of  $0.42 \mu\text{m}$ ) are observed that may render PVA-based, waterborne coatings interesting for food packaging applications.

### 1. Introduction

Roughly one-third of food produced for human consumption, amounting to around 1.3 billion tons per year, is wasted at some point in the supply chain, and 95–115 kg of food per capita per year is wasted by consumers in developed countries [1]. Roughly one-third of these food products have brief periods from purchase to expiration or best before date, for instance, meat, fish, milk and milk-based products. More than 13% of food packages are thrown into the bin without ever being opened [2]. It is, therefore, reasonable to conclude that extending the date of expiry will reduce the amount of food waste and, thereby, the resources which go into their production [3]. The primary factor behind determining the expiration date is the permeability of the packaging. Industry prefers technically benign, water-based, chlorine- and metal-free materials with improved flex-crack resistance to meet the challenge of creating sustainable flexible packaging. Most, if not all packaged food requires restricting permeability for both hydrophobic ( $\text{O}_2$ ,  $\text{N}_2$ ) and hydrophilic (water vapor,  $\text{CO}_2$ ) permeates. Such multi-permeate barriers can only be realized by less favorable laminated structures of polar and nonpolar polymers or by reducing diffusion rates in a nonselective manner.

The gas barrier of polymer films can be improved by decreasing the solubility of permeates or by increasing the density and, consequently,

reducing the free volume, for instance, by improving hydrogen bonding or enlarging crystalline domains. Alternatively, the diffusion path may be elongated by the incorporation of platy, impermeable fillers, an approach which has long been established as a tortuous path [4]. The latter introduces a large interphase area and will, of course, also modify the structure and/or crystallinity of the polymer matrix. Layered silicates are most commonly used as nanofillers to improve the barrier of food packaging. Fluorohectorite, for example, belongs to the 2:1 smectite family and shows a sandwich-like structure comprising two tetrahedral and one octahedral layers with a composition such as  $[\text{Na}_{0.5}]^{\text{inter}}[\text{Mg}_{2.5}\text{Li}_{0.5}]^{\text{oct}}[\text{Si}_4]^{\text{tet}}\text{O}_{10}\text{F}_2$  (NaHec) [5] for the synthetic fluorohectorite used here. Melt-synthesized clay nanosheets, moreover, come in high aspect ratios ( $> 20000$ ), qualifying synthetic fluorohectorite as a superb filler in nanocomposite materials. Additionally, this synthetic clay can be thoroughly delaminated into single layers simply by osmotic swelling [6].

Polyvinyl alcohol (PVA) is a well-known, mass-produced, cheap, biodegradable, water-soluble polymer that has a great oxygen barrier at low relative humidity (RH). On the one hand, hydrogen bonding of hydroxyl groups minimizes free volume; on the other hand, the polarity limits the solubility of nonpolar gases, such as  $\text{O}_2$  in PVA. Moreover, non-swollen crystalline domains of the semi-crystalline matrix are regarded as impermeable. The PVA films, however, show high solubility,

\* Corresponding author at: Bavarian Polymer Institute, Universitätsstraße 30, Bayreuth 95447, Germany.  
E-mail address: [Josef.Breu@uni-bayreuth.de](mailto:Josef.Breu@uni-bayreuth.de) (J. Breu).

<http://dx.doi.org/10.1016/j.memsci.2017.06.051>

Received 9 May 2017; Received in revised form 19 June 2017; Accepted 21 June 2017

Available online 21 June 2017

0376-7388/ © 2017 Published by Elsevier B.V.

hygroscopicity and swelling in water and, consequently, their water vapor permeability (WVP) is high. Moreover, water uptake by swelling at an elevated RH (> 35%) leads to a drastic increase of permeability not only of water vapor, but also of oxygen [7,8]. The oxygen permeability (OP) of a typical PVA film, for instance, increases by over 500% when going from 0% to 55% RH to an absolute oxygen transmission rate (OTR) for a 6- $\mu\text{m}$  thick film of  $3.1 \text{ cm}^3 \text{ m}^{-2} \text{ day}^{-1} \text{ bar}^{-1}$  [8]. This pronounced sensitivity to water vapor renders PVA unsuitable for flexible food packaging. Grunlan et al. [8] have shown that the critical RH, where swelling followed by a significant loss of the oxygen barrier sets in, can be shifted to a higher RH by the incorporation of Nantmorillonite as a platy impermeable filler. We have recently reported [9] that a waterborne spider silk protein-nanoclay composite is hydrophobized upon film formation to the degree where it not only becomes insoluble in water, but also shows only limited swelling at an elevated RH. In comparison to the uncoated substrate, the water vapor transmission rate (WVTR) of the bio-nanocomposite at 50% RH decreased by 96% to  $0.18 \pm 0.05 \text{ g m}^{-2} \text{ day}^{-1}$ . This would suggest that layered silicates not only reduce permeability in a nonselective manner via the tortuous path mechanism, but are also capable of hydrophobizing water-soluble polymer matrices to the point where waterborne formulations might result in barrier films that are not only rendered insoluble in water, but might also be an excellent oxygen barrier and possibly even a water vapor barrier. This would ideally render water-soluble polymers, which may be processed easily and in an environmentally friendly way, suitable for flexible food packaging.

Here we show that applying large aspect ratio clay that has been modified with 6-aminocaprohydroxamic acid hydrochloride, which can form hydrogen bonds with PVA, hampers the swelling of PVA nanocomposites to the degree where superior barriers for both water vapor and oxygen are observed even at 90% RH. This is surprising for such a hydrophilic, waterborne polymer system and might bring PVA back into the game for food packaging.

## 2. Experimental

### 2.1. Materials

The  $[\text{Na}_{0.5}]^{\text{inter}}[\text{Mg}_{2.5}\text{Li}_{0.5}]^{\text{oct}}[\text{Si}_4]^{\text{tet}}\text{O}_{10}\text{F}_2$  employed was synthesized via melt synthesis according to an established procedure in literature [6,10–12]. The material featured a cation exchange capacity (CEC) of  $1.27 \text{ mmol g}^{-1}$  and a high aspect ratio (> 20000) [6]. The NaHec was ion-exchanged with 6-aminocaprohydroxamic acid hydrochloride. A typical synthesis procedure is described in literature [13]. Briefly, 164 g (1 mol) of hydroxylamine sulfate (Sigma Aldrich) was added to 226 g (2 mol) of molten  $\epsilon$ -caprolactam (Sigma Aldrich). The mixture was stirred and heated for 5 h at  $100^\circ\text{C}$ . Then, 200 mL of methanol (VWR International, France) was added and heating was continued for another 5 h. Thereafter, 500 mL methanol was added to the hot reagent mixture and the unreacted hydroxylamine sulfate was filtrated. After methanol evaporation, unreacted caprolactam was removed by extraction with boiling trichloroethylene (Sigma Aldrich, four times 500 mL each). The product was then dissolved in methanol (100 mL) and gaseous ammonia (Rießner-Gase GmbH, Germany) was passed through the solution to completely precipitate the sulfate, which was then filtered off. Crystallization of 6-aminocaprohydroxamic acid was triggered by seeding and cooling the solution. It was purified by recrystallization in methanol ( $^1\text{H}$  (300 MHz,  $\text{D}_2\text{O}$ )  $\delta$  ppm 1.38 (s, 2H), 1.5–1.8 (m, 4H), 2.13 (t, 2H), 2.99 (t, 2H)). The PVA (Merck, Germany) with a molecular weight of 145000 and degree of hydrolysis  $\geq 98\%$  was used. An amount of 5 g of PVA was dissolved in 95 g of Millipore water by heating at  $90^\circ\text{C}$  for 3 h to obtain a 5 wt% solution. A corona-treated polyethylene terephthalate (PET) ( $36 \mu\text{m}$ ) film was used as a substrate (Bleher KG, Germany).

### 2.2. Nanocomposite film fabrication

#### 2.2.1. Preparation of suspensions

**2.2.1.1. PVA films.** An amount of 5 g of a PVA stock solution (5 wt%) was diluted with 95 g of Millipore water to obtain a 0.25 wt% solution for spraying PVA coatings.

**2.2.1.2. PVA-NaHec films.** The NaHec (0.5 g) was delaminated by immersing it into Millipore water (100 g, 0.5 wt%) and this was mixed with 10 g of the PVA stock solution (5 wt%). The mixture was then diluted with 290 g of Millipore water to obtain a suspension with a total solid content of 0.25 wt% for spraying. The PVA:NaHec ratio of this suspension was 1, yielding dry coatings with 50 wt% NaHec, corresponding to 34 vol% NaHec.

**2.2.1.3. PVA-HA Hec films.** Crystalline 6-aminocaprohydroxamic acid (HA) was added to a NaHec suspension, made as described above, in 1.5-fold excess of the CEC and the pH was adjusted with 1 M HCl (Gruessing GmbH, Germany) to  $\text{pH} = 8$  to protonate the modifier. The suspension was then mixed thoroughly in an overhead shaker overnight. Thereafter, the HA Hec suspension was centrifuged, washed with Millipore water and the procedure was repeated once. Completeness of ion exchange was checked by energy dispersive X-ray analysis. Moreover, weight loss, observed by thermogravimetric analysis (TGA), corresponds to the organic content expected based on the CEC (Fig. S1). The solid content of the suspension was determined by drying 10 mL. The HA content of this HA Hec was determined by TGA to be 16 wt%. The suspension was then diluted with Millipore water to obtain silicate content of 0.5 wt%. An amount of 119 g of this suspension was mixed with 8.1 g of the PVA stock solution (5 wt%). The mixture was then diluted with 273 g of Millipore water to obtain a suspension with a total solid content of 0.25 wt% for spraying. The (PVA + HA): Hec ratio of this suspension was 1, yielding dry coatings with 50 wt% of neat silicate filler (50 wt% of Hec, 8 wt% of HA and 42 wt% of PVA), corresponding to 34 vol% NaHec.

#### 2.2.2. Spray coating

Barrier films were prepared by a fully automated spray coating system (Fig. 1) equipped with a SATA 4000 LAB HVLP 1.0 mm spray gun (SATA GmbH & Co. KG, Germany). A fixed airbrush (Fig. 1a) sprayed the suspension (4 bars,  $1 \text{ mL s}^{-1}$ ) onto the PET substrate attached to the conveyor belt, which moved at a constant speed. The speed of the conveyor belt/substrate was set to  $1 \text{ m s}^{-1}$  and the distance between the airbrush and substrate was fixed at 24 cm. The thickness of the suspension layer applied in one spraying step was  $\approx 2 \mu\text{m}$ , which corresponds to a dry film thickness of  $\approx 5 \text{ nm}$ . The

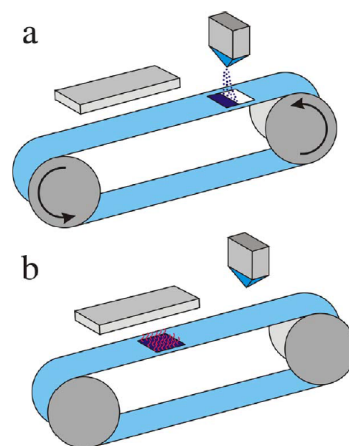


Fig. 1. Schematic representation of the spray coating process: (a) spraying, (b) drying.

sample was stopped under infrared lamps until evaporation of the solvent was complete to dry the suspension layer (Fig. 1b). The drying time was 120 s and the power of the lamps was adjusted to obtain a substrate surface temperature of 50 °C. The spraying/drying cycle was repeated until the barrier film thickness desired was obtained. A sample thickness was chosen to get films with barriers in the range of measurement of the various devices used to measure permeabilities 100–1000 cycles). The quality of the texture of these sprayed films is independent of the number of cycles and, hence, the thickness of the film. Our focus was on producing coatings of different thicknesses with a comparable quality of texture. Only then can the transmissions rates that vary by several orders of magnitude with the variation of RH be adjusted to meet the sensitivity range of the two devices used (Mocon PERMATRAN-W 3/33 and Sempa HiBarSens). The solid content would, of course, have to be increased for a technically benign processing, but this is out of the scope of this manuscript.

### 2.3. Nanocomposites characterization

The OTR were determined on a “super-OX-TRAN” instrument (Mocon OX-TRAN 2/21 M10x) with a lower detection limit of  $0.0005 \text{ cm}^3 \text{ m}^{-2} \text{ day}^{-1} \text{ bar}^{-1}$ . A mixture of 95% nitrogen and 5% hydrogen was used as the carrier gas and pure oxygen (> 99.95%, Linde Sauerstoff 3.5) as the permeate gas. The measurements were conducted at 23 °C and 50%, 75% and 90% RH. Double-cell film testing mode was applied to the total film surface area of  $100 \text{ cm}^2$ . The WVTR were measured applying a Mocon PERMATRAN-W model 3/33 at 23 °C and RH of 50% and 90%. The lower detection limit of the device was  $0.05 \text{ g m}^{-2} \text{ day}^{-1}$ . Water vapor partial pressure at 100% RH is 0.02811 bar at 23 °C. Thereby, water vapor partial pressure at 50% RH is 0.01405 bar, and at 90%, RH = 0.02530 bar. These partial pressures are needed to convert WVTR into WVP. The WVTR were measured on a HiBarSens HBS 2.0 HT (Sempa Systems GmbH, Dresden, Germany), with a lower detection limit of  $1 \times 10^{-6} \text{ g m}^{-2} \text{ day}^{-1}$ , for samples with WVTR below the detection limit of the Mocon PERMATRAN-W. The thicknesses of the films were measured with a Veeco Dektak 150 profilometer with a repeatability < 6 Å. Ten measurements were taken at different spots of the films and averaged. Unfortunately, an ellipsometer is not suitable for measuring film thickness, because the refractive indices of substrate and coating are too similar. X-ray diffraction (XRD) patterns were obtained using nickel-filtered Cu-K $\alpha$  radiation ( $\lambda = 1.54187 \text{ \AA}$ ) on a Bragg-Brentano type diffractometer (XPRT-PRO, PANalytical B.V.) equipped with an X'Celerator Scientific RTMS detector. All patterns were analyzed using Panalytical's Highscore Plus software. Prior to measurement, samples were equilibrated at a fixed RH in an Anton Paar temperature and humidity chamber. All small angle X-ray scattering (SAXS) data were measured using the SAXS system “Double Ganesha AIR” (SAXSLAB, Denmark). The X-ray source of this laboratory-based system is a rotating anode (copper, MicoMax 007HF, Rigaku Corporation, Japan) providing a micro-focused beam. The data are recorded by a position sensitive detector (PILATUS 300 K, Dectris). Different detector positions were used to cover the range of scattering vectors between  $0.004$  and  $1.0 \text{ \AA}^{-1}$ . The measurements of the suspensions were carried out in 1-mm glass capillaries (Hilgenberg, Germany) at room temperature. Transmission electron microscopy (TEM) images were taken on a Zeiss CEM 922 at accelerating voltages of 200 kV. Cross-sections of the nanocomposite coatings were prepared with an Cryo Ion Slicer IB-09060CIS (JEOL GmbH, Germany). The TGA were obtained using a NETZSCH STA 449 C (Erich Netzsch GmbH & Co. Holding KG, Germany) thermogravimetric analyzer. Measurements were performed in aluminum oxide pans under air atmosphere (80/20; N<sub>2</sub>/O<sub>2</sub>) at a heating rate of  $10 \text{ }^\circ\text{C min}^{-1}$  from 30 to 1000 °C. Fourier transform infrared spectroscopy (FTIR) was performed using a Jasco FT/IR-6100 spectrometer.

## 3. Results and discussion

### 3.1. Barrier properties

Here, we compare the OTR (50%, 75% and 90% RH) and WVTR (50% and 90% RH) of unfilled PVA coatings with those filled with synthetic Na-hectorite (PVA-NaHec) and those filled with the same hectorite modified with 6-aminocaprohydroxamic acid hydrochloride (PVA-HAHec). When immersing synthetic NaHec into deionized water, it is gently, but completely delaminated, without mechanical agitation, into single layers [14]. Due to the melt-synthesis, these clay nanosheets, moreover, come in high aspect ratios (> 20000) (Fig. S2). The Na<sup>+</sup> ions can be easily exchanged by 6-ammoniumcaprohydroxamic acid in the delaminated stage. Ion exchange does not trigger any re-stacking, as evidenced by the lack of a reflection at the basal spacing of HAHec stacks ( $\approx 15 \text{ \AA}$ ) in the SAXS curves of aqueous suspensions (5.3 wt%) (Fig. S3).

Ion exchange of Na<sup>+</sup> ions by 6-ammoniumcaprohydroxamic acid, on the one hand, reduces the hydrophilicity of the filler to some extent; nevertheless, aqueous suspensions of HAHec remain stable for months. Moreover, synthesis of 6-aminocaprohydroxamic acid from  $\epsilon$ -caprolactam is straightforward and cheap, allowing for industrial scaling. On the other hand, the modifier is known to form very strong hydrogen bonds [15] via the hydroxamic acid functional group (–R–C(O)–N(H)–OH). A slight shift of the OH band to lower frequencies is observed in the infrared spectrum (Fig. S4), which might indicate hydrogen bonding with PVA hydroxyl groups [16] which, in turn, would be expected to minimize free volume and potentially also to limit swelling. The strongly polarizing clay surface might, however, also improve intramolecular hydrogen bonding of PVA. Therefore, the shift observed is not conclusive for hydrogen bonding between HA and PVA.

The stability of both NaHec and HAHec suspensions is not affected by mixing with PVA solutions, as indicated by the lack of reflections at the basal spacing of NaHec (15.2 Å) or HAHec stacks ( $\approx 15 \text{ \AA}$ ) in the SAXS patterns (Fig. S3). These highly stable delaminated suspensions of 1:1 (in wt%) mixtures of dissolved PVA and NaHec or HAHec were spray-coated onto PET substrates, whereupon thin, flexible and transparent (Fig. S5) barrier films were obtained. Neat, unfilled PVA films were fabricated in the same way for comparison.

All films have been carefully conditioned at the temperature and RH (50%, 75% and 90%) prior to measuring the OTR and WVTR values (Table 1). Equilibration may take more than three months for high barrier films (Fig. S6).

Absolute transmission rates are the relevant figures for applications. Transmission rates are, however, largely influenced by the thickness of the barrier coatings and even the transmission rate of the substrate. The performance of barrier coatings can, therefore, only be compared if transmission rates are converted into permeabilities, OP and WVP, whereby, it is generally assumed that the rate is inversely proportional

**Table 1**  
The OTR and WVTR of nanocomposite films at 23 °C and 50%, 75% and 90% RH.

	RH %	Coating thickness, $\mu\text{m}$			
		PET	PVA	PVA-NaHec	PVA-HAHec
		0	$0.70 \pm 0.06$	$0.45 \pm 0.06$	$0.42 \pm 0.06$
OTR $\text{cm}^3 \text{ m}^{-2} \text{ day}^{-1} \text{ bar}^{-1}$	50	36.7	0.44	$9 \times 10^{-4}$	$6 \times 10^{-4}$
	75	34.3	22.8	0.01	$1.8 \times 10^{-3}$
	90	33.0	30.8	0.24	0.11
WVTR $\text{g m}^{-2} \text{ day}^{-1}$	50	3.6	2.0	0.01*	$6 \times 10^{-4**}$
	90	6.3	3.8	0.95	0.18

\*,\*\* WVTR of these samples were below the detection limit of the MOCON PERMATRAN-W model 3/33 device. Therefore, samples with increased coating thicknesses were prepared (\* =  $5.10 \pm 0.15$ , \*\* =  $5.65 \pm 0.15 \mu\text{m}$ ) and measured on the more sensitive SEMPA device.

to the thickness. This might, however, not be strictly true for the WVP of PVA coatings, as pointed out by Xianda et al. [17]. The range of film thicknesses of the samples we compared in the following is, however, small and the potential error in the conversion of WVTR to WVP will be small. Moreover, the contribution of the substrate is separated, applying a series expansion, as suggested by Roberts et al. [18], which requires that the value for the substrate is reported. Comparison with literature values is difficult because test conditions vary significantly and various units are used. Pressure differences are sometimes not recorded or are simply omitted in the conversions.

The PET substrate already shows an appreciable oxygen barrier. The OTR decreases moderately, while WVTR increases slightly with increasing RH (Table 1). In contrast to PET, the transmission rates of much more polar PVA is very sensitive to humidity. The OTR increases by a factor of 70 and WVTR by a factor of  $\approx 2$  when increasing the RH from 50% to 90%. The comparatively small increase of WVTR is expected, since the WVTR of the PVA-coated PET are mainly determined by the hydrophobic PET substrate that already has a very low permeability.

As expected in tortuous path theory, incorporation of the large aspect ratio NaHec filler reduces the OTR about 500 times compared to the unfilled film at 50% RH. This comparison even ignores that the thickness of the nanocomposite film is only 65% of that of the PVA film. Direct comparison is greatly assisted by the conversion into permeabilities (Fig. 2). The OTR measured for PVA-NaHec is only marginally above the detection limit of the Mocon OX-TRAN 2/21 M10x, which is equal to  $0.0005 \text{ cm}^3 \text{ m}^{-2} \text{ day}^{-1} \text{ bar}^{-1}$ . Spray coating allows the film thickness to be easily adjusted to the point where permeability values are within measurement range. The WVP of PVA-NaHec compared to PVA films is reduced by a factor of 63 at 50% RH. Both the OP (250 times) and WVP (5.5 times) for PVA-NaHec increase significantly when going from 50% to 90% RH.

As expected, both the absolute transmission rates and the sensitivity to humidity can be further improved by switching to the modified filler: The OP and WVP of PVA-HAHeC were found to be lower compared to

PVA-NaHec at all RH. At 50% RH, OP was found to be lower by a factor of 1.6, while the WVP was lower by a factor of 15. For potential application in food packaging, the performance at elevated RH is of prime importance. In this respect, the performance of PVA-HAHeC is surprisingly good. Compared to an unfilled PVA coating, the OP of PVA-NaHec at 90% RH is lower by a factor of 3230, while for PVA-HAHeC, it is lower by a factor of 6460. The same trend holds for WVP, where, compared to an unfilled PVA coating, at 90% RH the WVP of PVA-NaHec is lower by a factor of 13.4, while for PVA-HAHeC it is lower by a factor of 88.3. The sensitivity to humidity is much lower for PVA-HAHeC, indicating that the hydrogen bonding interaction between modified nanoplatelets and polymer might be capable of restricting the swelling of PVA.

As already mentioned, comparison of the results obtained with literature values is not straightforward, because test conditions vary significantly and various units are used. We cite the original values and, in parenthesis, the values converted to the standard units used in this manuscript to assist comparison. Gaume et al. [19] prepared PVA-montmorillonite nanocomposite coatings, comprising 5 wt% of the clay, and reported an OP of  $1.1 \times 10^{-17} \text{ cm}^3 \text{ cm cm}^{-2} \text{ Pa}^{-1} \text{ s}^{-1}$  ( $9.5 \text{ cm}^3 \mu\text{m m}^{-2} \text{ day}^{-1} \text{ bar}^{-1}$ ) at  $38^\circ\text{C}$  and 0% RH. The WVP of this nanocomposite at  $38^\circ\text{C}$  and 100% RH was found to be equal to  $9.1 \times 10^{-13} \text{ g cm cm}^{-2} \text{ s}^{-1}$  ( $118 \text{ g } \mu\text{m m}^{-2} \text{ day}^{-1} \text{ bar}^{-1}$ ). The 2  $\mu\text{m}$  PVA nanocomposite films filled with 10 wt% of saponite and coated on 12  $\mu\text{m}$  PET showed an OTR of  $1.67 \text{ cm}^3 \text{ m}^{-2} \text{ day}^{-1} \text{ atm}^{-1}$  at  $23^\circ\text{C}$  and 0% RH [20] that corresponds to an OP of  $3.3 \text{ cm}^3 \mu\text{m m}^{-2} \text{ day}^{-1} \text{ bar}^{-1}$ . Grunlan et al. [8] investigated the influence of the clay concentration and RH on the barrier properties of clay nanocomposites. They reported an OP for a film of a 3 wt% PVA-montmorillonite nanocomposite below  $2.5 \times 10^{-2}$  and  $2 \text{ cm}^3 \mu\text{m m}^{-2} \text{ day}^{-1} \text{ bar}^{-1}$  at  $23^\circ\text{C}$ , 35% and 55% RH, respectively. Increasing the filler content to 20 wt% reduced the OP to less than  $2.5 \times 10^{-2} \text{ cm}^3 \mu\text{m m}^{-2} \text{ day}^{-1} \text{ bar}^{-1}$  at 55% RH. Liu et al. [21] reported a WVP of  $2.36 \times 10^{-10} \text{ g m m}^{-2} \text{ Pa}^{-1} \text{ s}^{-1}$  ( $2 \times 10^6 \text{ g } \mu\text{m m}^{-2} \text{ day}^{-1} \text{ bar}^{-1}$ ) for a PVA nanocomposite filled with 5 wt% Na-montmorillonite at  $25^\circ\text{C}$  and 50% RH.

Given the moisture sensitivity discussed in the introduction, it is not surprising that all studies of clay-nanocomposites did not investigate the barrier properties at an elevated RH. Where some benchmarks exist at 50% RH and  $23^\circ\text{C}$  in literature, the permeabilities reported in this work for PVA-HAHeC are about two orders of magnitude better than results published previously. In the present work, the best OP is equal to  $2.5 \times 10^{-4} \text{ cm}^3 \mu\text{m m}^{-2} \text{ day}^{-1} \text{ bar}^{-1}$  at  $23^\circ\text{C}$  and 50% RH.

The better barrier performance and lower moisture sensitivity is certainly partially related to the high aspect ratio of the synthetic hectorite. As indicated by the comparison of PVA-NaHec and PVA-HAHeC coatings, H-bonding of the modifier might also contribute to the moisture tolerance and the superior barrier performance of PVA-HAHeC at an elevated humidity, which is more relevant for real applications.

The PXRD and SAXS analyses were consulted in an effort to understand the factors that might be responsible for the significant shift of the onset of permeability increase triggered by swelling and the factors limiting swelling.

### 3.2. PXRD analysis of Swelling

As discussed before, SAXS data (Fig. S3) show that completely delaminated clay nanosheets in the ternary system (PVA + clay + water) are homogeneously dispersed. Surprisingly, the XRD of dried nanocomposite coatings, however, suggests that (partial) phase separation occurred upon drying (Fig. 3). Clay platelets in the dry nanocomposite films are no longer uniformly distributed in the PVA matrix. Rather, interferences are observed for both nanocomposites that correspond to re-stacked NaHec and HAHeC domains, respectively. No estimate may be given from PXRD data regarding the degree of restacking.

Not surprisingly, the segregated NaHec stacks swell as a function of RH and the d-spacings increase with RH (13.3, 15.0 and  $15.9 \text{ \AA}$  at 50%,

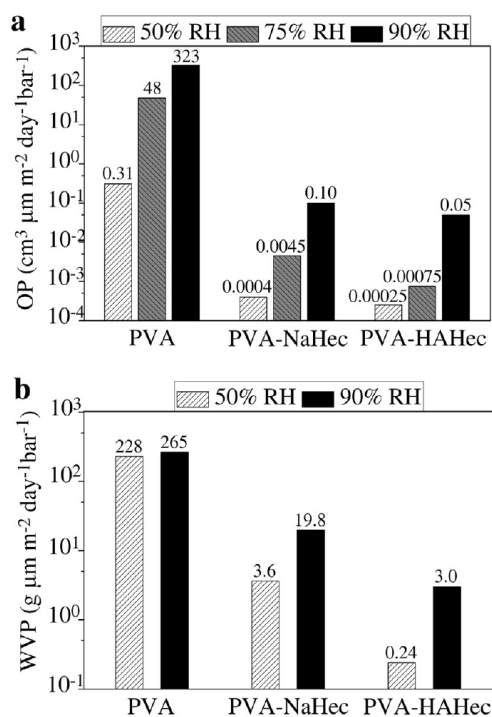


Fig. 2. The OP (a) and WVP (b) of coatings at  $23^\circ\text{C}$  and 50%, 75% and 90% RH.

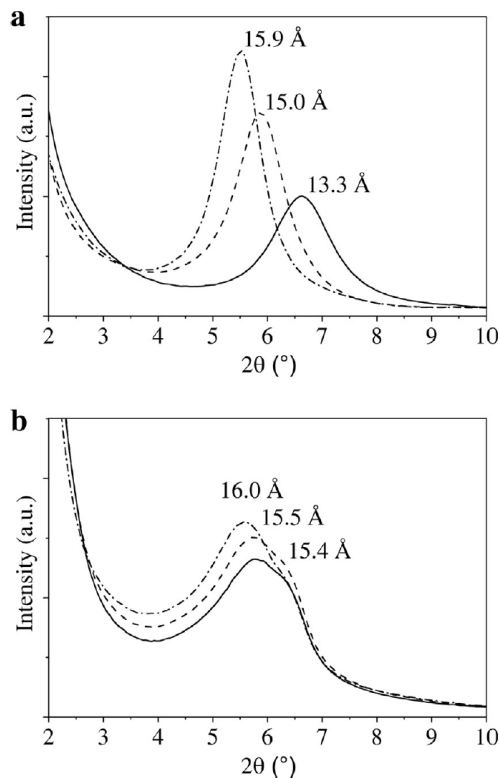


Fig. 3. The PXRD diffractograms of PVA-NaHec (a) and PVA-HAhec (b) at 50% (solid), 75% (dash) and 90% (dash dot) RH.

75% and 90% RH, respectively; Fig. 3a). This swelling will contribute to the overall water vapor sensitivity of the PVA-NaHec nanocomposite, as manifested in the barrier performance. Interestingly, modification of the NaHec with 6-ammoniumcaprohydroxamic acid reduces the swelling a great deal. The d-spacing increases only slightly (15.4, 15.5 and 16.0 Å at 50%, 75% and 90%, respectively; Fig. 3b). Not surprisingly, modification of the clay reduces the hydrophilicity of the segregated clay domains.

More surprisingly, the crystalline domains of the separated PVA matrix show reduced water vapor sensitivity. According to the work of Gaume et al. [19], the region between 17° and 21° 2θ refers to partially crystalline domains of PVA. In line with this, the unfilled PVA coating at > 50% RH showed a weak reflection at ≈ 18° 2θ (Fig. 4a). This reflection, however, corresponds to already swollen crystalline PVA domains, as indicated by a shift of this reflection upon drying at 0% RH to ≈ 20° 2θ. However, the moisture sensitivity of this PVA peak is significantly altered for both nanocomposites. The reflection associated with crystalline domains in PVA-NaHec remains at ≈ 20° 2θ at 50% RH and is still shifted to ≈ 18° 2θ at 75% and 90% RH (Fig. 4b). By contrast, swelling of the crystalline PVA domains for PVA-HAhec is hampered even at 90% RH (Fig. 4c). It appears that the onset of the swelling of clay and PVA domains regarding RH is correlated. The reason for this cooperativity is unclear.

The significantly reduced swelling sensitivity of both HAhec and crystalline PVA domains will contribute to the greatly reduced water sensitivity of the PVA-HAhec coatings. This might be related to potential hydrogen bonding between modifier and crystalline PVA domains attached to the filler surface. The swelling of crystalline PVA domains, in turn, might be responsible for the considerable deterioration of the barrier properties of neat PVA at RH > 35% [8].

The PVA peaks appear to be more intense with the nanocomposite coatings, which might indicate that the filler surface may act as a

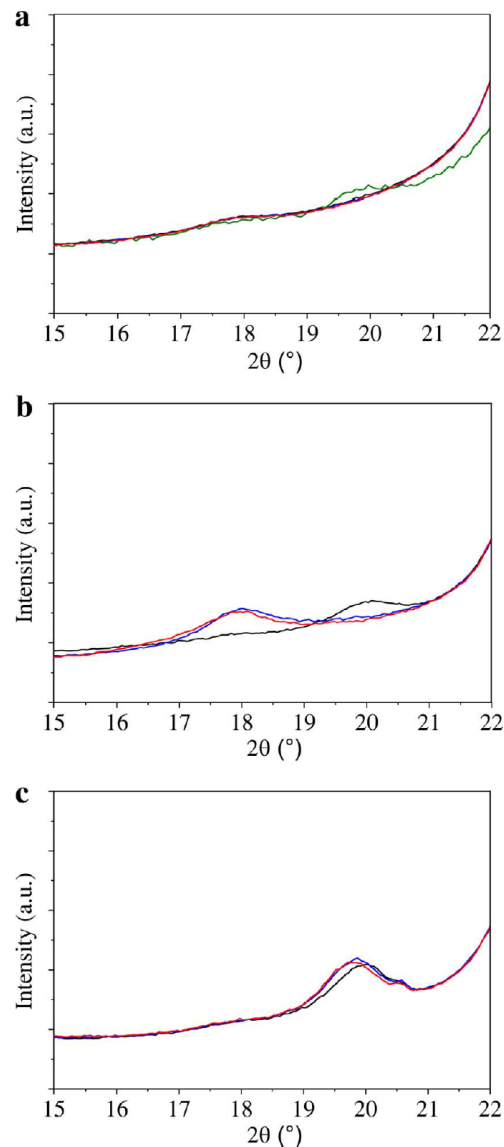


Fig. 4. Diffractograms of PVA (a), PVA-NaHec (b) and PVA-HAhec (c) in the region between 15 and 22° 2θ at 0% (green), 50% (black), 75% (blue) and 90% (red) RH. (For interpretation of the references to color in this figure legend, the reader is referred to the web version of this article.)

nucleation site increasing the crystallinity of the PVA matrix. This would be comparable to the increase of beta sheet content observed for spider silk protein-nanoclay composites reported recently [9]. Quantification based on X-ray intensities is, however, not justified, because epitaxial growth of PVA domains on oriented clay sheets might be the dominating impact on intensity changes.

### 3.3. Film texturing

Two-dimensional SAXS, moreover, shows that spray coating yields a perfectly textured film. The PET substrate consists of parallel oriented domains (~10 nm size, Fig. 5a). The 001 Bragg reflexes of NaHec and HAhec stacks (Fig. 5b, c) appear horizontally, proving a perfect parallel orientation of stacks. The mean derivation angle of the orientation distribution of the stacks is 1.45° (Fig. S7). This high quality of parallel

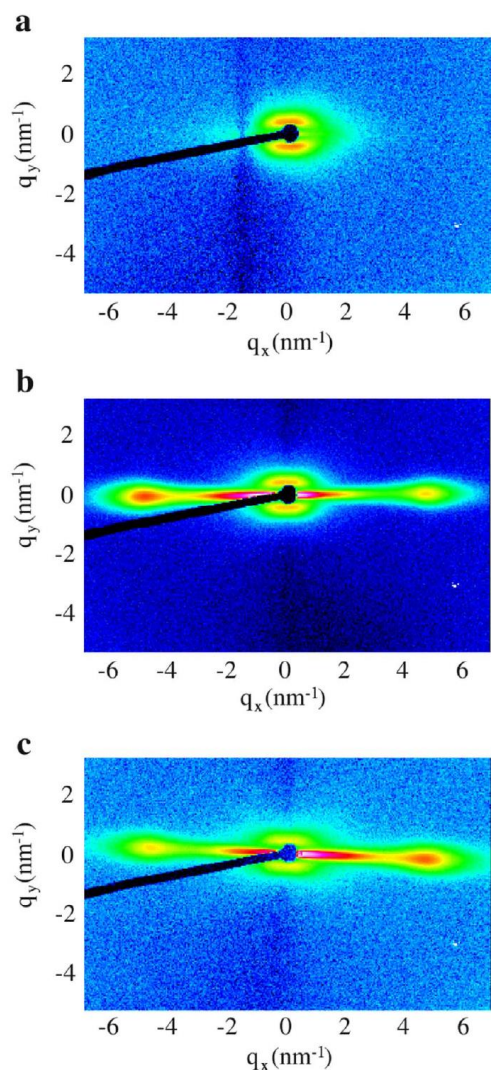


Fig. 5. Two-dimensional SAXS pattern of textured films measured in parallel geometry: PET (a), PVA-NaHec (b) and PVA-HAHeC (c).

orientation of clay platelets is the key for an appreciable tortuous pathway and will, therefore, contribute significantly to the superior barrier properties. During the spraying process, the very dilute suspension containing highly anisotropic platelets crashes onto the substrate surface at a huge speed. Upon collision, droplets spread onto the surface and clay platelets tend kinetically to occupy denser parallel positions above the substrate. In addition, after every spraying step, a thin liquid film of the suspension forms on the surface, giving sufficient mobility. The thickness of the liquid film is estimated to be about 2  $\mu\text{m}$  and with drying times of 2 min, the nanoplatelets also have sufficient time to adopt the most advantageous parallel position.

The perfect parallel orientation of the large aspect ratio nanoplatelets of PVA-HAHeC was confirmed by a TEM cross-sectional image (Fig. 6).

#### 4. Conclusions

Applying large aspect ratio synthetic clay that has been modified with 6-aminocaprohydroxamic acid hydrochloride hampers the swelling of PVA-nanocomposites to the degree where superior barriers for

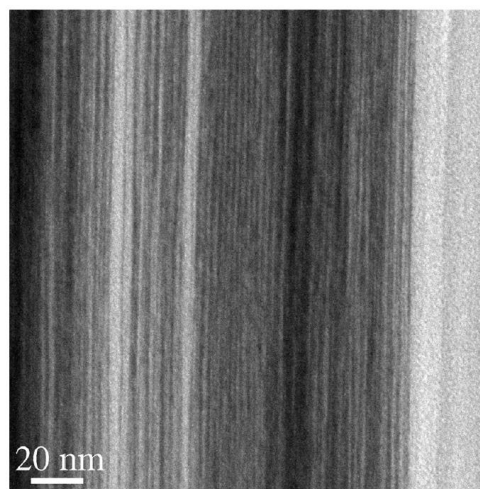


Fig. 6. TEM image of PVA-HAHeC nanocomposite film.

both water vapor and oxygen are observed even at 90% RH. This surprisingly low sensitivity to humidity might be attributed to a combination of potential hydrogen bonding of the modifier with the PVA matrix, the large aspect ratio of the synthetic clay applied and the perfect texture achieved by spray coating. We expect that the concept can be transferred to other hydrophilic polymer systems, bringing waterborne barrier formulations back into the game for food packaging.

#### Acknowledgements

The authors thank both electronic and mechanical workshops of Bayreuth University for building the automatic spray coating machine. The authors thank Florian Puchtl for synthesizing the clay and Marco Schwarzmann for sample preparation and TEM measurements. This work was supported by the German Science Foundation (DFG) within the collaborative research project SFB 840.

#### Appendix A. Supporting information

Supplementary data associated with this article can be found in the online version at <http://dx.doi.org/10.1016/j.memsci.2017.06.051>.

#### References

- [1] J. Gustavsson, C. Cederberg, U. Sonesson, R. v. Otterdijk, A. Meybeck, Global Food Losses and Food Waste, Save Food Congress, Düsseldorf 16.05.2011.
- [2] T. Quested, L. Murphy, Household food and drink waste: A product focus. <<http://www.wrap.org.uk/>>, June 2014.
- [3] D. Gunasekera, Cut food waste to help feed world, *Nature* 524 (2015) 415.
- [4] J.P. DeRocher, B.T. Gettelfinger, J. Wang, E.E. Nuxoll, E.L. Cussler, Barrier membranes with different sizes of aligned flakes, *J. Membr. Sci.* 254 (2005) 21–30.
- [5] B.K.G. Theng, Formation and Properties of Clay-polymer Complexes 4 Elsevier Science, LandcareResearch, Palmerston North, New Zealand, 2012.
- [6] M. Stöter, D.A. Kunz, M. Schmidt, D. Hirsemann, H. Kalo, B. Putz, J. Senker, J. Breu, Nanoplatelets of sodium hectorite showing aspect ratios of  $\approx 20\,000$  and superior purity, *Langmuir* 29 (2013) 1280–1285.
- [7] C. Mo, W. Yuan, W. Lei, Y. Shijiu, Effects of temperature and humidity on the barrier properties of biaxially-oriented polypropylene and polyvinyl alcohol films, *J. Appl. Packag. Res.* 6 (2014) 40–46.
- [8] J.C. Grunlan, A. Grigorian, C.B. Hamilton, A.R. Mehrabi, Effect of clay concentration on the oxygen permeability and optical properties of a modified poly(vinyl alcohol), *J. Appl. Polym. Sci.* 93 (2004) 1102–1109.
- [9] E. Doblhofer, J. Schmid, M. Riess, M. Daab, M. Suntinger, C. Habel, H. Bargel, C. Hugenschmidt, S. Rosenfeldt, J. Breu, T. Scheibel, Structural insights into water-based spider silk protein-nanoclay composites with excellent gas and water vapor barrier properties, *ACS Appl. Mater. Interfaces* 8 (2016) 25535–25543.
- [10] J. Breu, W. Seidl, A.J. Stoll, K.G. Lange, T.U. Probst, Charge homogeneity in synthetic fluorohectorite, *Chem. Mater.* 13 (2001) 4213–4220.
- [11] H. Kalo, M.W. Möller, M. Ziadeh, D. Dolejš, J. Breu, Large scale melt synthesis in an

## Appendix 1

---

- open crucible of Na-fluorohectorite with superb charge homogeneity and particle size, *Appl. Clay Sci.* 48 (2010) 39–45.
- [12] M. Stöter, S. Rosenfeldt, J. Breu, Tunable exfoliation of synthetic clays, *Annu. Rev. Mater. Res.* 45 (2015) 129–151.
- [13] E.N. Zilberman, O.D. Strizhakov, S.V. Svetozarskiy, Synthesis of  $\epsilon$ -aminocaprohydroxamic acid, *J. Gen. Chem. USSR (Engl. Transl.)* 35 (1965) 857–860.
- [14] S. Rosenfeldt, M. Stöter, M. Schlenk, T. Martin, R.Q. Albuquerque, S. Förster, J. Breu, In depth insights into the key steps of delamination of charged 2D nanomaterials, *Langmuir* 32 (2016) 10582–10588.
- [15] R. Kohli, *Hydrogen Bonding Abilities of Hydroxamic Acid and Its Isosteres*, Anchor Academic Publishing, Hamburg, 2016.
- [16] M. Gorman, The evidence from infrared spectroscopy for hydrogen bonding: a case history of the correlation and interpretation of data, *J. Chem. Educ.* 34 (1957) 304.
- [17] Y. Xianda, W. Anlai, C. Suqin, Water-vapor permeability of polyvinyl alcohol films, *Desalination* 62 (1987) 293–297.
- [18] A.P. Roberts, B.M. Henry, A.P. Sutton, C.R.M. Grovenor, G.A.D. Briggs, T. Miyamoto, M. Kano, Y. Tsukahara, M. Yanaka, Gas permeation in silicon-oxide/polymer (SiO<sub>x</sub>/PET) barrier films: role of the oxide lattice, nano-defects and macro-defects, *J. Membr. Sci.* 208 (2002) 75–88.
- [19] J. Gaume, C. Taviot-Gueho, S. Cros, A. Rivaton, S. Therias, J.L. Gardette, Optimization of PVA clay nanocomposite for ultra-barrier multilayer encapsulation of organic solar cells, *Sol. Energy Mater. Sol. Cells* 99 (2012) 240–249.
- [20] J.H. Yeun, G.S. Bang, B.J. Park, S.K. Ham, J.-H. Chang, Poly(vinyl alcohol) nanocomposite films: thermo-optical properties, morphology, and gas permeability, *J. Appl. Polym. Sci.* 101 (2006) 591–596.
- [21] G. Liu, Y. Song, J. Wang, H. Zhuang, L. Ma, C. Li, Y. Liu, J. Zhang, Effects of nanoclay type on the physical and antimicrobial properties of PVOH-based nanocomposite films, *LWT – Food Sci. Technol.* 57 (2014) 562–568.

## Supporting information

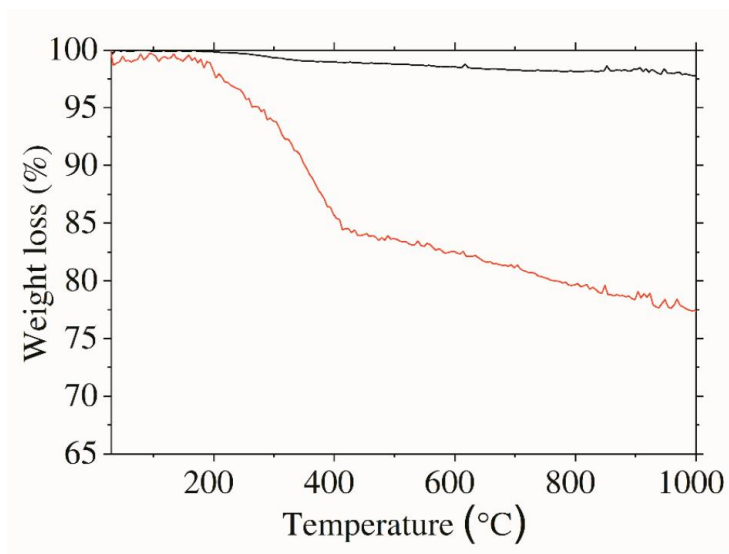


**Figure S1.** TGA curves of NaHec (black) and HAHec (red). The weight loss below 400 °C corresponds to the modifier content and amounts to 16 wt% which is in agreement with expectations based on cation exchange capacity of NaHec.

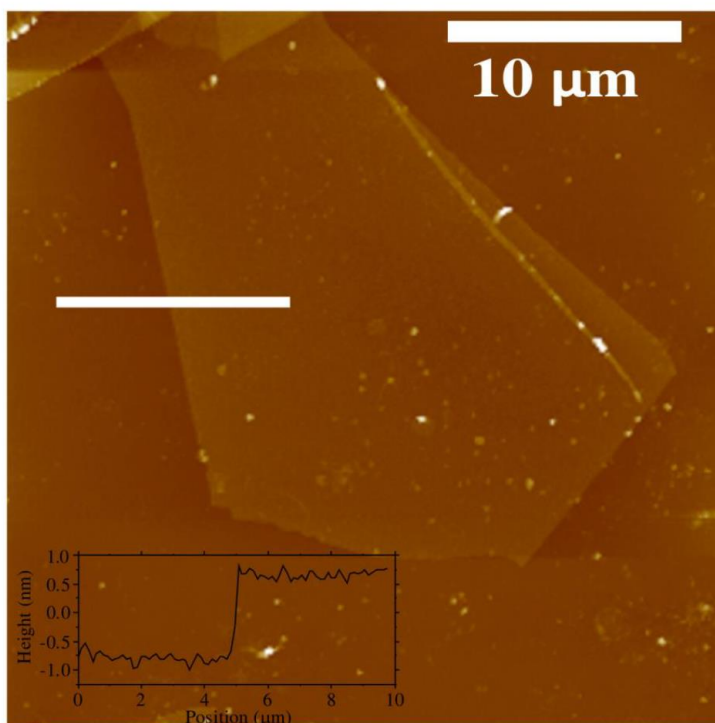


**Figure S2.** Typical AFM picture of delaminated NaHec.

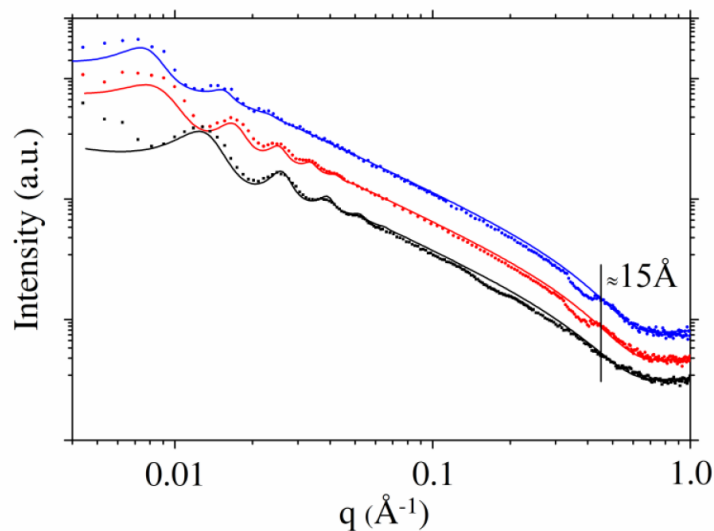


**Figure S3.** 1D-SAXS pattern of aqueous suspensions (5.3 wt%) of HAHeC (black squares), PVA-HAHeC (red circles) and PVA-NaHeC (blue circles). The vertical line marks the basal spacing expected for stacks of NaHeC ( $\approx 15.2$  Å) and HAHeC ( $\approx 15$  Å); no sign of restacking upon blending with PVA in water is observed. The continuous lines correspond to calculated intensities based on a model of stacked discs with a radius of  $9 \mu\text{m}$  and a thickness of  $8.5$  Å. The rational  $00l$  series observed at low  $q$  ( $< 0.1 \text{ \AA}^{-1}$ ) indicate a rather uniform separation of delaminated clay nanoplatelets to  $48 \pm 5$  nm for HAHeC,  $74 \pm 8$  nm for PVA-HAHeC and  $80 \pm 13$  for PVA-NaHeC, respectively.

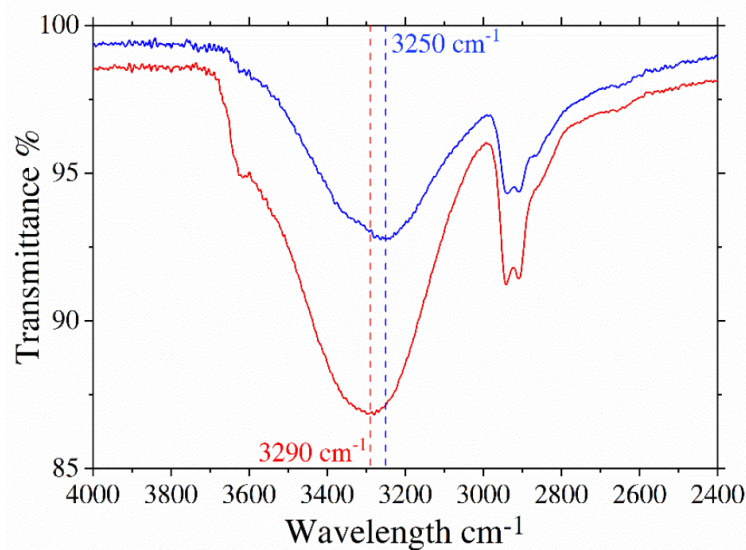


**Figure S4.** FTIR spectra of the PVA-NaHeC (red) and PVA-HAHeC (blue) nanocomposite films.

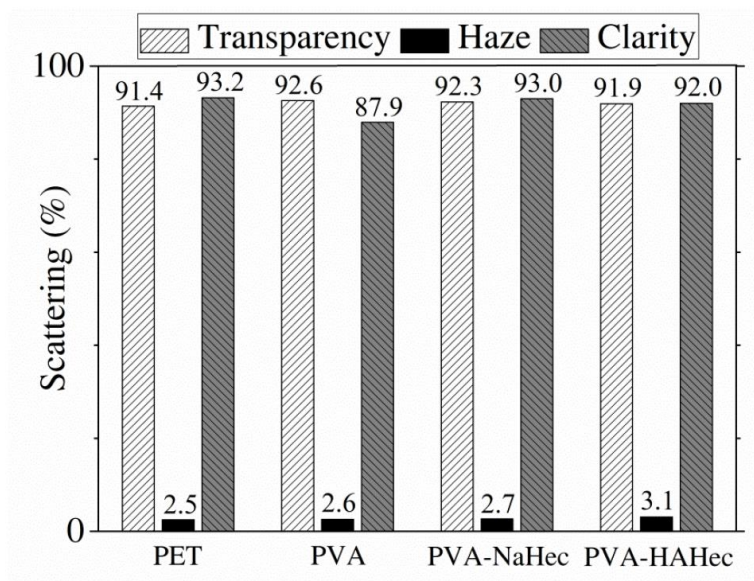


**Figure S5.** Optical properties of the films. PVA, PVA-NaHec and PVA-HAHec films are highly transparent, colorless and flexible.

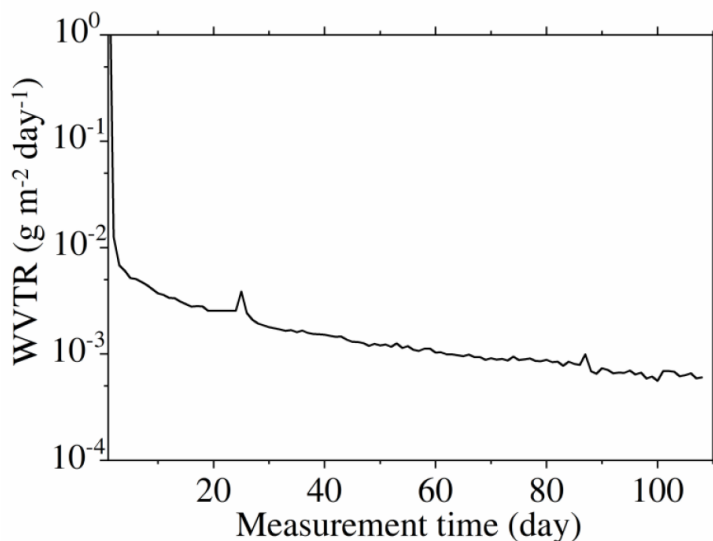


**Figure S6.** The example of WVTR measurement on the HiBarSens HBS 2.0 HT. All films have been carefully conditioned at RH of measurement and reported values have been measured at equilibrium. On the Figure is WVTR measurement of PVA-HAhec at 23 °C and 50% RH.

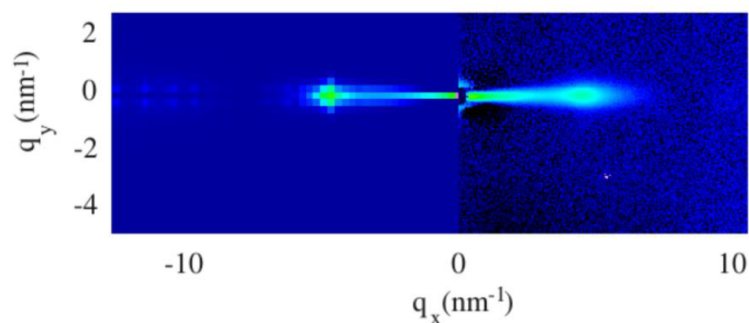


**Figure S7.** Calculated (left) and experimental (right) 2D-SAXS pattern of the inorganic content in PVA-NaHec (0.45  $\mu\text{m}$  thick coating of 34 vol% NaHec, 66 vol% PVA on a 36  $\mu\text{m}$  PET substrate). The experimental data are obtained by subtracting the scattering of a PVA film (0.7  $\mu\text{m}$  on top of a 36  $\mu\text{m}$  PET substrate) from the scattering of the PVA-NaHec. The  $001$  reflex is calculated using parallel stacks of discs in a distance of 1.5 nm with a deviation of 0.05 nm. The discs are assumed to have a radius of 9  $\mu\text{m}$  and a thickness of 0.85 nm. The mean derivation angle of the orientation distribution of the restacked platelets is  $1.45^\circ$ .

## 6.2. Appendix 2

### **Large scale self-assembly of smectic nanocomposite films by doctor blading versus spray coating: impact of crystal quality on barrier properties**

Evgeny S. Tsurko,<sup>†,‡,°</sup> Patrick Feicht,<sup>†,‡,°</sup> Frederik Nehm,<sup>§</sup> Kevin Ament,<sup>†,‡</sup> Sabine Rosenfeldt,<sup>†,⊥</sup>  
Ines Pietsch,<sup>||</sup> Konrad Roschmann,<sup>||</sup> Hussein Kalo,<sup>#</sup> and Josef Breu<sup>\*,†,‡</sup>

<sup>†</sup> Bavarian Polymer Institute, Universitätsstraße 30, Bayreuth, 95447, Germany

<sup>‡</sup> Department of Inorganic Chemistry I, University of Bayreuth, Universitätsstraße 30, Bayreuth, 95447, Germany

<sup>§</sup> Dresden Integrated Center for Applied Physics and Photonic Materials, TU Dresden, George-Bähr-Straße 1, Dresden, 01062, Germany

<sup>⊥</sup> Department of Physical Chemistry I, University of Bayreuth, Universitätsstraße 30, Bayreuth, 95447, Germany

<sup>||</sup> BASF SE, 67056 Ludwigshafen, Germany

<sup>#</sup> BYK Chemie GmbH, Stadtwald-Straße 44, 85368 Moosburg, Germany

\* Corresponding author:

Prof. Dr. Josef Breu

Universitätsstr. 30

95440 Bayreuth

Germany

\* E-mail address: [Josef.Breu@uni-bayreuth.de](mailto:Josef.Breu@uni-bayreuth.de)

Macromolecules, DOI: 10.1021/acs.macromol.7b00701.

# Large Scale Self-Assembly of Smectic Nanocomposite Films by Doctor Blading versus Spray Coating: Impact of Crystal Quality on Barrier Properties

Evgeny S. Tsurko,<sup>†,‡,○</sup> Patrick Feicht,<sup>†,‡,○</sup> Frederik Nehm,<sup>§</sup> Kevin Ament,<sup>†,‡</sup> Sabine Rosenfeldt,<sup>†,⊥</sup> Ines Pietsch,<sup>||</sup> Konrad Roschmann,<sup>||</sup> Hussein Kalo,<sup>#</sup> and Josef Breu<sup>\*,†,‡,⊥</sup>

<sup>†</sup>Bavarian Polymer Institute, Universitätsstraße 30, Bayreuth, 95447, Germany

<sup>‡</sup>Department of Inorganic Chemistry I, University of Bayreuth, Universitätsstraße 30, Bayreuth, 95447, Germany

<sup>§</sup>Dresden Integrated Center for Applied Physics and Photonic Materials, TU Dresden, George-Bähr-Straße 1, Dresden, 01062, Germany

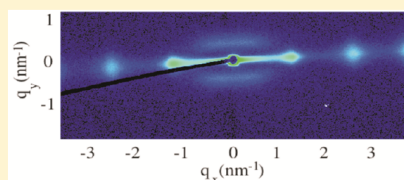
<sup>⊥</sup>Department of Physical Chemistry I, University of Bayreuth, Universitätsstraße 30, Bayreuth, 95447, Germany

<sup>||</sup>BASF SE, 67056 Ludwigshafen, Germany

<sup>#</sup>BYK Chemie GmbH, Stadtwald-Straße 44, 85368 Moosburg, Germany

## Supporting Information

**ABSTRACT:** Flexible transparent barrier films are required in various fields of application ranging from flexible, transparent food packaging to display encapsulation. Environmentally friendly, waterborne polymer–clay nanocomposites would be preferred but fail to meet in particular requirements for ultra high water vapor barriers. Here we show that self-assembly of nanocomposite films into one-dimensional crystalline (smectic) polymer–clay domains is a so far overlooked key-factor capable of suppressing water vapor diffusivity despite appreciable swelling at elevated temperatures and relative humidity (R.H.). Moreover, barrier performance was shown to improve with quality of the crystalline order. In this respect, spray coating is superior to doctor blading because it yields significantly better ordered structures. For spray-coated waterborne nanocomposite films (21.4  $\mu\text{m}$ ) ultra high barrier specifications are met at 23 °C and 50% R.H. with oxygen transmission rates (OTR)  $< 0.0005 \text{ cm}^3 \text{ m}^{-2} \text{ day}^{-1} \text{ bar}^{-1}$  and water vapor transmissions rates (WVTR) of  $0.0007 \text{ g m}^{-2} \text{ day}^{-1}$ . Even in the most challenging environments (38 °C and 90% R.H.), values as low as  $0.24 \text{ cm}^3 \text{ m}^{-2} \text{ day}^{-1} \text{ bar}^{-1}$  and  $0.003 \text{ g m}^{-2} \text{ day}^{-1}$  were found for OTR and WVTR, respectively.



## INTRODUCTION

Flexible transparent barrier coatings are required in applications ranging from food packaging<sup>1,2</sup> to display encapsulation.<sup>3,4</sup> Most if not all barriers require restricted permeability for both hydrophobic ( $\text{O}_2$ ,  $\text{N}_2$ ,  $\text{CO}_2$ ) and hydrophilic (water vapor) permeates. In general, the permeability ( $P$ ) of the barrier coating is given by  $P = S \times D$ , where  $S$  and  $D$  are solubility and diffusivity of the permeates, respectively.<sup>5</sup> Concerted adjustment of both  $S$  and  $D$  allow for fine-tuning the barrier performance and produces barriers for both kinds of permeates simultaneously.  $S$  depends on the affinity of permeates to the matrix wherein polar molecules are basically more soluble in polar than in nonpolar matrices and vice versa. Waterborne (hydrophilic) polymers possess excellent barrier properties for hydrophobic permeates like oxygen in particular at very low relative humidities (R.H.). However, at ambient R.H. the gas barrier performance degrades severely due to swelling of the polymer matrix; their water vapor barrier is generally poor because of the high solubility of the permeate.  $D$  can be influenced by the incorporation of impermeable platelets like layered silicates (clay) thus increasing the diffusion path

(tortuous pathway). According to the Cussler theory,<sup>6</sup>  $D$  mainly depends on the aspect ratio ( $\alpha$ ) and volume fraction ( $\phi$ ) of the filler, while parallel alignment (texture) is assumed to be given.

Equidistant positioning of filler platelets into a smectic lyotropic phase would have to rely on self-assembly and is difficult to be realized experimentally. Only very few examples of such one-dimensionally (1D) ordered nanocomposites have been reported in the literature: Recently, Wong et al.<sup>7</sup> reported self-assembly of an epoxy–zirconium phosphate nanocomposite into a smectic phase by spray coating. We have recently reported that a waterborne spider silk protein–nanoclay composite is self-assembled into a 1D crystal upon film formation.<sup>8</sup> 1D crystallinity amplifies Coulomb attractions (Madelung constant) between negatively charged nanoplatelets and the positively charged matrix between them which, e.g., is expected to restrain swelling of the nanocomposite. A

**Received:** April 3, 2017

**Revised:** May 9, 2017

**Published:** May 16, 2017

systematic study on the impact of the quality of the crystalline order of such smectic nanocomposites on barrier performance is so-far lacking. Here we apply two different processing techniques, doctor blading and spray coating, that happen to yield nanocomposite films of distinctly different smectic crystallinity. As a polymer matrix we apply a mixture of ethoxylated polyethylenimine (PEIE) and poly(acrylic acid)-PAA provided by BASF SE<sup>9,10</sup> which is a waterborne, amorphous polyelectrolyte system that gives stable cocarvate suspensions similar to a PEI/PAA system recently introduced by Grunlan et al.<sup>11</sup> This polyelectrolyte system is then combined with an utterly delaminated synthetic layered silicate.

## ■ EXPERIMENTAL SECTION

**Materials.** The employed  $[\text{Na}_{0.5}]^{\text{inter}}[\text{Mg}_{2.5}\text{Li}_{0.5}]^{\text{oct}}[\text{Si}_4]^{\text{tet}}\text{O}_{10}\text{F}_2$  (NaHec) was synthesized via melt synthesis according to an established literature procedure.<sup>12</sup> The material featured a cation exchange capacity (CEC) of 1.27 mmol  $\text{g}^{-1}$ . The NaHec was ion-exchanged with 6-aminocaprohydroxamic acid hydrochloride which was synthesized according to literature.<sup>13</sup> 164 g (1 mol) of hydroxylamine sulfate (Sigma-Aldrich, Germany) were added to 226 g (2 mol) of molten  $\epsilon$ -caprolactam (Sigma-Aldrich, Germany). The mixture was stirred and heated for 5 h at 100 °C. Then 200 mL of methanol (VWR International, France) were added and heating was continued for another 5 h. 500 mL methanol were added to the hot reagent mixture and the unreacted hydroxylamine sulfate was filtrated. After methanol evaporation unreacted caprolactam was removed by extraction with boiling trichloroethylene (Sigma-Aldrich, Germany, 4 times 500 mL each). The product was then dissolved in methanol (100 mL) and gaseous ammonia was passed through the solution to completely precipitate the sulfate which was then filtered off. Crystallization of 6-aminocaprohydroxamic acid was triggered by seeding and cooling the solution. It was purified by recrystallization in methanol. Ethoxylated polyethylenimine (PEIE) solution (80 wt %,  $M_w = 13000$  g/mol) and poly(acrylic acid)(PAA) solution (35 wt %,  $M_w = 100000$  g/mol) in water were provided by BASF SE, Germany. Ammonia solution (25 wt %) was provided by Bernd Kraft GmbH, Germany, hydrochloric acid (1 M) was provided by Grüssing GmbH, Germany. Corona treated polyethylene terephthalate (PET) (36  $\mu\text{m}$ ) film was used as substrate (Bleher KG, Germany). All chemicals were used as received without further purification.

**Preparation of the Nanocomposite Suspension.** NaHec (0.5 g) was delaminated by immersing it into Millipore water (100 g, 0.5 wt %). To the NaHec suspension was added crystalline 6-aminocaprohydroxamic acid in 1.5-fold excess of the CEC, and the pH was adjusted with 1 M HCl to pH = 8 to protonate the modifier. The suspension was then mixed thoroughly in an overhead shaker overnight. Thereafter the clay suspension was centrifuged, washed with Millipore water and the procedure was repeated. Completeness of ion exchange was checked by energy dispersive X-ray analysis. Moreover, weight loss as observed by thermogravimetric analysis (TGA) corresponds to the organic content expected based on the CEC (Figure S1). Finally, 6-ammoniumcaprohydroxamic acid modified NaHec (HAHec) was redispersed in water (0.5 wt %).

Then 8 g of PAA solution were mixed with 10 g of Millipore water and 0.1 g of ammonia solution (25 wt %). The mixture was stirred for 5 min, and after 1.5 g of PEIE solution was added, stirring was continued for 1 h. This polyelectrolyte mixture (19.6 g, 20.5 wt %) was first diluted with 282.3 g of Millipore water, and then 201.2 g of the 0.5 wt % HAHec suspension was added. The obtained nanocomposite formulation had a total solid content of 1 wt % with 20 wt % of the solid content being attributed to HAHec. For doctor blading, a slightly higher total solid content of 1.7 wt % was used to obtain thicker barrier films.

**Nanocomposite Film Fabrication.** Spray-coated (SC) nanocomposite films were prepared applying a fully automated spray coating system equipped with a SATA 4000 LAB HVLP 1.0 mm spray gun (SATA GmbH & Co. KG, Germany). A fixed airbrush sprays the

suspension (4 bar, 1 mL  $\text{s}^{-1}$ ) on the PET substrate attached to the conveyor belt, which moves with a certain speed. The speed of the conveyor belt/substrate was set to 1 m  $\text{s}^{-1}$  and the distance between airbrush and substrate was fixed at 24 cm. The thickness of the suspension layer applied in one spraying step is  $\approx 2$   $\mu\text{m}$  which corresponds to  $\approx 20$  nm dry film thickness. For drying the suspension layer, the sample is stopped under infrared lamps until evaporation of the solvent is complete. The drying time was 180 s and the power of the lamps was adjusted to obtain a substrate surface temperature of 50 °C. Films were prepared by repeating 1000 spraying/drying cycles. The quality of the texture and crystallinity obtained is independent of the number of cycles and hence the film thickness.

Doctor-bladed (DB) films were prepared using an automated device (Zehntner ZAA 2300, Zehntner GmbH Testing Instruments, Switzerland). The substrate temperature was 67 °C, the blade speed was 1.2 cm  $\text{s}^{-1}$ , and the blade height was 90  $\mu\text{m}$ . The thickness of the dried nanocomposite film is typically 1.5  $\mu\text{m}$ .

For DB films the maximum film thickness that can be thoroughly dried without triggering blisters<sup>14</sup> is  $< 2$   $\mu\text{m}$ . SC processing allows preparation of thicker films that then reach the ultrahigh barrier region.

All nanocomposite films were cured by evaporating the volatile base  $\text{NH}_3$  at 80 °C.

**Nanocomposites Characterization.** Oxygen transmission rates (OTR) were measured on a Mocon OX-TRAN 2/21 XL instrument (Minneapolis, MN) with a lower detection limit of 0.0005  $\text{cm}^3 \text{m}^{-2} \text{day}^{-1} \text{bar}^{-1}$ . The measurements were conducted at 23 °C/50% R.H. and at 38 °C/90% R.H. Double-cell film testing mode was applied with a total film surface area of 100  $\text{cm}^2$ .

Water vapor transmission rates (WVTR) of DB nanocomposite films were measured applying a Mocon PERMATRAN-W model 3/33 at 23 °C/50% R.H. and at 38 °C/90% R.H. The lower detection limit of the device was 0.05  $\text{g m}^{-2} \text{day}^{-1}$ .

WVTR measurements of the SC nanocomposite films were performed using electrical calcium corrosion tests (Ca-Tests)<sup>15</sup> as described by Nehm et al.<sup>16</sup> Here, the conductivity of a thin-film Ca sensor behind the barrier is monitored in a controlled climate. Upon water ingress, metallic Ca reacts to  $\text{Ca}(\text{OH})_2$ , resulting in a conductivity loss. The slope of the conductivity over time is directly proportional to the WVTR. The measurements were made at 23 °C/50% R.H. and 38 °C/90% R.H. The lower detection limit of the device is  $1 \times 10^{-5} \text{g m}^{-2} \text{day}^{-1}$ . For further details on the setup, please see ref 16.

Spray coating allows for simultaneously coating a small piece of a silicon waver next to the PET substrate. The thickness of SC nanocomposites could then be measured on the silicon substrate with a Veeco Dektak 150 profilometer with a repeatability  $< 0.6$  nm. Ten measurements were taken at different spots and averaged. This technique could not be applied with DB coatings, and therefore, the thickness was calculated assuming a uniform spreading of the solid content applied over the complete substrate.

Powder X-ray diffraction (PXRD) patterns were obtained using nickel filtered Cu  $K\alpha$  radiation ( $\lambda = 1.54187$  Å) on a Bragg-Brentano-type diffractometer (XPRT-PRO, PANalytical B.V.) equipped with an X'Celerator Scientific RTMS detector. All patterns were analyzed using Panalytical's Highscore Plus software. Prior to measurement, samples were carefully equilibrated at 23 °C/0% R.H., 23 °C/50% R.H., and at 38 °C/90% R.H. in an Anton Paar temperature - humidity chamber.

All small-angle X-ray scattering (SAXS) data were measured using the SAXS system "Double Ganesha AIR" (SAXSLAB, Denmark). The X-ray source of this laboratory-based system is a rotating anode (copper, MicoMax 007HF, Rigaku Corporation, Japan) providing a microfocussed beam. The data are recorded by a position sensitive detector (PILATUS 300 K, Dectris). To cover the range of scattering vectors between 0.05 and 10  $\text{nm}^{-1}$  different detector positions were used. The measurements of the suspensions were done in 1 mm glass capillaries (Hilgenberg, code 4007610, Germany) at room temperature.

TGA were obtained using NETZSCH STA 449C (Erich Netzsch GmbH & Co. Holding KG, Germany) thermogravimetric analyzer for

NaHec, HAec samples and TGA/SDTA 851 (Mettler Toledo, Germany) for SC nanocomposite film. Measurements were performed in aluminum oxide pans under air atmosphere (80/20; N<sub>2</sub>/O<sub>2</sub>) at a heating rate of 10 °C min<sup>-1</sup> from 30 to 1000 °C.

Transmission electron microscopy (TEM) images were taken on a Zeiss CEM 922 at accelerating voltages of 200 kV.

## RESULTS AND DISCUSSION

**Polymer–Clay Suspension.** Layered silicates are readily available and affordable fillers and have therefore been most commonly employed for polymer nanocomposites.<sup>17–22</sup> Here, a synthetic sodium fluorohectorite (NaHec, [Na<sub>0.5</sub>]<sup>inter</sup>[Mg<sub>2.5</sub>Li<sub>0.5</sub>]<sup>oct</sup>[Si<sub>4</sub>]<sup>tet</sup>O<sub>10</sub>F<sub>2</sub>) is applied<sup>23</sup> that has been shown to utterly delaminate into single layers of median aspect ratio of ≈20000 as shown by static light scattering and atomic force measurements (see ref 12 for details) when immersed in deionized water.<sup>12</sup> Because of the large aspect ratio, at concentrations as low as 1 vol % NaHec is able to form a nematic phase as evidenced by the small-angle X-ray scattering (SAXS).<sup>24</sup>

The interlayer Na<sup>+</sup> ions can be easily exchanged by organic cations to adjust surface tension and suspensibility. In this line, 6-aminocaprohydroxamic acid hydrochloride (HA) was used as a surface modifier that renders the surface more hydrophobic and at the same time is capable of forming strong hydrogen bonds<sup>25</sup> via the hydroxamic acid functional group (–R–C(O)–N(H)–OH). Aqueous suspensions of surface modified NaHec (HAHec) represent nematic phases as evidenced by a rational 00 $l$  series in the SAXS pattern with an interlayer distance of 48 nm at 2 vol % (Figure S2). The lack of a peak at 1.5 nm indicates that no restacking has been triggered upon ion exchange.

HAHec suspensions were mixed with a suspension of the two-component polyelectrolyte system (ethoxylated polyethyleneimine (PEIE) and poly(acrylic acid)(PAA), BASF SE, Germany). The SAXS pattern of a concentrated gel (26.8 wt % PEIE–PAA and 8.2 wt % HAHec) proves perfect homogeneity (Figure 1). Singular silicate layers are separated

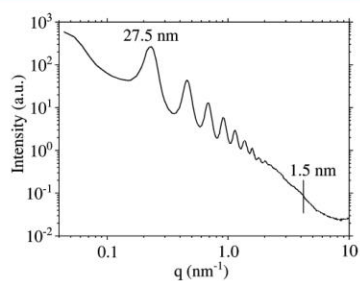


Figure 1. 1D-SAXS pattern of polyelectrolyte–HAHec gel.

to a uniform distance of 27.5 nm as indicated by a 00 $l$  series visible up to the tenth order. In this quaternary system any aggregation into stacks with small separations of adjacent silicate layers corresponding to intercalated HA or PEIE can be ruled out as indicated by the absence of peaks below  $q = 4.2$  nm<sup>-1</sup> (1.5 nm).

**Self-Assembly of Smectic Polymer–Clay Domains.** Dilute (1–2 wt % total solid content) polyelectrolyte–HAHec suspensions were applied to a PET substrate by doctor blading or spray coating (Figure 2). The filler content of dried

nanocomposite films was checked by thermogravimetric analysis (Figure S3).

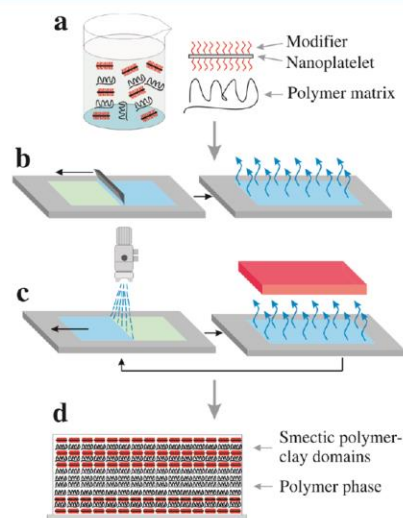


Figure 2. Homogeneous polyelectrolyte–HAHec suspensions (a) were applied on PET substrates by doctor blading (b) or spray coating (c). Upon evaporation of water, the components self-assemble into smectic nanocomposite films (d).

The texture of both doctor-bladed (DB) and spray-coated nanocomposite films (SC) was analyzed by 2D-SAXS measurements (Figure 3) where films were located parallel to the beam direction. The peaks along the  $q_x$  axis represent platelets aligned parallel to the substrate. The weak halos above and below the line of 00 $l$  reflections are characteristic for PET (Figure S4). Besides these halos no intensity is observed off the  $q_x$  direction

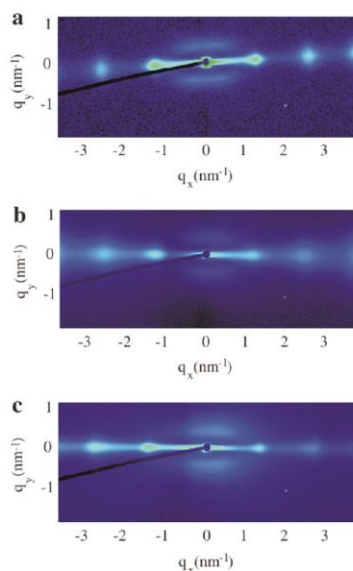
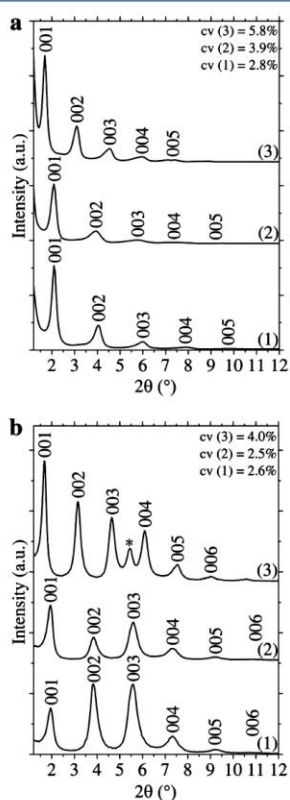


Figure 3. 2D-SAXS patterns of the nanocomposites recorded at ambient conditions ( $T = 23$  °C, R.H. ≈ 40%). (a, b) Spray-coated nanocomposite film, (c) Doctor-bladed nanocomposite film.

indicating perfectly parallel arrangement of the clay platelets to PET.

For both nanocomposite films along [001], Bragg reflections are visible up to the fourth order (004) and indicate an interlayer distance of 4.5 nm. The nanocomposite films are 1D crystalline with 1 nm thick clay platelets being separated by 3.5 nm of polymer matrix. Diffuse scattering (streaking) between the Bragg reflections indicates some degree of variation of the separation of clay platelets in the nanocomposites. While the degree of streaking varies slightly from sample to sample (SC films in Figure 3, parts a and b), DB films (Figure 3c) generally show more diffuse scattering indicating a less precisely defined separation (lower 1D crystallinity) of adjacent clay platelets by polymer volume in the smectic nanocomposite film.

The 1D crystalline nature of both nanocomposite films is confirmed by powder X-ray diffraction (PXRD) (Figure 4).



**Figure 4.** PXRD patterns of nanocomposite films equilibrated at different temperature/R.H. conditions. (a) Doctor-bladed nanocomposite film. (b) Spray-coated nanocomposite film recorded at 23 °C/0% R.H. (1), 23 °C/50% R.H. (2), and 38 °C/90% R.H. (3), respectively.

According to Meuring's rules<sup>26</sup> in PXRD patterns, the quality of the 1D crystalline order is indicated by the coefficient of variation (*cv*) and the intensity and maximum visible order of the 00*l* series. DB films have a significantly higher *cv* and the intensities of the 00*l* reflections fall off much quicker with increasing scattering angle.

At 23 °C/0% R.H. the interlayer spacing for DB films is 4.21 nm while for the SC films it is 4.55 nm. Quite surprisingly for a

waterborne nanocomposite, upon increasing the R.H. to 50%, no significant swelling with water vapor is observed as indicated by no significant changes in interlayer distances. The interlayer spacing observed in PXRD corresponds well with the SAXS value.

Significant swelling, however, sets in at 38 °C/90% R.H. where the interlayer distance increases by some 15% corresponding to a significant volume of water being dissolved in the nanocomposite films. For the swollen, well ordered SC films, moreover, the shift of the 00*l* series to lower diffraction angles reveals an additional peak (marked with an asterisk in Figure 4b(3)) that at low R.H. is superimposed on the 003 reflection. The interlayer distance of 1.5 nm corresponding to this peak may be related to silicate layers separated by only HA. This is a first hint that upon removal of solvent from the perfectly homogeneous quaternary suspension (Figure 1) partial phase separation may be triggered.

Assuming a density of 1.15 g cm<sup>-3</sup> for the organic volume between two silicate layers of 1 nm thickness and a density of 2.8 g cm<sup>-3</sup>, the nanocomposite films prepared contain ≈10 vol % of filler. Therefore, for homogeneous, single phase 1D crystalline (smectic) nanocomposite film with utterly delaminated equidistantly distributed HA/Hec in the polymer an interlayer distance of 10 nm (1 nm platelet thickness + 9 nm organic volume) is expected. Clearly, with both DB and SC nanocomposite films significantly lower interlayer distances are observed. Obviously a thermodynamically favored partial phase separation occurs upon drying the nanocomposite films. Cutting the nanocomposite film samples with a cryo-ion-slicer allows for a direct visualization of the phase separation by transmission electron microscopy (TEM) (Figure 5). Smectic

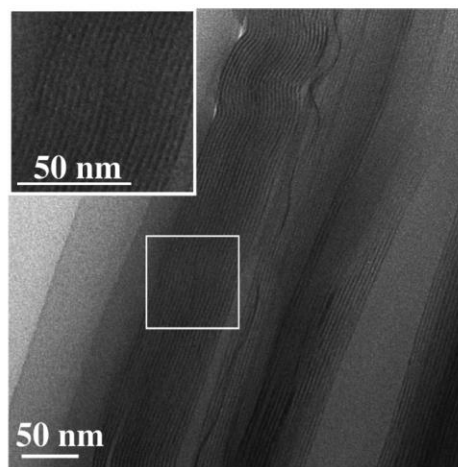


**Figure 5.** TEM image of free-standing SC nanocomposite film. Phase separation is observed where polymer–clay domains (dark area) alternate with polymer phase (bright area).

polymer–clay domains with an interlayer spacing corresponding to the values seen in SAXS and PXRD (see inset in Figure 5) alternate with the polymer phase. Very rarely a domain with a smaller separation corresponding to HA/Hec can be found (Figure S5).

**Oxygen and Water Vapor Barriers of the Nanocomposites.** Oxygen (OTR) and water vapor (WVTR) transmission rates for DB and SC nanocomposite films were

**Table 1.** OTR and WVTR of the Films at 23 °C/50% R.H. and 38 °C/90% R.H.

	temp, °C/R.H., %	coating thickness, $\mu\text{m}$		
		0 (PET)	1.5 (DB)	21.4 (SC)
OTR, $\text{cm}^3 \text{m}^{-2} \text{day}^{-1} \text{bar}^{-1}$	23/50	37.2	0.024	<0.0005
	38/90	57.5	12.2	0.24
WVTR, $\text{g m}^{-2} \text{day}^{-1}$	23/50	3.6	0.09	0.0007
	38/90	15.3	4.1	0.0030

**Table 2.** OP and WVP of the Films at 23 °C/50% R.H. and 38 °C/90% R.H.

	temp, °C/R.H., %	coating thickness, $\mu\text{m}$		
		0 (PET)	1.5 (DB)	21.4 (SC)
OP, $\text{cm}^3 \mu\text{m m}^{-2} \text{day}^{-1} \text{bar}^{-1}$	23/50	1339	$3.6 \times 10^{-2}$	$<1 \times 10^{-2}$
	38/90	2070	23.2	5.1
WVP, $\text{g } \mu\text{m m}^{-2} \text{day}^{-1} \text{bar}^{-1}$	23/50	9220	9.9	1.1
	38/90	9226	140.7	1.1

measured at 23 °C/50% R.H. and 38 °C/90% R.H. (Table 1). For DB films the maximum film thickness that can be thoroughly dried without triggering blisters<sup>14</sup> is <2  $\mu\text{m}$ . SC processing allows preparation of thicker films that then reach the ultrahigh barrier region.

All films have been carefully conditioned at the temperature and R.H. of the measurement. For some of the samples equilibration takes up to 13 days. All reported values have been measured at equilibrium (Figures S6–S8). Most remarkably, OTR and WVTR at 23 °C/50% R.H. of SC nanocomposite films are  $<0.0005 \text{ cm}^3 \text{m}^{-2} \text{day}^{-1} \text{bar}^{-1}$  and  $0.0007 \text{ g m}^{-2} \text{day}^{-1}$  respectively, already satisfying the tough requirements for encapsulation of organic photovoltaics.<sup>27</sup> While as expected both OTR and WVTR increase with higher temperature and R.H., amplification of WVTR is significantly more pronounced for DB nanocomposite films (45 times) as compared to SC nanocomposite films (4.3 times). Quite surprisingly, the transmission rate of the hydrophobic permeate, oxygen, appears to be more sensitive to swelling: OTR increases 510 times and 480 for DB and SC films, respectively.

The performances of different barrier coatings can only be compared when transmission rates are converted to permeabilities, oxygen permeability (OP) and water vapor permeability (WVP), whereby in a first approximation<sup>28</sup> it is generally assumed that the rate is inversely proportional to the thickness (Table 2). The contribution of the substrate is separated applying a series expansion as suggested by Roberts et al.<sup>29</sup> For WVP R.H., moreover, have to be converted into water vapor partial pressures at 23 and 38 °C, respectively. Comparing OP and WVP underlines the superior performance of SC over DB nanocomposite films at all conditions. At 23 °C/50% R.H. OP of the SC film is lower by a factor of more than 3.6 whereas at 38 °C/90% R.H. the factor increases to 4.5. The difference in performance between processing techniques is more pronounced for WVP. At 23 °C/50% R.H. the WVP of SC films is only lower by a factor of 9 while at 38 °C/90% R.H. the factor increases to 128. Quite surprisingly, WVP of the SC film does not increase at 38 °C/90% R.H. despite the significant swelling of the smectic polymer–clay domains observed by PXRD (Figure 4) that increases the dissolved volume of the permeate by some 15%.

As the processing technique has a significant impact on the quality of the 1D crystallinity of the smectic polymer–clay domains, the order in the nanocomposite film might indeed be a so-far overlooked key factor for the barrier performance.

Excellent optical properties and flexibility of both nanocomposite (Figure 6a–d) films make these barrier materials

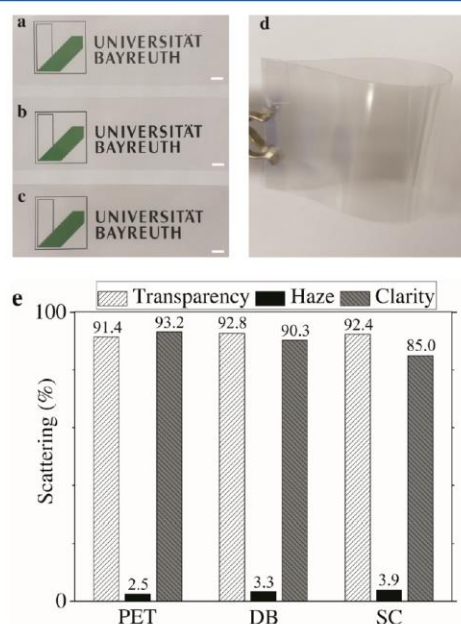


**Figure 6.** Photographs of the nanocomposite films: (a) 36  $\mu\text{m}$  PET substrate; (b) DB (thickness 1.5  $\mu\text{m}$ ); (c) SC (thickness 21.4  $\mu\text{m}$ ). Scale bar in parts a, b, and c is 1 cm. (d) Bended SC. (e) Optical transmittance, haze, and clarity of neat PET foil and nanocomposite coatings with PET foil as substrate.

very promising candidates for applications requiring optical transparency like food or optoelectronic. While optical transmittance and haze of coated substrates are comparable to the neat PET foil, clarity decreases moderately upon coating (Figure 6e).

## CONCLUSIONS

It is generally accepted that fine-tuning of diffusivity and solubility is required to concomitantly achieve good barrier performance for both hydrophobic and hydrophilic permeates. Our results suggest that smectic polymer–clay domains and the

quality of this 1D crystallinity are so far overlooked key factors for barrier film performance. Spray coating yields a better 1D crystallinity as compared to doctor blading. We suggest, that the improved regularity enhances the electrostatic interaction between filler and matrix via the Madelung constant which eventually reduces the transmission rates. With such smectic polymer–clay films even ultra high water vapor barriers can be realized with waterborne formulations.

Although these waterborne formulations were found to be perfectly homogeneous, 6-ammoniumcaprohydroxamic acid fails to ensure complete miscibility of the modified clay filler with the polymer matrix triggering partial phase separation upon solvent removal. We expect that barrier performance can be further improved if this partial phase separation can be avoided employing a more appropriate modifier.

## ■ ASSOCIATED CONTENT

### Supporting Information

The Supporting Information is available free of charge on the ACS Publications website at DOI: 10.1021/acs.macromol.7b00701.

Additional 1D and 2D SAXS, TEM image, TGA plots, and OTR and WVTR measurements (PDF)

## ■ AUTHOR INFORMATION

### Corresponding Author

\*(J.B.) E-mail: Josef.Breu@uni-bayreuth.de. Telephone +49-921-55-2530. Fax: +49 921 55 2788.

### ORCID

Josef Breu: 0000-0002-2547-3950

### Author Contributions

These authors (E.S.T. and P.F.) contributed equally to this manuscript.

### Notes

The authors declare no competing financial interest.

## ■ ACKNOWLEDGMENTS

The authors thank both the electronic and mechanical workshops of Bayreuth University for building the automatic spray coating machine. The authors also thank Professor Karl Leo, Technische Universität Dresden, for making electrical calcium corrosion test equipment available. We, moreover, thank Prof. S. Förster, Bayreuth, for making the SAXS system available. The authors thank Florian Puchtl for synthesizing the clay and Marco Schwarzmann for sample preparation and TEM measurements. E.S.T. would like to thank Josef Hausner for his help with processing the XRD data. This work was supported by the German Science Foundation (DFG) within the Collaborative Research Project SFB 840.

## ■ REFERENCES

- (1) Arora, A.; Padua, G. W. Review: Nanocomposites in Food Packaging. *J. Food Sci.* **2010**, *75* (1), R43–R49.
- (2) Lange, J.; Wyser, Y. Recent Innovations in Barrier Technologies for Plastic Packaging – a Review. *Packag. Technol. Sci.* **2003**, *16*, 149–158.
- (3) Choi, M.-C.; Kim, Y.; Ha, C.-S. Polymers for Flexible Displays: From Material Selection to Device Applications. *Prog. Polym. Sci.* **2008**, *33* (6), 581–630.
- (4) Logothetidis, S. Flexible Organic Electronic Devices: Materials, Process and Applications. *Mater. Sci. Eng., B* **2008**, *152* (1–3), 96–104.

- (5) Sabu, T.; Kuruvilla, J.; Malhotra, S. K.; Goda, K.; Sreekala, M. S. *Polym. Compos.*; Wiley-VCH: Weinheim, Germany, 2013; Vol. 2, Nanocomposites.
- (6) DeRoche, J. P.; Gettelfinger, B. T.; Wang, J.; Nuxoll, E. E.; Cussler, E. L. Barrier Membranes with Different Sizes of Aligned Flakes. *J. Membr. Sci.* **2005**, *254* (1–2), 21–30.
- (7) Wong, M.; Ishige, R.; White, K. L.; Li, P.; Kim, D.; Krishnamoorti, R.; Gunther, R.; Higuchi, T.; Jinnai, H.; Takahara, A.; Nishimura, R.; Sue, H.-J. Large-Scale Self-Assembled Zirconium Phosphate Smectic Layers via a Simple Spray-Coating Process. *Nat. Commun.* **2014**, *5*, 3589.
- (8) Doblhofer, E.; Schmid, J.; Rieß, M.; Daab, M.; Suntinger, M.; Habel, C.; Bargel, H.; Hugenschmidt, C.; Rosenfeldt, S.; Breu, J.; Scheibel, T. Structural Insights into Water-Based Spider Silk Protein – Nanoclay Composites with Excellent Gas and Water Vapor Barrier Properties. *ACS Appl. Mater. Interfaces* **2016**, *8*, 25535–25543.
- (9) Andre, V.; Bertleff, W.; Borzyk, O.; Huff, J.; Nörenberg, R. Verwendung alkoxilierter polyvinylamine zur modifizierung von oberflächen. Patent EP1290071B1, DE10029027A1, EP1290071A1, US7268199, US20030143908, WO2001096453A1. May 11, 2005.
- (10) Pietsch, I.; Weiss, A.; Preishuber-Pflügl, P.; Bippus, P.; Hunerfauth, K. Use of aqueous polyanion-polyethyleneimine solutions for producing polymer films with oxygen-barrier properties. Patent EP2859035B1, CN104350091A, EP2859035A1, US20150086734, WO2013182444A1. July 13, 2016.
- (11) Haile, M.; Sarwar, O.; Henderson, R.; Smith, R.; Grunlan, J. C. Polyelectrolyte Coacervates Deposited as High Gas Barrier Thin Films. *Macromol. Rapid Commun.* **2017**, *38*, 1600594.
- (12) Stöter, M.; Kunz, D. A.; Schmidt, M.; Hirsemann, D.; Kalo, H.; Putz, B.; Senker, J.; Breu, J. Nanoplatelets of Sodium Hectorite Showing Aspect Ratios of  $\approx 20\ 000$  and Superior Purity. *Langmuir* **2013**, *29* (4), 1280–1285.
- (13) Zilberman, E. N.; Strizhakov, O. D.; Svetozarskiy, S. V. Synthesis of  $\epsilon$ -aminocaprohydroxamic acid. *J. Gen. Chem. USSR (Engl. Transl.)* **1965**, *35*, 857–860.
- (14) Möller, M. W.; Lunkenbein, T.; Kalo, H.; Schieder, M.; Kunz, D. A.; Breu, J. Barrier Properties of Synthetic Clay with a Kilo-Aspect Ratio. *Adv. Mater.* **2010**, *22* (46), 5245–5249.
- (15) Paetzold, R.; Winnacker, A.; Henseler, D.; Cesari, V.; Heuser, K. Permeation Rate Measurements by Electrical Analysis of Calcium Corrosion. *Rev. Sci. Instrum.* **2003**, *74* (12), S147–S150.
- (16) Nehm, F.; Dollinger, F.; Klumbies, H.; Leo, K.; Müller-Meskamp, L. Device-like Electrical Calcium Corrosion Test for WVTR Measurements of Ultra-Barrier. Presented at the 58th Annual Society of Vacuum Coaters Technical Conference, 2015.
- (17) Schütz, M. R.; Kalo, H.; Lunkenbein, T.; Breu, J.; Wilkie, C. A. Intumescent-like Behavior of Polystyrene Synthetic Clay Nanocomposites. *Polymer* **2011**, *52* (15), 3288–3294.
- (18) Schütz, M. R.; Kalo, H.; Lunkenbein, T.; Gröschel, A. H.; Müller, A. H. E.; Wilkie, C. A.; Breu, J. Shear Stiff, Surface Modified, Mica-like Nanoplatelets: A Novel Filler for Polymer Nanocomposites. *J. Mater. Chem.* **2011**, *21* (32), 12110–12116.
- (19) Walther, A.; Bjurhager, I.; Malho, J. M.; Pere, J.; Ruokolainen, J.; Berglund, L. A.; Ikkala, O. Large-Area, Lightweight and Thick Biomimetic Composites with Superior Material Properties via Fast, Economic, and Green Pathways. *Nano Lett.* **2010**, *10* (8), 2742–2748.
- (20) Podsiadlo, P.; Liu, Z.; Paterson, D.; Messersmith, P. B.; Kotov, N. A. Fusion of Seashell Nacre and Marine Bioadhesive Analogs: High-Strength Nanocomposite by Layer-by-Layer Assembly of Clay and L-3,4-Dihydroxyphenylalanine Polymer. *Adv. Mater.* **2007**, *19* (7), 949–955.
- (21) Yang, Y.-H.; Haile, M.; Park, Y. T.; Malek, F. A.; Grunlan, J. C. Super Gas Barrier of All-Polymer Multilayer Thin Films. *Macromolecules* **2011**, *44*, 1450–1459.
- (22) Kunz, D. A.; Schmid, J.; Feicht, P.; Erath, J.; Fery, A.; Breu, J. Clay-Based Nanocomposite Coating for Flexible Optoelectronics Applying Commercial Polymers. *ACS Nano* **2013**, *7* (5), 4275–4280.
- (23) Theng, B. K. G. *The Clay Minerals*, 2nd ed.; Elsevier B.V.: 2012, Vol. 4.

- (24) Rosenfeldt, S.; Stöter, M.; Schlenk, M.; Martin, T.; Albuquerque, R. Q.; Förster, S.; Breu, J. In *Depth Insights into the Key Steps of Delamination of Charged 2D Nano Materials*. *Langmuir* **2016**, *32*, 10582–10588.
- (25) Kohli, R. *Hydrogen Bonding Abilities of Hydroxamic Acid and Its Isoesters*. Anchor Academic Publishing: Hamburg, Germany, 2016.
- (26) Moore, D. M.; Reynolds, R. C., Jr. *X-Ray Diffraction and the Identification and Analysis of Clay Minerals*, 2nd ed. Oxford University Press: Oxford, U.K. and New York; 1997.
- (27) Tscherner, M.; Konrad, C.; Bizzarri, A.; Suppan, M.; Cajlakovic, M.; Ribitsch, V.; Stelzer, F. Opto-Chemical Method for Ultra-Low Oxygen Transmission Rate Measurement. *IEEE Sensors Conference* **2009**, 1660–1665.
- (28) Xianda, Y.; Anlai, W.; Suqin, C. Water-Vapor Permeability of Polyvinyl Alcohol Films. *Desalination* **1987**, *62*, 293–297.
- (29) Roberts, A. P.; Henry, B. M.; Sutton, A. P.; Grovenor, C. R. M.; Briggs, G. A. D.; Miyamoto, T.; Kano, M.; Tsukahara, Y.; Yanaka, M. Gas Permeation in Silicon-Oxide/polymer (SiO<sub>x</sub>/PET) Barrier Films: Role of the Oxide Lattice, Nano-Defects and Macro-Defects. *J. Membr. Sci.* **2002**, *208* (1–2), 75–88.

## Supporting information

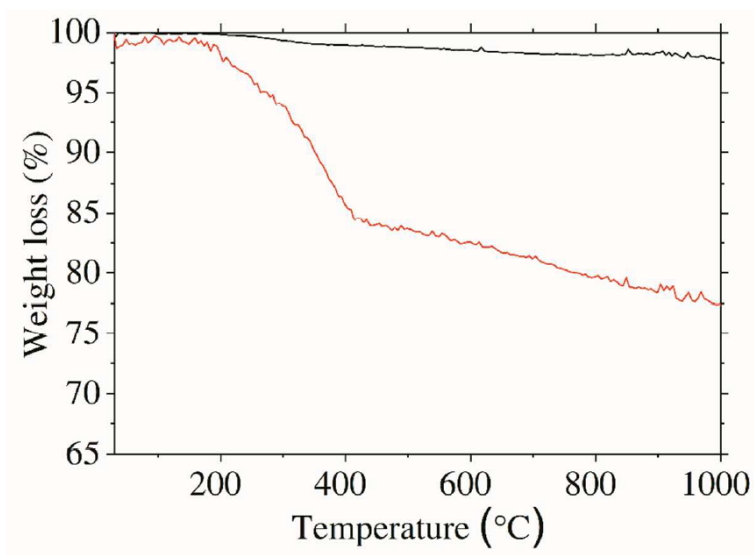


**Figure S1.** TGA curves of NaHec (black) and HAHec (red). The weight loss below 400 °C corresponds to the modifier content and amounts to 16 wt% which is in agreement with expectations based on cation exchange capacity of NaHec.

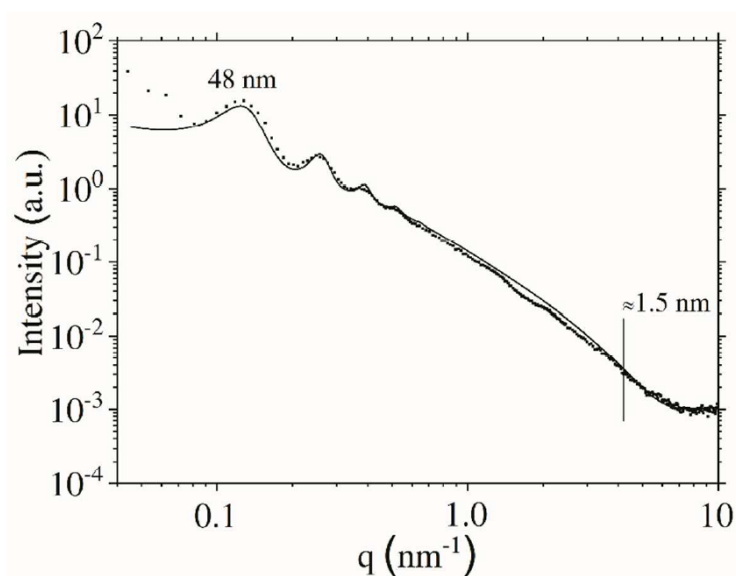


**Figure S2.** 1D-SAXS pattern of HAHec aqueous suspension (2 vol%). The vertical line marks the basal spacing expected for stacks of HAHec ( $\approx 1.5$  nm); no sign of restacking in water is observed. The continuous line corresponds to calculated intensity based on a model of stacked discs with a radius of 9  $\mu\text{m}$  and a thickness of 1 nm. The rational  $00l$  series observed at low  $q$  ( $< 1 \text{ nm}^{-1}$ ) indicates a rather uniform separation of delaminated clay nanoplatelets to  $48 \pm 5$  nm.

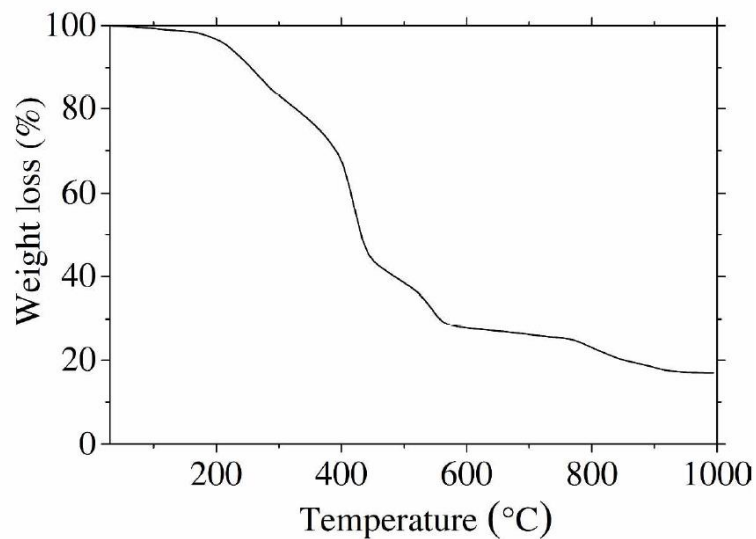


**Figure S3.** TGA curve of the free-standing SC nanocomposite with a hectorite loading of 10 vol%. The weight loss observed corresponds to the polymer:clay ratio of the suspension applied. Please note that NaHec is a fluoro-hectorite and does not decompose before 800 °C.

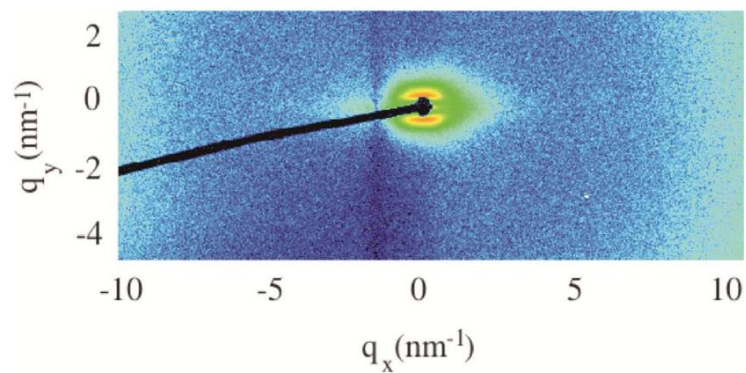


**Figure S4.** 2D-SAXS pattern of PET substrate measured in parallel geometry.

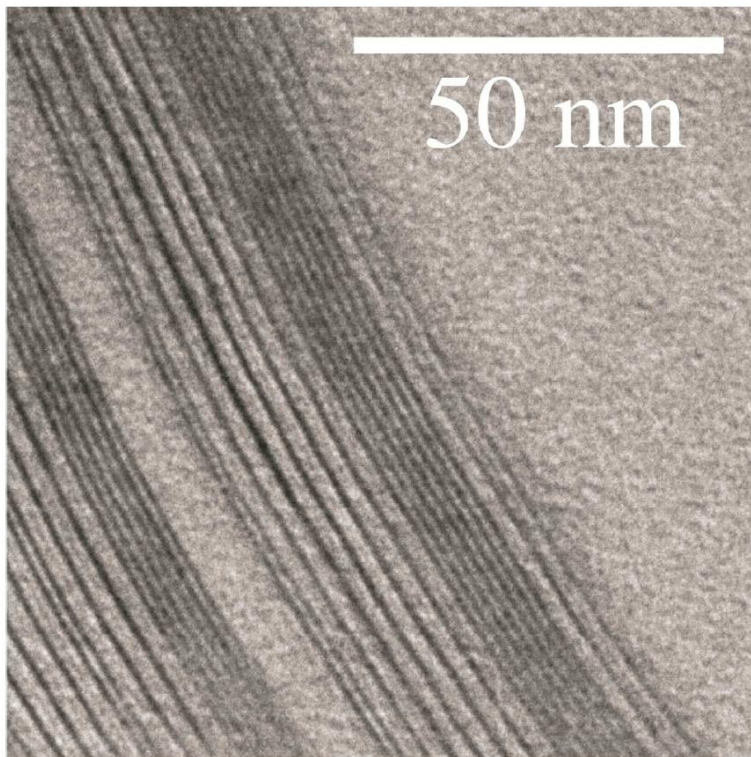


**Figure S5.** TEM image of free-standing SC nanocomposite film. Very rarely a domain with a smaller separation corresponding to HAHeC can be found.

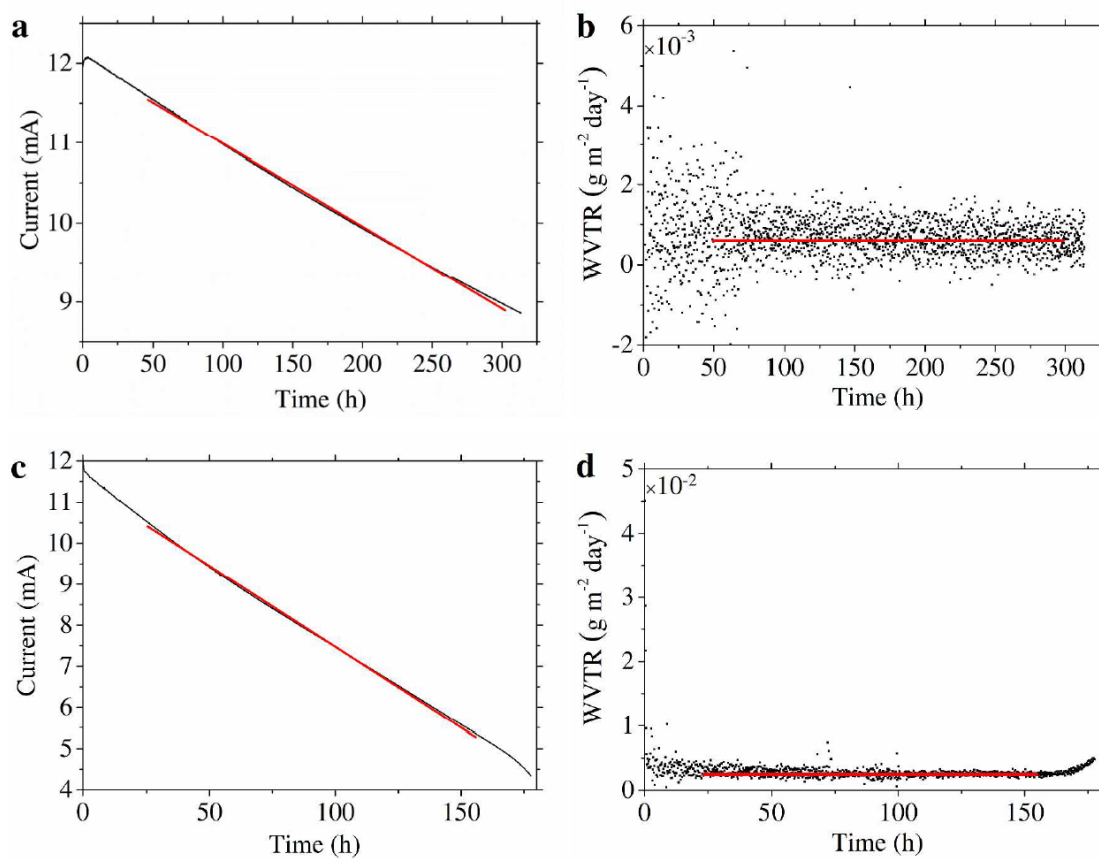


**Figure S6.** An example of WVTR measurements of SC nanocomposite using electrical calcium corrosion tests. (a, b) 23 °C / 50% R.H.; (c, d) 38 °C / 90% R.H.. The red line indicates the average value.

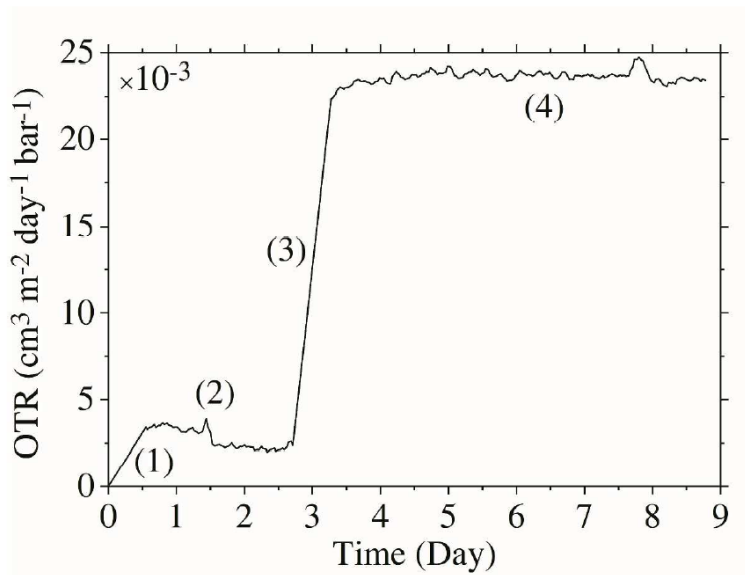


**Figure S7.** An example of OTR measurement of DB nanocomposite at 23 °C / 50% R.H. using a Mocon OX-TRAN 2/21 XL. The measurement consists of conditioning (1); measurement of device individual zero (2); conditioning (3) and finally measuring OTR (4) at equilibrium.

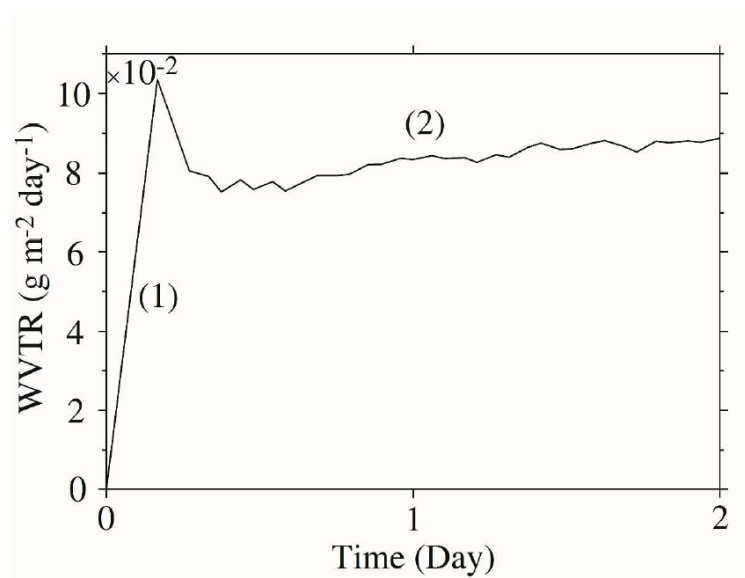


**Figure S8.** An example of WVTR measurement of DB nanocomposite at 23 °C / 50% R.H. using Mocon PERMATRAN-W model 3/33. The measurement consists of conditioning (1) and measurement of the nanocomposite WVTR (2) at equilibrium.

### 6.3. Appendix 3

#### **An excellent helium barrier for lighter than air applications**

Christoph Habel<sup>a,b</sup>, Evgeny S. Tsurko<sup>a,b</sup>, Patrick Feicht<sup>a,b</sup>, Matthias Daab<sup>a,b</sup>, Sabine Rosenfeldt<sup>a,c</sup>,  
Josef Breu<sup>a,b,\*</sup>

<sup>a</sup> Bavarian Polymer Institute, Universitätsstraße 30, Bayreuth 95447, Germany

<sup>b</sup> Department of Inorganic Chemistry I, University of Bayreuth, Universitätsstraße 30, Bayreuth 95447, Germany

<sup>c</sup> Department of Physical Chemistry I, University of Bayreuth, Universitätsstraße 30, Bayreuth 95447, Germany

\* Corresponding author:

Prof. Dr. Josef Breu

Universitätsstr. 30

95440 Bayreuth

Germany

\* E-mail address: [Josef.Breu@uni-bayreuth.de](mailto:Josef.Breu@uni-bayreuth.de)

This work will be submitted in Journal of Membrane Science

## ABSTRACT

New wind energy concepts in which helium acts as a lifting agent require new materials with an excellent multi-permeate barrier behavior against helium, oxygen and water vapor. This is an important factor do not lose too much of this lifting agent and, moreover, not wasting the lifting gas with oxygen or water vapor. In this work it has been examined whether polar polymeric composite systems concerning layered silicates have such excellent barriers. Therefore, we dispersed a melt-synthesized sodium fluorohectorite (NaHec) with a homogenous charge distribution and an aspect ratio of about 20000 in a polar polyvinyl alcohol (PVA) matrix. With a 1  $\mu\text{m}$  coating of the PVA-NaHec nanocomposite with an inorganic content of about 50 wt% we obtained helium permeability values of about 1000 times better than the bare PVA matrix.

Keywords: layered silicates, polymer nanocomposites, helium barrier, waterborne systems, lighter-than-air vehicles

**1. Introduction**

The barrier of polymer films can be improved by decreasing the solubility of permeates or by reducing the free volume with increasing the density. Alternatively, the diffusion path may be elongated by incorporation of platy, impermeable fillers, an approach which has long been established as tortuous path [1]. The latter will introduce a large interphase area and this way of course will also modify the structure and/or crystallinity of the polymer matrix.

Layered silicates are most commonly used as nanofillers. Fluorohectorite, as an example, belongs to the 2:1 smectite family and shows a sandwich-like structure comprising two tetrahedral and one octahedral layers with a composition like  $[\text{Na}_{0.5}]^{\text{inter}}[\text{Mg}_{2.5}\text{Li}_{0.5}]^{\text{oct}}[\text{Si}_4]^{\text{tet}}\text{O}_{10}\text{F}_2$  (NaHec) [2] as for the synthetic fluorohectorite used here. Melt-synthesized clay nanosheets, moreover, come in high aspect ratios ( $> 20000$ ) qualifying synthetic fluorohectorite as superb filler in nanocomposite materials. Additionally, this synthetic clay can be utterly delaminated into single layers simply by osmotic swelling [3].

Besides the upcoming hydrogen economy, lighter-than-air vehicles using the wind energy are hot topics in the alternative energy generation [4,5]. In this applications it is necessary do not waste the lifting agent helium and to reduce the loss of it. Therefore, the barrier of the used polymer matrices against incoming gases like oxygen and water vapor and against helium itself has to be

increased. Moreover, these materials should be lightness, flexible and mechanically stable. Classic barrier materials are multilayer systems or metalized polymers [6,7]. On the one hand it is quite difficult to detect possible defects in these multilayer systems and to remove them. On the other hand, both material systems are brittle and therefore not the preferred choice for applications with the described requirements. Consequently, such multi-permeate barriers (helium, oxygen, water vapor) can only be realized by a flexible single-layer coating with a customized matrix [8–10].

Polyvinyl alcohol (PVA) is a well-known, mass produced, low cost, biodegradable, water soluble polymer that at low relative humidity (RH) shows a great oxygen barrier. Generally, in the presence of moisture, water soluble polymers like PVA, however, swell [11]. Water uptake results in plasticization of the polymer chains because polymer chain interactions via hydrogen bonding worsen leading to an increase of permeability not only of water vapor but also of oxygen [12]. For instance, the oxygen permeability (OP) of a typical PVA film increases by over 500% when going from 0% to 55% RH to an absolute oxygen transmission rate (OTR) for a 6  $\mu\text{m}$  thick film of  $3.1 \text{ cm}^3 \text{ m}^{-2} \text{ day}^{-1} \text{ bar}^{-1}$  [13]. Water vapor permeability (WVP) for PVA is of course even more sensitive to moisture [12].

Here we show that nanocomposite systems out of this waterborne polymer and with synthetic hectorite with a huge aspect ratio as filler are favorable for lighter than air applications. These applications require a great barrier against nonpolar gases like helium and oxygen, but also for polar gases like water vapor. We have already shown [14] that these nanocomposite systems have an excellent barrier against oxygen and water vapor and here we show these great barrier properties further against the much more sophisticated gas helium.

## 2. Experimental

### 2.1. Materials

The employed  $[\text{Na}_{0.5}]^{\text{inter}}[\text{Mg}_{2.5}\text{Li}_{0.5}]^{\text{oct}}[\text{Si}_4]^{\text{tet}}\text{O}_{10}\text{F}_2$  was synthesized via melt synthesis according to an established literature procedure [3,15–17]. The material featured a cation exchange capacity of  $1.27 \text{ mmol g}^{-1}$ .

Polyvinyl alcohol (PVA) (Sigma Aldrich, Germany) with different molecular weight and degree of hydrolysis was used: Mowiol 10-98 ( $M_w = 61000$ , 98.0 – 98.8 mol% hydrolysis); Mowiol 18-88 ( $M_w = 130000$ , 86.7-88.7 mol% hydrolysis); Mowiol 20-98 ( $M_w = 125000$ , 98.0 – 98.8 mol% hydrolysis). 5 g of PVA were dissolved in 95 g of Millipore water by heating at  $95 \text{ }^\circ\text{C}$  for 4 hours to obtain a 5 wt% solution.

A corona treated polyethylene terephthalate (PET) ( $36 \text{ }\mu\text{m}$ ) film was used as a substrate (Bleher KG, Germany).

### 2.2. Nanocomposite films fabrication

*PVA-NaHec films:* NaHec (0.5 g) was delaminated by immersing it into Millipore water (100 g, 0.5 wt%) and this was mixed with a PVA solution (5 wt%) and the dispersion was stirred about 10 minutes. The total solid content in the end was 2.5 wt%. Upon drying, the mixture will yield barrier films with 10 wt%, 20 wt% and 50 wt% filler content.

The resulting suspensions were doctor-bladed automatically onto the PET substrate and the resulting films were dried at  $80 \text{ }^\circ\text{C}$  for 3 days. It is quite difficult to determine the exact resulting heights of the coatings. Elipsometry as method is not possible because of the refractive indices of the different components are too similar. To detect the resulting heights via atomic force microscopy a silicium wafer has to be coated in the same way like the sample substrates. Comparing with spray coating as method is quite impossible. Therefore, the resulting heights of the coatings are calculated with considering the densities of the PVA and the NaHec, the filler content and the height of the automatic doctor blading system that was set to  $60 \text{ }\mu\text{m}$ . The resulting heights are given in **Table 1**.

**Table 1.** Resulting coating thicknesses at different filler contents.

Filler content (wt%)	Coating thickness ( $\mu\text{m}$ )
0	1.4
10	1.3
20	1.2
50	1.0

### 2.3. Nanocomposites characterization

X-ray diffraction (XRD) patterns were obtained using nickel filtered Cu-K $\alpha$  radiation ( $\lambda = 1.54187 \text{ \AA}$ ) on a Bragg-Brentano-type diffractometer (XPRT-PRO, PANalytical B.V.) equipped with an X'Celerator Scientific RTMS detector. All patterns were analyzed using Panalytical's Highscore Plus software.

All small angle X-ray scattering (SAXS) data were measured using the small-angle X-ray system "Double Ganesha AIR" (SAXSLAB, Denmark). The X-ray source of this laboratory-based system is a rotating anode (copper, MicoMax 007HF, Rigaku Corporation, Japan) providing a micro-focused beam. The data are recorded by a position sensitive detector (PILATUS 300K, Dectris). To cover the range of scattering vectors between 0.003-2.2  $\text{\AA}^{-1}$  different detector positions were used. The measurements of the suspensions were done in 1 mm glass capillaries (Hilgenberg, Germany) at room temperature.

The measurement of the helium transmission rate (HeTR) was done with a pressure difference method on the GDP-C of the Brugger company and on the measurement institute Permlab. The relative humidity of 75% RH was set with a sulfuric acid solution (DIN 50008-2).

### 3. Results and discussion

At low RH PVA is a very good barrier material to nonpolar gases like oxygen. On the one hand hydrogen bonding of hydroxyl groups minimizes free volume; on the other hand, the polarity limits the solubility of nonpolar gases in PVA. Moreover, non-swollen crystalline domains of the semi-crystalline matrix are regarded impermeable. PVA films, however, show high solubility, hygroscopicity and swelling in water and consequently their WVP is high. Moreover, as already mentioned, water uptake by swelling at elevated RH (> 35%) leads to a drastic increase of permeability not only of water vapour but also of oxygen. This pronounced sensitivity to water vapour renders PVA unsuitable for flexible food packaging. Grunlan *et al.* [13] has shown that the critical RH, where swelling followed by a significant loss of oxygen barrier sets in, can be shifted to higher RH by incorporation of Na-montmorillonite as platy impermeable filler. We have recently reported [18] that a waterborne spider silk protein-nanoclay composite is hydrophobized upon film formation to the degree where it not only becomes insoluble in water but also shows only limited swelling at elevated RH. In comparison to the uncoated substrate the WVTR of the bio-nanocomposite decreased by 96% to  $0.18 \pm 0.05 \text{ g m}^{-2} \text{ day}^{-1}$ . Moreover, we already reported [14] that PVA has an excellent barrier against oxygen and even against water vapor. Surprisingly this phenomenon also occurs at high RH (> 75%). Nevertheless, even for lighter than air applications the barrier against much more sophisticated gases like helium are an important point.

#### 3.1. SAXS and XRD

To create a highly effective tortuous path according to Cussler [1] a huge aspect ratio is required. Therefore, it is indispensable that NaHec as a filler is completely delaminated in the PVA before the doctor blading step. We have already reported, that NaHec is well dispersed in the used solvent water [19]. To show this delamination also in the triple phase system (polymer, solvent, clay) small angle x-ray scattering (SAXS) measurements were done (**Fig. 1**).

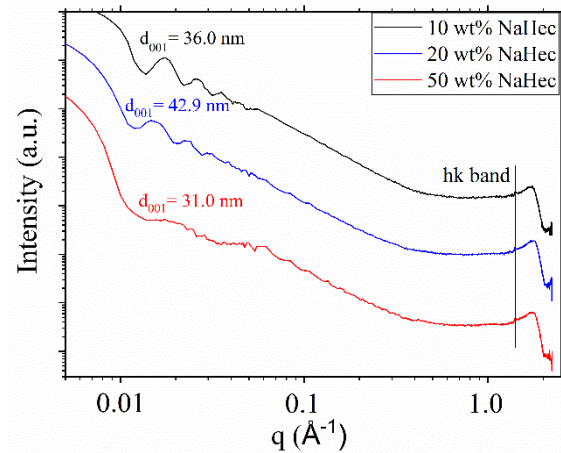


**Fig. 1.** SAXS measurement of PVA-NaHec gels at different filler loading. NaHec contents in gel are 2.4 vol% (10 wt% NaHec), 2.0 vol% (20 wt% NaHec), 2.9 vol% (50 wt% NaHec).

The distance between the single platelets is between 30-45 nm and that indicates, that NaHec as a filler is delaminated even in the triple state with PVA as matrix. In the next producing step, the jellylike dispersion is doctor-bladed on a PET substrate and dried as described. The distance between the single NaHec platelets after the drying process was determined using XRD analysis (**Fig. 2**).

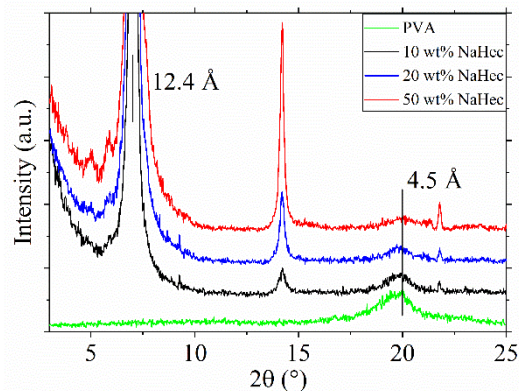


**Fig. 2.** XRD measurement of the composites with different filler contents.

There is one characteristic peak of semi-crystalline PVA at about  $20^\circ$  with a broad width [20]. The samples with NaHec as a filler moreover show a  $d_{001}$  value of about  $12.4 \text{ \AA}$  that is independent of the filler content. This value matches with the d-value of a single-hydrated interlayer cation sodium. Normally one would expect an increasing d-spacing with an increasing polymer content. At a NaHec content of about 50 wt%, i.e. about 30 vol%, there should be a distance between the layers of about  $30 \text{ \AA}$  if the NaHec is homogenously dispersed in the

polymer matrix. This result shows, that during the drying process and the removal of the solvent, the surface tensions get too high because of the different surface energies of NaHec and PVA. Therefore, the NaHec platelets restack and a phase segregation occurs.

### 3.2 Helium barrier

The helium transmission rates were measured (**Table 2**) to estimate the effect of the incorporation of NaHec platelets into the polymer matrix.

**Table 2.** The HeTR and the calculated permeabilites of the composites at 2-10% RH.

Polymer	NaHec (wt%)	HeTR	Permeability
		$\text{cm}^3 \text{ m}^{-2} \text{ day}^{-1} \text{ atm}^{-1}$	$\text{cm}^3 \mu\text{m m}^{-2} \text{ day}^{-1} \text{ atm}^{-1}$
PET	0	1740	62640
PET + PVA 20-98	0	531	19860
PET + PVA 20-98	20	1.7	63
PET + PVA 10-98	20	1.45	54
PET + PVA 20-98	50	1.2	44
PET + PVA 18-88	50	1.0	37
PET + PVA 10-98	50	0.5	18.5

Even the coating with neat PVA lead to a decrease of the permeability of the complete system of about 68%. As discussed before, the X-ray measurements show a restacking and therefore a single hydrated interlayer. This polar interlayer acts as a good barrier against the nonpolar gas helium. With NaHec as filler, the permeability decreases by a huge factor of up to 1000. These results match with the model of Cussler [1]; an increasing filler content lead to decreasing transmission rates. That effect is independent of the polymer matrix. To compare the effectivity of the different coatings the permeabilities of the neat coatings with the same filler loading are calculated. Therefore, the thicknesses of these coatings are taken into account [21] (**Table 2**).

The resulting permeabilities of the coatings depend on the molar mass of the polymer matrix. With an increasing molar mass, the permeability of the composite is increasing. This is the consequence of the increasing number of entanglements. Therefore, the free volume increases and the barrier properties decrease. With incorporation of 50 wt% the permeability of PVA-NaHec nanocomposite decreases by factor of about 1000 compare to unfilled PVA coating.

One of the disadvantages of PVA as matrix is the plasticization effect at a RH over 35%. We have already shown [14] a decreasing plasticization effect for oxygen and water vapor and therefore, we also expect it with helium as test gas (**Table 3**).

**Table 3.** HeTR of the nanocomposite systems at 0% and 75% RH.

Sample	HeTR	Permeability
	$\text{cm}^3 \text{ m}^{-2} \text{ day}^{-1} \text{ atm}^{-1}$	$\text{cm}^3 \mu\text{m m}^{-2} \text{ day}^{-1} \text{ atm}^{-1}$
	<i>0% RH / 75% RH</i>	<i>0% RH / 75% RH</i>
PET + PVA + 10 wt%	<i>0.8</i>	<i>31.3</i>
NaHec	<b><i>7.1</i></b>	<b><i>266.3</i></b>
PET + PVA + 50 wt%	<i>0.8</i>	<i>30.3</i>
NaHec	<b><i>1.7</i></b>	<b><i>63.3</i></b>

As it was expected, the transmission rates at a relative humidity of about 75% increased because of the polymer plasticization. Nevertheless, this plasticization effect is much lower than in the neat polymer matrix because then, the permeability at about 75% RH would have been in the region of the neat PET substrate with a permeability of about  $60000 \text{ cm}^3 \mu\text{m m}^{-2} \text{ day}^{-1} \text{ atm}^{-1}$ . Moreover, the increase of the transmission rate of the sample with 50 wt% filler content is less than the increase of the sample with 10 wt%.

#### 4. Conclusions

Applying large aspect ratio synthetic clay increases the barrier properties of the waterborne polymer PVA against helium by a factor of about 1000. On the one hand this is due to the elongated tortuous path caused by the huge platelets and the used polar polymer PVA. Moreover, we were able to show, that the molar mass of the polymer is important for the resulting barrier properties of the systems. A lower molar mass leads to decreasing permeabilities. This can be explained by the decreased number of entanglements and therefore the reduced free volume. With transferring to other hydrophilic polymer matrices we are sure to further increase the barrier properties of the layered silicate-polymer-composites.

#### Acknowledgements:

The authors thank Florian Puchtler for producing the synthetic clay. This work was supported by the German Science Foundation (DFG) within the collaborative research project SFB 840.

---

**References**

- [1] J.J.P. DeRocher, B.T. Gettelfinger, J.Wang, E.E. Nuxoll, E.L. Cussler, Barrier membranes with different sizes of aligned flakes, *J. Membr. Sci.* 254 (2005) 21–30.
- [2] B.K.G. Theng, Formation and Properties of Clay-polymer Complexes, Elsevier Science, Landcare Research, Palmerston North, New Zealand, 2012. Volume 4.
- [3] M.Stöter, D.A. Kunz, M. Schmidt, D. Hirsemann, H. Kalo, B. Putz, J. Senker, J. Breu, Nanoplatelets of sodium hectorite showing aspect ratios of  $\approx 20\ 000$  and superior purity, *Langmuir.* 29 (2013) 1280–1285.
- [4] R.J.M. Penedo, T.C.D. Pardal, P.M.M.S. Silva, N.M. Fernandes, T.R.C. Fernandes, *Airborne Wind Energy*, 2013, 491–500.
- [5] N. Fernandes, HAWE report summary, 2011, project reference: 256714.
- [6] X. Liang, D.M. King, M.D. Groner, J.H. Blackson, J.D. Harris, S.M. George, A.W. Weimer, Barrier properties of polymer / alumina nanocomposite membranes fabricated by atomic layer deposition, *J. Membr. Sci.* 322 (2008) 105–112.
- [7] L.J. Van Rooyen, J. Karger-Kocsis, O.C. Vorster, L.D. Kock, Helium gas permeability reduction of epoxy composite coatings by incorporation of glass flakes, *J. Membr. Sci.* 430 (2013) 203–210.
- [8] P. Tzeng, E.L. Lugo, G.D. Mai, B.A. Wilhite, J.C. Grunlan, Super Hydrogen and Helium Barrier with Polyelectrolyte Nanobrick Wall Thin Film, *Macromol. Rapid Commun.* 36 (2015) 96–101.
- [9] S. Campbell, J.C. Johnston, L. Inghram, L. Mccorkle, B. Park, E. Silverman, NASA /TM-2003\_212221 (2003).
- [10] T. Ogasawara, Helium gas permeability of montmorillonite / epoxy nanocomposites, *Composites.* 37 (2006) 2236–2240.
- [11] H.B. Hopfenberg, A. Apicella, D.E. Saleeby, Factors affecting water sorption in and solute release from glassy ethylene-vinyl alcohol copolymers, *J. Membr. Sci.* 8 (1981) 273–282.
- [12] C. Mo, W. Yuan, W. Lei, Y. Shijiu, Effects of Temperature and Humidity on the Barrier Properties of Biaxially-oriented Polypropylene and Polyvinyl Alcohol Films, *J. Appl. Packag. Res.* 6 (2014) 40–46.
- [13] J.C. Grunlan, A. Grigorian, C.B. Hamilton, A.R. Mehrabi, Effect of clay concentration on the oxygen permeability and optical properties of a modified poly(vinyl alcohol), *J. Appl. Polym. Sci.* 93 (2004) 1102–1109.
- [14] E.S. Tsurko, P. Feicht, C. Habel, T. Schilling, M. Daab, S. Rosenfeldt, J. Breu, Can Water Vapour Tolerant High Oxygen and Water Vapour Barrier Nanocomposite Coatings be Obtained with a Waterborne Formulation?, *J. Membr. Sci.* 540 (2017) 212–218.
- [15] J. Breu, W. Seidl, A.J. Stoll, K.G. Lange, T.U. Probst, Charge homogeneity in synthetic fluorohectorite, *Chem. Mater.* 13 (2001) 4213–4220.
- [16] H. Kalo, M.W. Möller, M. Ziadeh, D. Dolejš, J. Breu, Large scale melt synthesis in an

- open crucible of Na-fluorohectorite with superb charge homogeneity and particle size, *Appl. Clay Sci.* 48 (2010) 39–45.
- [17] M. Stöter, S. Rosenfeldt, J. Breu, Tunable Exfoliation of Synthetic Clays, *Annu. Rev. Mater. Res.* 45 (2015) 129–151.
- [18] E. Doblhofer, J. Schmid, M. Riess, M. Daab, M. Suntinger, C. Habel, H. Bargel, C. Hugenschmidt, S. Rosenfeldt, J. Breu, T. Scheibel, Structural Insights into Water-Based Spider Silk Protein-Nanoclay Composites with Excellent Gas and Water Vapor Barrier Properties, *ACS Appl. Mater. Interfaces.* 8 (38) (2016) 25535–25543.
- [19] S. Rosenfeldt, M. Stöter, M. Schlenk, T. Martin, R.Q. Albuquerque, S. Förster, J. Breu, In Depth Insights into the Key Steps of Delamination of Charged 2D NanoMaterials, *Langmuir.* 32 (41) (2016) 10582–10588.
- [20] J. Gaume, C. Taviot-Gueho, S. Cros, A. Rivaton, S. Therias, J. L. Gardette, Optimization of PVA clay nanocomposite for ultra-barrier multilayer encapsulation of organic solar cells, *Sol. Energy Mater. Sol. Cells.* 99 (2012) 240–249.
- [21] A.P. Roberts, B.M. Henry, A.P. Sutton, C.R.M. Grovenor, G.A.D. Briggs, T. Miyamoto, M. Kano, Y. Tsukahara, M. Yanaka, Gas permeation in silicon-oxide/polymer (SiO<sub>x</sub>/PET) barrier films: Role of the oxide lattice, nano-defects and macro-defects, *J. Membr. Sci.* 208 (2002) 75–88.

## **7. Declaration – Erklärung**

Hiermit erkläre ich, dass keine Tatsachen vorliegen, die mich nach den gesetzlichen Bestimmungen über die Führung akademischer Grade zur Führung eines Doktorgrades unwürdig erscheinen lassen.

Hiermit erkläre ich mich damit einverstanden, dass die elektronische Fassung meiner Dissertation unter Wahrung meiner Urheberrechte und des Datenschutzes einer gesonderten Überprüfung hinsichtlich der eigenständigen Anfertigung der Dissertation unterzogen werden kann.

Hiermit erkläre ich eidesstattlich, dass ich die Dissertation selbstständig verfasst und keine anderen als die von mir angegebenen Quellen und Hilfsmittel benutzt habe.

Ich habe die Dissertation nicht bereits zur Erlangung eines akademischen Grades anderweitig eingereicht und habe auch nicht bereits diese oder eine gleichartige Doktorprüfung endgültig nicht bestanden.

Hiermit erkläre ich, dass ich keine Hilfe von gewerblichen Promotionsberatern bzw. –vermittlern in Anspruch genommen habe und auch künftig nicht nehmen werde.

Bayreuth, 08. December 2017

---

Evgeny S. Tsurko